VILNIUS UNIVERSITY
CENTER FOR PHYSICAL SCIENCES AND TECHNOLOGY

JAROSLAVAS BELOVICKIS

ULTRASONIC AND DIELECTRIC SPECTROSCOPY OF COMPOSITES BASED ON POLYMERS AND ORGANIC OR INORGANIC NANOPARTICLES

Doctoral dissertation
Physical Science, Physics (02P)

Vilnius, 2017

VILNIAUS UNIVERSITETAS
FIZINIŲ IR TECHNOLOGIJOS MOKSLŲ CENTRAS

JAROSLAVAS BELOVICKIS

KOMPOZITŲ, SUDARYTŲ IŠ POLIMERŲ IR ORGANINIŲ BEI NEORGANINIŲ NANODALELIŲ, ULTRAGARSINĖ IR DIELEKTRINĖ SPEKTROSKOPIJA

Daktaro disertacija
Fiziniai mokslai, Fizika (02P)

Vilnius, 2017

The dissertation was prepared at Vilnius University in 2013 – 2017.

Scientific supervisor– Prof. habil. Dr. Jūras Banys (Vilnius University, Physical sciences, Physics – 02P).

Scientific advisor– assoc. Prof. Dr. Vytautas Samulionis (Vilnius University, Physical sciences, Physics – 02P).

Acknowledgements

Here I would like to let some people know how much I have appreciated their help over the past four years. They deserve my thanks for a variety reasons.

First of all, I am grateful to my scientific supervisor Prof. habil. Dr. Jūras Banys for supervision and guidance in preparing the thesis, the help concerning other not less important issues over my PhD.

I sincerely appreciate the ever-ready help provided by my scientific advisor assoc. Prof. Dr. Vytautas Samulionis, with whom I had the pleasure of spending time these past four years, and the invaluable knowledge which he has shared with me.

Besides my supervisor and scientific advisor, I would like to thank Dr. Jan Macutkevic for providing the opportunity to investigate polydimethylsiloxane based composites and his insightful comments during writing articles.

I would like to thank Dr. Maxim Silibin for consulting and supplying samples which gave rise to the fruitful cooperation in the form of the work and several articles.

I wish to express my heartfelt gratitude to Prof. Daumantas Čiplys and assoc. Prof. Dr. Romualdas Rimeika for formation of my interest in the world of acoustics during my Bachelor and Master programmes. In addition, the International Student Grant of the Acoustical Society of America, given in the year 2014, would have been impossible without the research results in the field of acousto-optic modulation obtained under the supervision and help of my wise supervisors at the laboratory of Physical acoustics.

I extend my gratitude to the present colleagues in the laboratory of microwave spectroscopy and the colleagues I worked with: Dr. Vidmantas

Kalendra, Dr. Šarūnas Bagdzevičius, Dr. Maksim Ivanov, Dr. Edita Palaimienė Dr. Martynas Kinka, Dr. Saulius Rudys, Rūta Mackevičiūtė, Ieva Kranauskaitė, Ilona Zamaraitė, Mantas Šimėnas, Šarūnas Svirskas, Džiugas Jablonskas and Sergejus Balčiūnas for the nice working atmosphere and the kind help. I appreciate their assistance in performing lots of experiments and the time we spent together outside the lab.

Ich möchte gerne Herrn Priv.-Doz. Dr. Ingo Alig und Prof. Mario Kupnik für mein Praktikum danken, das ich an dem Fraunhofer LBF auszuführen konnte. Während der Zeit habe ich wertvolles Wissen und unschätzbare Erfahrung erworben.

Darüber hinaus möchte ich herzliche mich bei den Mitarbeiterinnen und den Mitarbeitern der Gruppe Morphologie und Dynamik bedanken. Ich habe mich sehr gefreut, Ihre nette Gesellschaft kennen zu lernen. Ich bin für die begeisternde Atmosphäre und Zusammenarbeit in diesen Monaten sehr dankbar.

I much appreciate valuable advices from my teacher Vladimir Ovčinikov and his genuine interest in the world of Physics.

I would to take the opportunity to thank my good friend Aliaksei Kurylenka for inspiration and multifold help.

Gern nutze ich die Gelegenheit, um Frank Lemke für die Inspiration und weise Ratschläge im abgelaufenen Jahr zu danken.

Finally, I wish to thank my Family and especially my Mother for her support and understanding throughout the PhD and my life.

Table of contents

1 Introduction 8
1.1 Aim of the work 12
1.2 Scientific novelty 13
1.3 Statements presented for defence 14
1.4 List of publications included into the thesis 15
1.5 Other papers 16
1.6 Conference presentations 16
1.6.1 Oral presentations 16
1.6.2 Poster presentations 17
1.6.3 Other presentations based on the results 19
1.7 Author‘s contribution 19
2 Overview 20
2.1 Nanocomposites 20
2.2 Types of polymers used in nanocomposites 20
2.4 Processes related to semicrystalline polymers 28
2.5 Ferroelectricity and phase transition dynamics 30
2.6 Dynamics of relaxational polarization 36
2.7 Ultrasonic spectroscopy 42
2.8 Importance of PDMS and P(VDF-TrFE) as a composite matrix 45
2.9 Fillers in nanocomposites 49
3 Experimental 52
3.1 Means of dielectric spectroscopy 52
3.2 Means of ultrasonic specroscopy 54
3.3 Means for ferroelectric characterisation 56
3.4 Other techniques 57
3.5 Materials 59
4 Experimental results 61

4.1 PDMS/ZnO 61
4.1.1 Summary 72
4.2 (PVDF-TrFE)/BPZT 73
4.2.1 Modelling and experiment of polarization reversal 73
4.2.1.1 Summary 83
4.2.2 Dielectric, ferroelectric and piezoelectric investigation 84
4.2.2.1 Summary 95
4.2.3 Ultrasonic spectroscopy 96
4.2.3.1 Summary 106
4.2.4 P(VDF-TrFE)/CNT 107
4.2.4.1 DSC and DMA results 109
4.2.4.2 Ultrasonic studies 115
4.2.4.3 Dielectric studies 119
4.2.4.4 TSDC studies 120
4.2.4.5 SEM analysis 123
4.2.4.6 Summary 124
5 Conclusions 126
6 References 128

1 Introduction

During the last decades nanotechnology has reached a great importance in the research world. The branch of technology is operating in various fields of application as communications and medicine. The main reason behind the use of nanocomposites is the enhancement of various properties when compared to individual components. Produced nanomaterials can display unique properties which are supported by morphological evidence at nanometer scale. For this reason, it is very important to understand, how properties of nano- and microcomposites depend on the ratio and type of its constituents. Hence, a proper improvement of mechanical, piezoelectric or ferroelectric properties of the nanocomposites is the main goal in inventing new devices with potential applications. Moreover, it is important to determine the reliability and durability of a material prior to the massive production on the market. Therefore, conducted repetitive experiments under various conditions (e.g. increased temperature) could contribute to understanding the interfaces between various fillers and the surrounding medium within a nanocomposite.

Polymer based composites with embedded solid fillers can incorporate mechanical and electrical properties of its constituents. In comparison with classical inorganic piezoelectrics, piezoelectric polymers have a number of advantages, namely good mechanical flexibility, easy processability, low cost of production, robustness, and lightness, whereas ceramics are typically brittle and more difficult to process [1-5]. Here the ferroelectric copolymer poly(vinylidene fluoride trifluoroethylene) (PVDF-TrFE) distinguishes amongst other polymers [6-9]. Strong piezoelectric and pyroelectric activity allows applications of P(VDF-TrFE) in high performance actuators, contact switches, strain measurements, motion sensors, medical diagnostics such as blood and urine analysis, drug delivery monitoring, homeland security

applications, warfare detection, environmental and food quality monitoring and in artificial organs (due to its chemical stability) [10-14]. A wide application field of the piezoelectric polymers is developing for piezoelectric transducers and, especially, ultrasonic sensor arrays [15]. Further efforts to improve piezoelectric, dielectric and elastic properties of the polymers for above mentioned applications have been done by mixing these ferroelectric copolymers with electroactive fillers [1, 16]. Fillers of the well-known piezoelectrics, such as barium-doped lead zirconate titanate (BPZT, ferroelectric to paraelectric phase transition at Curie temperature, T_C = 453 K) or barium titanate (BTO, T_C = 393 K), are perfect for the incorporation due to their high electromechanical coupling coefficients, dielectric permittivity values, and piezoelectric strain constants [1, 16-18]. Therefore, we focus our attention on properties of such P(VDF-TrFE) based piezoelectric composites. In spite of numerous investigations of polymer elastic properties performed over a wide frequency range: at low frequencies by Dynamic Mechanical Analysis (DMA) methods [19], at ultrasonic frequencies by pulse echo reflection [20, 21] and pulse echo transmission methods [22], and at high frequencies by Brillouin scattering experiments [23], there is a lack of ultrasonic investigations of P(VDF-TrFE) copolymers, especially in the phase transition region. As far as we know, for the PVDF polymers there has only been one experiment investigating temperature dependences of ultrasonic wave velocity and attenuation at 2 MHz frequency [24]. On the frequency scale, acoustic waves of frequencies near to 10 MHz are commonly used in diagnostic ultrasound techniques, e.g., in ophthalmology where most scanning probes use frequencies from 10 MHz to 20 MHz. Therefore, results of ultrasonic investigation of pure P(VDF-TrFE) and its composites with BPZT at 10 MHz are of peculiar importance. In this work ultrasonic anomalies, related to the ferroelectric phase transitions in the materials under investigation, are discussed. Results of dielectric and differential scanning calorimetry (DSC) investigations of these new P(VDF-TrFE)/BPZT composites are also presented.

However, the aforementioned polymer matrix distinguishes above other ferroelectric materials by its negative piezoelectricity, i.e. a contraction of the material upon an electric field in the direction of the polarization [25, 26]. I. Katsouras et al. proposed a new model in addition to the previous contradictory models [25, 27-29], in which the unusual negative piezoelectric coefficient is explained by electromechanically coupled contractions of crystalline lamellae and amorphous parts. Therefore, figuring out a single model for improvement of electromechanical properties of PVDF and P(VDF-TrFE) based composites is complicated by the opposite signs of piezoelectric coefficients of the polymer matrix with regard to the coefficients of ceramic fillers. Hence, the question is still open and requires more elucidation.

Carbon nanotubes (CNT) are perfect fillers to reinforce mechanical properties or tune electrical properties of polymer materials due to their large Young's modulus of elasticity (1000 MPa) and high electrical conductivity, respectively [30-32]. A small addition of the conductive fillers can increase the sensing capability of the polymer based composites as it has been reported elsewhere [30, 31]. Therefore, CNT has been chosen as organic fillers in the nanocomposites under the study.

Meanwhile, several groups have reported on the effect of annealing and thermal cycling on properties of P(VDF-TrFE) [33-38]. This makes interesting to carry out investigations of the polymer based composites with various compositions of fillers [7]. Therefore, an important part of the study is to report on detailed investigations of the effect of thermal cycling and annealing on ferroelectric phase transition in P(VDF-TrFE) based composites and to compare results obtained by ultrasonic, dielectric and calorimetric measurements of the same composite samples.

For a non-ferroelectric polymer matrix a pure polydimethylsiloxane (PDMS) has been chosen. It is a good electrical insulator with the lowest temperature of vitrification (T_g= 148 K) among polymers [39], nevertheless, it can be doped, for example, with conducting fillers to become electrically

conducting [40, 41]. Among other nanofillers (like carbon nanotubes, carbon black etc.) which are often used for polymer composite preparation, ZnO nanoparticles and nanorods are very interesting due to their unique semiconducting, photoconducting and piezoelectric properties [42-44]. Both ZnO nanomaterials [45-48] and PDMS [39, 49, 50] attract much attention duo to their high potential of various electronic application, however little has been published about the mechanical and dielectric properties of PDMS composites filled with ZnO nanoparticles. Additional purpose of the work was to study the influence of ZnO nanoparticles on the mechanical and dielectric properties of PDMS in a wide temperature range. Hence, analysing properties of the composite by two experimental techniques can provide better understanding of relaxation processes in nanocomposites of PDMS/ZnO.

1.1 Aim of the work

For this research the following purposes were addressed:

- To characterize the composites in order to understand the influence of electroactive ceramic powders on the electromechanical properties of the P(VDF-TrFE) copolymer based composites.
- To discuss ultrasonic and dielectric anomalies, related to the ferroelectric phase transitions and other processes characteristic to the ferroelectric polymer based nanocomposites.
- To investigate the impact of conductive organic fillers on the dielectric and the mechanical properties of the ferroelectric composites.
- To perform detailed investigations of the effect of thermal cycling and annealing on ferroelectric phase transition in P(VDF-TrFE) based composites and to compare results obtained by ultrasonic, dielectric and calorimetric measurements of the same composite samples.
- To study the influence of ZnO nanoparticles on the mechanical and dielectric properties of PDMS in a wide temperature range.
- To compare and contrast impact of organic and inorganic fillers on the properties and functionality of the polymer based nanocomposites.

1.2 Scientific novelty

- For the first time results of temperature dependences of ultrasonic wave velocity and attenuation in P(VDF-TrFE) composites with BPZT were presented.
- A large thermal hysteresis, typical for the first order ferroelectric phase transition, was observed in both temperature dependences of ultrasonic velocity and piezovoltage in the investigated composites.
- Dielectric properties and ferroelectric characteristics of P(VDF-TrFE) based composites are presented and explained in frames of the Lichtenecker's effective medium approximation model.
- For the first time a detailed investigation of the effect of thermal cycling and annealing in P(VDF-TrFE) based composites obtained by ultrasonic measurements is presented.
- At the first time the frequency dependence of the piezoelectric coefficients of piezoelectric polymers was demonstrated.
- Thermally stimulated discharge current measurements of the P(VDF-TrFE)/CNT composites, combined with ultrasonic measurements, revealed a strong dependence of the TSDC current's electret component on the presence of CNT nanoparticles.
- For the first time mechanical and dielectric properties of PDMS composites filled with ZnO nanoparticles are presented.
- Existence of the dielectric hysteresis between cooling and heating cycles and its strong dependence on the concentration of ZnO nanoparticles is shown.

1.3 Statements presented for defence

As a part of this study, the investigation included some research hypotheses:

- In composites of piezoelectric polymer (PVDF-TrFE) with inorganic piezoelectric BPZT particles the dielectric, ultrasonic and piezoelectric properties are determined not only by simple influence of components calculated by mixing rule of Lichtenecker's approximation model but also by change of morphology, thermal treatment, and of the glass-crystalline (ferroelectric- paraelectric) state of host polymer matrix which is modified by the BPZT.
- Both the Curie and melting temperatures of P(VDF-TrFE)/BPZT decrease with the addition the BPZT fillers.
- In composites of (PVDF-TrFE) polymer with small amount of organic CNTs the dielectric and mechanical properties depend not only on the increased conductivity of composite determined by large conductivity of CNT, but also by CNTs acting as nucleation centers for a subsequent growth of spherulites. Such change of conformation in glass-crystalline-amorphous polymer matrix results in the change of the loss maxima temperature anomalies related to the glass or ferroelectric- paraelectric transition.
- In composites of non-piezoelectric PDMS with ZnO nanoinclusions the temperature dependent dielectric and mechanical relaxation anomalies are dependent on ZnO particles acting as nucleation centers in glass-crystalline state, or scattering centers in amorphous high temperature state of PDMS. Room temperature increase of ultrasonic attenuation in the strongly doped PDMS/ZnO composites is due to increased scattering centers for ultrasonic wave.

1.4 List of publications included into the thesis

1. **J. Belovickis**, V. Samulionis, J. Banys, M. Silibin, A. Solnyshkin, K. Nekludov, A. Sysa. Effect of Thermal Cycling on Ferroelectric Phase Transition of PVDF-TrFE Based Composites as Investigated by Ultrasonic Spectroscopy, Ferroelectrics, 512, pp. 65- 70 (2017).
2. **J. Belovickis**, V. Samulionis, J. Banys, M. Silibin, A. Solnyshkin, Y. Shilyaeva, K. Nekludov, S. Gavrilov, V. Rubanik Jr., V. Rubanik, V.V. Shvartsman. Ultrasonic spectroscopy of copolymer based P(VDF-TrFE) composites with fillers on lead zirconate titanate basis, Polymer Testing, 53, pp. 211- 216 (2016).
3. M. Silibin, **J. Belovickis**, S. Svirskas, M. Ivanov, J. Banys, A. Solnyshkin, S. Gavrilov, O. Varenyk, A. Pusenkova, N. Morozovsky, V. Shvartsman, A. Morozovska. Polarization reversal in organic-inorganic ferroelectric composites: modeling and experiment. Appl. Phys. Lett., 107, 142907 (2015).
4. **J. Belovickis**, J. Macutkevic, S. Svirskas, V. Samulionis, J. Banys, O. Shenderova, and V. Borjanovic. Ultrasonic and dielectric relaxations in PDMS/ZnO nanocomposite. Phys. Status Solidi B, 252, 2778–2783 (2015).
5. **J. Belovickis**, J. Macutkevic, Š. Svirskas, V. Samulionis, J. Banys, O. Shenderova, V. Borjanovic. Dielectric spectroscopy of polymer based PDMS nanocomposites with ZnO nanoparticles. Ferroelectrics, 479, 82-89 (2015).

1.5 Other papers

6. I. Anusca, S. Balciunas, P. Gemeiner, Š. Svirskas, M. Sanlialp, G. Lackner, C. Fettkenhauer, **J. Belovickis**, V. Samulionis, M. Ivanov, B. Dkhil, J. Banys, V. V. Shvartsman and D. C. Lupascu. Dielectric Response: Answer to Many Questions in the Methylammonium Lead Halide Solar Cell Absorbers. Adv. Energy Mater., **7**, 1700600 (2017).
7. **J. Belovickis**, A. Kurylenko, V. Murashko. Effect of open ultraviolet germicidal irradiation lamps on functionality of excimer lasers used in cornea surgery - Brief report. International Journal of Ophthalmology, 10(9), 1474-1476 (2017).
8. V. Samulionis, J. Macutkevic, J. Banys, **J. Belovickis** and O. Shenderova. Ultrasonic and dielectric studies of polymer PDMS composites with ZnO and onion-like carbons nanoinclusions. IOP Conf. Series: Materials Science and Engineering, 87, 012010 (2015).
9. V. Samulionis, J. Macutkevic, J. Banys, **J. Belovickis**. Ultrasonic studies of onion-like carbons/polydimethylsiloxane composites. 2014 IEEE IUS, 1986-1987 (2014).

1.6 Conference presentations

1.6.1 Oral presentations

1. **J. Belovickis**, V. Samulionis, M. Ivanov, Š. Svirskas, J. Banys, M.V. Silibin, V. V. Shvartsman, S. Lanceros-Mendez, Dielectric, ferroelectric and ultrasonic investigation of polymer based P(VDF-TrFE) composites, 5th SEMINAR on Properties of ferroelectric and superionic systems, Uzhorod (26-27 October 2015).

2. **J. Belovickis**, V. Samulionis, Š. Svirskas, M. Ivanov, J. Banys, M.V. Silibin, V. V. Shvartsman, S. Lanceros-Mendez, Ferroelectric and ultrasonic studies on polymer based P(VDF-TrFE) composites with PZT, BTO and CFO inclusions, Joint The 5th International Workshop on Smart Materials & Structures (5th SM&S) and International Meeting on Materials for Electronic Applications IMMEA-2015 Marrakech (9-11 September 2015).
3. **J. Belovickis**, Š. Svirskas, M. Ivanov, V. Samulionis, J. Banys, M.V. Silibin, A.V. Solnyshkin, S. A. Gavrilov and A. A. Dronov, Ultrasonic and dielectric spectroscopy of polymer based PVDF-TrFE composites with PZT fillers, in: The 13th European Meeting on Ferroelectricity (EMF 2015), Porto (28 June - 3 July 2015).
4. **J. Belovickis**, Š. Svirskas, M. Ivanov, V. Samulionis, J. Banys, M. V. Silibin, A.V. Solnyshkin, S. A. Gavrilov and V. V. Shvartsman, Investigation of Polymer Based P(VDF-TrFE) Composites with Inorganic Fillers by Means of Dielectric Spectroscopy, in: ISAF-ISIF-PFM 2015, Singapore (24-27 May 2015).

1.6.2 Poster presentations

5. **J. Belovickis**, V. Samulionis J. Banys, M. Silibin, Effect of $LiNbO_3$ Nanofillers on Dielectric and Ferroeletric Properties of P(VDF-TrFE) Copolymer Based Composites, in: 42st Lithuanian National Conference on Physics, Vilnius University, Vilnius (4- 6 October 2017).

6. **J. Belovickis**, V. Samulionis, J. Banys, M. Silibin, A.V. Solnyshkin and A. Sysa, Impact of CNT on mechanical properties of ferroelectric polymer based composite, 4th International Scientific Conference on Modern Problems of Mechanics, Kyiv, Ukraine (28- 30 August, 2017).
7. **J. Belovickis**, V. Samulionis, J. Banys, M. Silibin, A.V. Solnyshkin and A. Sysa, Effect of Thermal Cycling On Ferroelectric Phase Transition Of PVDF-TrFe Based Composites As Investigated By Ultrasonic Spectroscopy, 13th Russia/CIS/Baltic/Japan Symposium on Ferroelectricity (RCBJSF) and International Workshop on Relaxor Ferroelectrics 2016 (IWRF), Matsue, Japan (19 – 23 June, 2016).
8. **J. Belovickis**, Š. Svirskas, V. Samulionis, M. Ivanov, J. Banys, M.V. Silibin, S. A. Gavrilov, K. N. Nekludov, A.V. Solnyshkin, V. V. Shvartsman, Investigation of dielectric and ultrasonic behavior of PVDF based polymer composites with ferroelectric fillers, Functional Materials and Nanotechnologies (FM&NT-2015), Vilnius (5-8 October 2015).
9. V. Samulionis, J. Macutkevic, J. Banys, **J. Belovickis**, O. Shenderova, Ultrasonic studies of Polydimethysiloxane based nanocomposites, in: 41st Lithuanian National Conference on Physics, Vilnius University, Vilnius (17- 19 June 2015).
10. **J. Belovickis**, J. Macutkevic, Š. Svirskas, V. Samulionis, J. Banys, O. Shenderova, Ultrasonic Wave Propagation in PDMS with ZnO nanoparticles, in: International Symposium RCBJSF – 2014 - FM&NT, Riga (29 September- 2 October 2014).
11. **J. Belovickis**, J. Macutkevic, Š. Svirskas, V. Samulionis, J. Banys, O. Shenderova, Dielectric spectroscopy of polymer based PDMS nanocomposites with ZnO nanoparticles. European Conference on Application of Polar Dielectrics 2014, Vilnius (7- 11 July 2014).

1.6.3 Other presentations based on the results

12. **J. Belovickis**, M. Ivanov, Š. Svirskas, J. Banys, M. Silibin, A.V. Solnyshkin and V. V. Shvartsman, Dielectric and Ferroelectric Investigation of P(VDF-TrFE)-based Composites, 13th Russia/CIS/Baltic/Japan Symposium on Ferroelectricity (RCBJSF) and International Workshop on Relaxor Ferroelectrics 2016 (IWRF), Matsue, Japan (19 – 23 June, 2016).
13. V. Samulionis, **J. Belovickis**, J. Banys, Š. Svirskas, M. Ivanov, M.V. Silibin, S. Lanceros-Mendez, Effect of CFO and PZT fillers on Dielectric and Ultrasonic Properties of P(VDF-TrFE) Copolymer Based Composites, 35th Symposium on Dynamical Properties of Solids, Freising (13- 17 September 2015).
14. V. Samulionis, J. Macutkevic, J. Banys, **J. Belovickis**, O. Shenderova, Ultrasonic and dielectric studies of polymer PDMS composites with ZnO and onion-like carbons nanoinclusions, in: 2015 Global Conference on Polymer and Composite Materials, Beijing (20- 23 May 2015).
15. V. Samulionis, J. Macutkevic, J. Banys, **J. Belovickis**, O. Shenderova and V. Borjanovic, Ultrasonic studies of onion-like carbons/polydimethysiloxane composites, in: 2014 International Ultrasonics Symposium, Chicago, Illinois (3- 6 September 2014).

1.7 Author‘s contribution

The student conducted the majority of the experiments independently, made substantial contributions to the conception and the design, acquisition, analysis and interpretation of the data used in the aforementioned articles and presentations.

2 Overview

In this chapter various types of composites and its fillers are described. In addition, its relevant properties are presented and overviewed more detailed.

2.1 Nanocomposites

Nanocomposites are widely used in structural, electronic, biological, medicinal and other applied sectors [51]. Any composite consists at least of two major components, i.e. matrix and reinforcement fillers. If the composite contains constituents of nanometer scale, then it is referred to as "nanocomposite". In the case of polymeric nanocomposites polymers act as matrices for the incorporation of filler materials. All composites are known to be interesting multiphase materials for their optional combination of components with different properties. Depending on the physical property to be improved, different filler materials are used in the preparation of polymeric nanocomposites. In such way various reinforcements of material are possible, i.e. mechanical strength, electrical conductivity, chemical stability, temperature and environmental stability. The miniaturization of the electronic devices is mostly due to the development of such novel functional nanocomposites. Nanocomposites have given a significant contribution to the development of various advanced branches of nanotechnology [51, 52].

2.2 Types of polymers used in nanocomposites

In Greek *Poly* means "many" and *mer* means "parts". Polymers are made of small units, monomers, joined in long chains by forming chemically strong

covalent bonds between atoms. Depending on the use in electronics polymers can be divided into two main types by its composition, i.e. organic and non-organic compounds. Organic polymers are chemically based on carbon, hydrogen, and other non-metallic elements (O, N, and Si) [51]. Furthermore, they consist of large chain-like molecular structures with a backbone of carbon atoms. Some of the commonly used polymers are polypropylene (PP), poly(vinylidene chloride)(PVDF), poly(dimethylsiloxane) (PDMS), polycarbonate (PC) and silicone rubber [52]. Their mechanical characteristics are generally different to metallic and ceramic materials, i.e. they are not as stiff nor as strong as the aforementioned materials. Due to low densities many of the polymers are extremely ductile and pliable (i.e. plastic), which means they are easily formed into complex shapes. The main drawback of polymers is their tendency to soften or decompose at higher temperatures. Sometimes low electrical conductivity can also limit their use. Therefore, for a long time polymers have been considered as simple insulators of electrical currents. The breakthrough has been done in the recent 30 years through a simple modification of ordinary organic conjugated polymers [51, 52]. One of the invented types of materials are electrically conducting polymers (ECP) which can combine electrical properties of metals with advantages of ordinary polymers such as lighter weight or resistance to corrosion [53]. Sometimes the materials are referred as the materials of the twenty first century [53]. These polymers have significant intrinsic electronic conductivity along with enhanced electrochemical properties. Unlike inorganic semiconductors this type of polymers is molecular and lacks long range order. Organic polymers can exhibit charge transport and optical properties analogous to crystalline network of semiconductors.

In spite the fact, that these polymers have several disadvantages as poor thermal and chemical stability, low mechanical strength and poor environmental stability, some properties can be improved in order to achieve necessary standards for technological application. These drawbacks can be

easily avoided if nanocomposites are prepared with carbon nanomaterials (CNMs) [51, 52]. Carbon nanomaterials are superior materials of the twenty-first century with unique properties, which are absent in any other material, i.e. high electronic conductivity and mechanical strength, light weight, large surface area, good environmental stability and high corrosion resistance. Unfortunately, CNMs face problems of insolubility and agglomeration in various solvents upon their addition [3, 51]. These drawbacks are very critical in their practical usages. The CNMs are strong in their specific properties, where the conducting polymers are not. Therefore, by combining ECPs and CNMs it appears possible to overcome these drawbacks. The ECP/CNM nanocomposites can possess good mechanical strength and high electronic conductivity combined with good temperature stability.

Polymers may also be classified into polar or non-polar because this feature strongly affects dielectric properties. Non-polar polymers do not contribute to dipole polarization and dielectric properties remain independent in an alternating electric field. The geometry of the polymer chain determines the polarity of material. The resulting dipole moment depends on whether the pendants reinforce or cancel each other. Many fluoropolymers as P(VDF-TrFE) are polar. P(VDF-TrFE) has a high dipole moment of $–CF_2$ unit at every second alternating carbon backbone. The organic- inorganic polymer networks can serve as an origin of relaxation processes in polymers [54].

Another important type of nanocomposites are polymer based composites with piezoceramic fillers, which have been developed principally for sonar and medical ultrasonic imaging technologies [5]. In these applications the transducer is usually interfacing with liquids or soft tissues of body or skin. The advantages over ordinary piezoceramics include better acoustic matching between transducer and medium, electromechanical coupling and higher band width. The transmission of ultrasound from one medium to another and its reflection depends on the “impedance matching”. These properties allow

processing of well-defined ultrasonic pulses and, as a consequence, better imaging resolution.

Depending on the manner in which phase connections are made in composites, physical properties can change by many orders of magnitude. Each phase in a composite can be self-connected in zero, one, two or three dimensions in respect to three perpendicular axes [55]. For diphasic composites ten connectivities can be realized during production. As an example, the connectivity pattern for a 3-0 composite is illustrated in Figure 2.2.1.

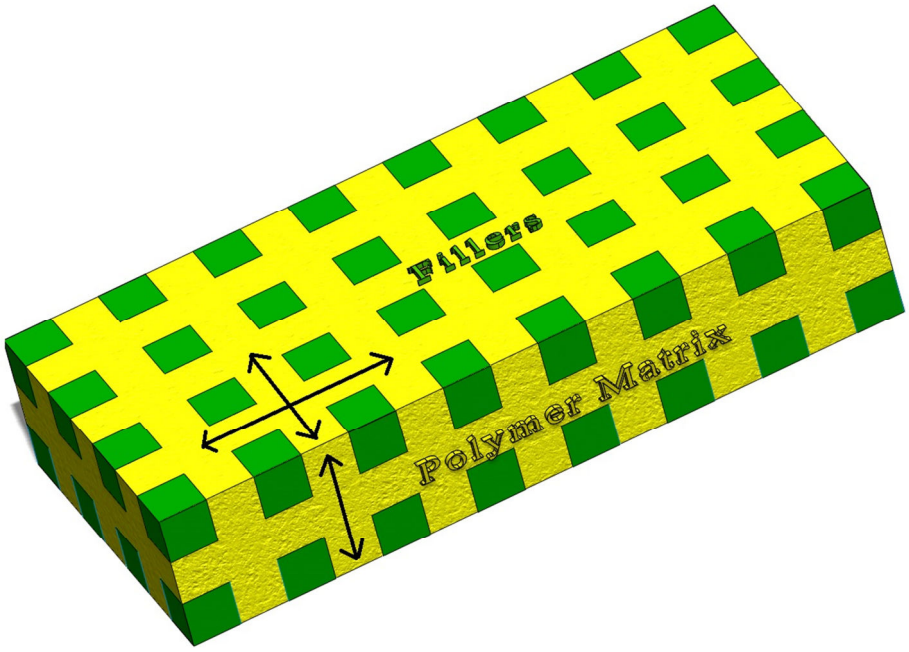

Figure 2.2.1. The connectivity pattern for a 3-0 composite. The green parts represent the fillers in a polymer matrix (yellow). Arrows are used to indicate the connected directions.

The 3-0 connectivity pattern has one phase self-connected in three-dimensional layers, i.e. in the lateral X, Y and Z directions. The other phase, the fillers, is not in contact being separated by the polymer matrix. The major positive advantages of the 0–3 composite is the ease of fabrication [5].

2.3 Semicrystalline polymers

Solid polymers can be distinguished into amorphous and semicrystalline categories. The majority of polymers, the semicrystalline polymers, can show regions of high order. Amorphous solid polymers can be either in the glassy or in the rubbery state with chain cross-linking [4, 52]. It had long been believed that single crystals could not be produced from polymer solutions until the existence of single crystals of 10 nm thick was reported and the perfectly ordered structures of crystals were shown by electron diffraction patterns [56, 57]. On the other hand, various dislocations analogous to those in metals have been found in these polymeric single crystals. The other important concept of statistical disorder or so-called paracrystallinity model was introduced by R. Hosemann in 1950 [56, 58], in which the creep and the recrystallization phenomena are explained by motions of dislocations. These two models still are of importance for polymer morphology combining folded chain molecules and paracrystallinity. Three general explanations for formation of polymer morphology are now accepted, i.e. an irregularly folded molecule in a glassy state, a folded chain in lamellar structure and an extended chain [56].

Crystallization in semicrystalline polymers is followed by separation of unmixed crystals from chain parts near entanglements in the amorphous regions. The crystallites are interspersed with amorphous regions composed of randomly oriented molecules [52]. Different end groups, short chain branches and stereo defects can oppose a transformation into a crystal, but can become accumulated in the amorphous parts of a partially crystalline polymer [4]. Many factors affect the degree of crystallinity of polymers, i.e. chain complexity, tacticity, randomness of copolymers, bulky side groups and thermal history [3, 4, 52]. In other words, the polymer structure affects the crystallinity, i.e. the more regular it is, the easier it will pack crystals.

The process of polymer crystallization is addressed to nucleation and growth of spherical objects or so-called spherulites [3, 4, 52]. The shape of the spherulites may be roughly spherical, consisting of an aggregate of chain-folded crystallites (lamellae) about 10 nm thick that radiate two-dimensionally outward from a single nucleation [3, 4, 52]. The chains in the crystallites are oriented either parallel or perpendicular to the spherulite radius [4]. A simplified structure of a spherulite in amorphous polymer region is illustrated schematically in Figure 2.3.1. The individual chain-folded lamellar crystals (blue lines) are separated by the amorphous material (yellow part), in which tie-chain molecules act as connecting links between adjacent lamellae.

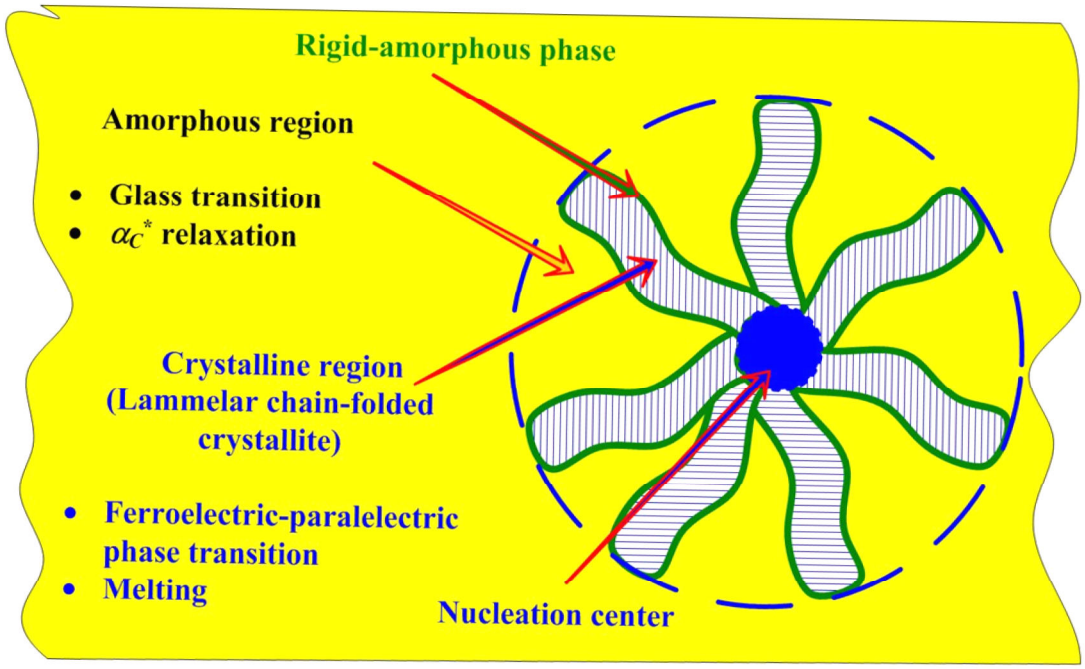

Figure 2.3.1. Schematic representation of polymer structure with specific properties attributed to amorphous and crystalline regions.

The spherulites usually grow with a constant rate up to the point where they start touching each other. The area of contact between spherulites can be planar or bent depending on the nucleation time. As the crystallization of a spherulitic structure approaches its completion, the spherulites begin to

impinge on one another, forming boundaries but maintaining spherical shape. The lamellar crystals start to twist as they extend like ribbons from the center. Spherulites are considered to be the polymer analogue of grains in polycrystalline metals and ceramics. Each spherulite may be composed of many different lamellar crystals with some amorphous material [52]. Their size of spherulites depend on the nucleation density and vary from several 100 nm up to several cm.

Spherulites are optically anisotropic objects, thus it is possibly to observe them by polarized light microscope. The shape, size, number, and distribution of crystallites in the amorphous polymer matrix strongly influences behaviour of the material. The birefringence is caused by stretched polymer chains in the crystallites. Polypropylene, poly(vinyl chloride) and nylon form a spherulitic structure when they crystallize from a melt. Sometimes it is possible to observe the spherulites by the means of ordinary light microscopy (Fig. 2.3.2).

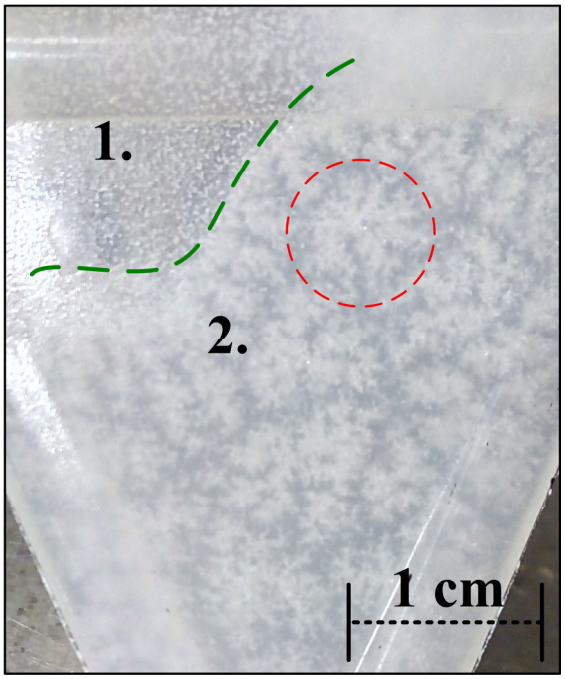

Figure 2.3.2. An example of partly crystallized polypropylene sample. For a better visualisation the green line separates two regions crystallized at different cooling rates (1. and 2.).

The sample of polypropylene consists of two regions crystallized at different cooling rates. The region 1 was formed in a relatively short period of time, about ten minutes. For the region 2 the cooling rate was lower than 0.5 K/min, thus providing appropriate conditions for the formation of the highly crystallized region. For a better visualisation the green line was used to distinguish the two regions. The red line presents a good example of a sprerulite growth from a centre.

Apart from the crystalline and amorphous fractures in semicrystalline polymers, a third fracture, rigid amorphous phase (RAP), may exist [59-62], which was extensively studied during the last twenty years. The RAP is usually attributed to an order-disorder interface located at the boundary of the crystal and the viscoelastic amorphous region (Fig. 2.3.1). The rigid-amorphous phase may originate by cross-linking or from pinning polymer chains on crystallites [59, 61] and does not represent a well-defined phase since the molecular mobility changes continuously between the crystal surface and the remaining melt-like regions. Cross-linking can make the amorphous phase more or less rigid and therefore reduce the phase boundaries. The relaxation of rigid amorphous phase has been reported in many semi-crystalline polymers as well as nanocomposites [62, 63]. It is assumed that each filler particle is covered by the RAP. With a high filler concentration within a nanocomposite the RAP may decrease due to particle agglomeration and disappear for the highest filler concentration [60].

The semicrystalline polymers can experience transitions of glass and ferroelectric-paraelectric phase, melting and so-called alpha crystalline relaxation (α_C^*). Melting of the polymer is due to structures that are only crystalline in parts [4]. It is supposed that in semicrystalline polymers with significant chain mobility inside the crystals the crystalline region melts after the surrounding rigid-amorphous phase, although, it still requires elucidation [59-62, 64]. In several polymers the RAP may even have a separate glass transition

[59]. The rigid-amorphous phase can affect the specific heat between the glass transition of the polymer matrix and the melting region [60]. The temperatures of glass transition and melting are important parameters of semicrystalline polymers, because they define the lower and upper temperature limits for numerous applications.

Depending on the symmetry of the crystalline region the semicrystalline polymers exhibit ferroelectricity, piroelectricity and piezoelectricity [2, 6, 7, 26, 36, 38, 65]. Some dipoles within the RAP cannot be oriented in an external electric field and therefore do not contribute to the polarization and the piezoelectric effect.

2.4 Processes related to semicrystalline polymers

There are several main relaxation processes in amorphous region of polymers which appear with different characteristic relaxation times (τ). These processes may be classified as α, β and γ with no physical meaning but reflecting the order in which these processes appear [3, 4, 66]. Moving from the region of low temperature to higher temperatures, the molecule becomes no longer tightly compressed and the first changes such as the solid-state transitions occur. The free volume increases due to expansion of the polymer matrix. This gives rise for side chain movements followed by localized bond movements as bending and stretching. These movements can be designated as the γ transition. After the free volume increases the whole side chains and localized groups of up to 50 backbone atoms begin to have enough space to rotate about C-C bond and the β transition occurs [3, 60, 66, 67]. As heating continues the chains in the amorphous regions begin to coordinate large scale motions and originate the main structural relaxation, i.e. the segmental α transition. Since the a relaxation is only attributed to amorphous material, in a

100% crystalline material this temperature would coincide with the melting temperature T_m [60, 66]. The α process is usually associated with micro-Brownian motion of the whole chain and a consecutive change of viscosity at a relatively short time scale. In most polymers the process is responsible for the glass transition of polymer matrix [3, 4].

The glass transition temperature is usually defined as a transition from a rubber-like to a solid state and may influence fabrication and processing procedures for polymers and polymer based composites [3, 4, 52, 56, 60, 66-68]. For a typical elastomeric material a shift to higher than the glass transition temperature brings a lower Young's modulus, while a shift to a lower temperature gives a higher value [68].

It is not a true first-order transition in the thermodynamic sense and is sometimes used in an ambiguous sense as it relates to the study of polymer viscoelasticity [68]. The transition occurs continuously in a systematic manner. Although, there is no real phase transition at T_g, or transition from a non-ergodic to an ergodic state, an abrupt change occurs of temperature dependence for volume, density, entropy and elastic constants. Qualitatively, the glass transition region can be interpreted as the onset of long-range, coordinated molecular motion [3]. An appropriate term for the transition temperature might be the temperature at which the storage modulus reaches an arbitrarily assigned value of mechanical storage G' or Young's E' moduli in the order of 10^8 Pa. At the temperature the thermal expansion coefficient undergoes a discontinuity [3, 68]. The T_g may depend on length and rigidity of the polymer chains, degree of crystallinity, pressure and even on the strength and nature of interactions between chains such as the Van der Waals intermolecular bonds. These forces are short in distance and strengthen with decrease of temperature, resulting in freezing of segmental relaxation when the polymer becomes brittle, i.e. the glass transition [3, 4, 51, 52, 56, 60, 66-68]. The glass transition temperature is relatively unaffected at low levels of crosslinking and is only sensitive to very low

molecular weight. The time needed for the chain disentangling increases with the molar mass [4]. The temperature T_g depends on cooling or heating rates, therefore, it is defined to consider the T_g as a segmental relaxation time of 100 sec.

Continued heating drives the semi-crystalline material through a so-called alpha crystalline relaxation (α_C^*) [63, 64, 69]. Sometimes the α_C^* structural relaxation is associated to hindered motions of amorphous phases within the crystalline segments [63, 69] and to a slippage between the crystallites [60, 64]. The relaxation is relatively broad in the frequency window and shifts towards a higher temperature as the frequency increases, therefore, the α_C^* relaxation is called as the size dependent structural relaxations concerning size of crystalline segments [69]. Although, in the case of a thermoset, a highly cross-linked material [3, 4], nothing happens after the glass transition temperature until the polymer degradation appears due the crosslinks preventing the chains from slipping past each other [63, 69]. In thermoplastics, polymers whose Van der Waals bonds may be weakened over and over again upon heating [3, 4] the α_C^* relaxation can be enlarged or decreased by the applied processing conditions or physical aging. At higher temperatures the α_C^* disappears due to melting of the crystalline region [64]. This relaxation is present in many flexible semi-crystalline polymers, including poly(ethlyene) (PE), poly(ethylene oxide) (PEO), isotatic popypropylene (PP) and poly(vinylidene fluoride) (PVDF) [63, 70].

2.5 Ferroelectricity and phase transition dynamics

In the middle of the twentieth century organic polymers as PVDF and its copolymers attracted a lot of scientific attention after it was reported that

ferroelectricity could also occur in organic solids [26]. A material is said to be ferroelectric if it has at least two orientational states in the absence of an external electric field [71, 72]. The temperature of paraelectric-ferroelectric phase transition is called Curie temperature. Below the temperature certain materials have a spontaneous electric polarization that can be reversed by the application of an external electric field. It is important to note, that the structure of the ferroelectric material (crystalline region in the case of ferroelectric polymers) does not change with the change of the direction of polarization. The property is only characteristic in crystals with no center of symmetry. Two classes of ferroelectric crystals are distinguished with respect to the type of structural phase transition occurring at Curie point. The first one is that of displacive phase transition and are described by propagation of polar vector modes, so-called "soft mode" or "optical phonon". With propagation of the soft mode at Curie temperature T_C "freezes" vibrations of atoms and produces a structure of lower symmetry below the T_C. The other class of ferroelectric crystals refers to order-disorder phase transitions, which are described in terms of propagation of scalar modes. Atoms in a previously random material become ordered on specific crystallographic sites, yielding (usually) a larger unit cell [71, 72]. Therefore, below the T_C the probability of finding a particle in one of two positions becomes different from zero. According to Landau's phenomenological model for phase transitions, the structural changes are described by the characteristic phase transition parameter- the order parameter η [71, 72]. If we denote N_1 and N_2 as probabilities to find atoms in positions 1 and 2, then the η can be expressed as:

$$\eta = \frac{N_1 - N_2}{N_1 + N_2} . \qquad (2.5.1)$$

At the phase transition point the value becomes different from zero. The polarization P is the order parameter in case of the proper ferroelectric phase transition. The η may also be considered as the orientation of a molecule [73].

The well-known ferroelectric polymers as PVDF and its copolymer P(VDF-TrFE) are considered to be of order-disorder type [33, 36, 37].

Ferroelectric phase transitions may be also classified by the change of spontaneous polarization on temperature, i.e. how abruptly does the order parameter η appears upon approaching the Curie temperature. If the decrease of η is step-like, the ferroelectric phase transition is attributed to the first order phase transition (Fig. 2.5.1a). At the second order phase transition the η decreases continuously upon approaching the Curie-temperature (Fig. 2.5.1b). The great majority of ferroelectric phase transitions are accompanied by an relatively small jump of the order parameter at $T = T_C$ but with a transformation of the symmetry group, thus relating the phase transition to a special class of first order transitions close to second order ones (Fig. 2.5.1c).

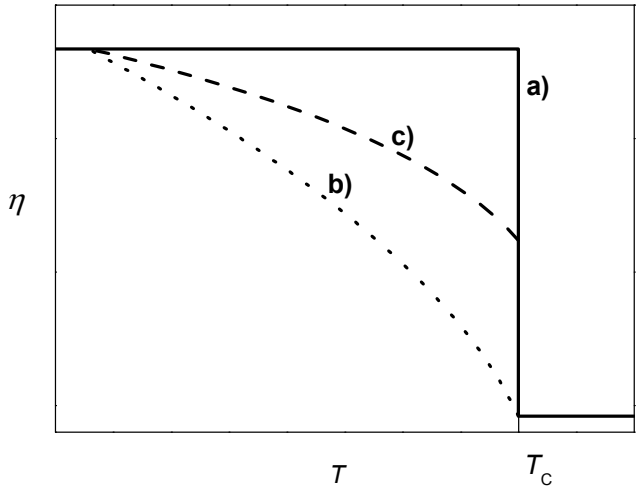

Figure 2.5.1. Temperatures dependence of the order parameter η in case of first, second and first close to second phase transitions.

According to Landau's phenomenological theory a proper ferroelectric phase transition of second order can be expressed through the thermodynamical potential F:

$$F(\sigma,T,\eta,E_2) = F_0(\sigma,T) + \frac{1}{2}\alpha(T-T_C)\cdot\eta^2 + \frac{1}{4}\beta\cdot\eta^4 - a\eta E_2, \quad (2.5.2)$$

where E_2 is a vector component of electric field parallel to the symmetry axis of the crystal, α is parameter achieved from the Devonshire approximation,T and σ are temperature and mechanical stress, relatively. The multiplication coefficient a may be treated as the density of the effective ionic charge in the case when the order parameter corresponds to a displacement of an ion in the unit cell. The coefficient β is positive in the case of second order phase transition. In the case of first phase transition a higher order term with respect to the order parameter must be taken into account as shown in equation (2.5.3):

$$F(\sigma,T,\eta,E_2)=F_0(\sigma,T)+\frac{1}{2}\alpha(T-T_C)\cdot\eta^2+\frac{1}{4}\beta\cdot\eta^4+\frac{1}{6}\gamma\cdot\eta^6-a\eta E_2 \quad , (2.5.3)$$

where γ is a coefficient, which must remain positive in order to have a stable crystal with a non-zero spontaneous polarization.

Let's determine the dependence of a spontaneous polarization as the order parameter (η= P) on the electric field in ferroelectric material in the case of a second order ferroelectric phase transition. In the absence of an external electric field (E_2= 0) the equilibrium value of the order parameter can be found from the condition when the thermodinamical potential has a minimum, therefore the conditions (2.5.4) must be fulfilled for equation (2.5.3):

$$\frac{\partial F(\sigma,T,P)}{\partial P}=0 \quad \text{and} \quad \frac{\partial^2 F(\sigma,T,P)}{\partial P^2}>0 \quad . \qquad (2.5.4)$$

After differentiating F with respect to P we obtain:

$$\frac{\partial F(P)}{\partial P}=\alpha(T-T_C)\cdot P+\beta\cdot P^3 \quad \text{and} \quad \frac{\partial^2 F(P)}{\partial^2 P}>\alpha(T-T_C)+3\beta\cdot P^2 \qquad (2.5.5)$$

It becomes clear from Eq. (2.5.4) and Eq. (2.5.5) that P changes continuously below T_C as it is shown in Fig. 2.5.1b and is expressed as:

$$P = \pm\sqrt{\frac{\alpha(T - T_C)}{\beta}} \quad . \tag{2.5.6}$$

By differentiating F with respect to P we obtain the dependence of the polarization as a function of the electric field:

$$E = \alpha(T - T_C)\cdot P + \beta \cdot P^3 \quad . \tag{2.5.7}$$

In a case of an external electric field the polarization is shown in Figure 2.5.2 for different temperatures around T_C.

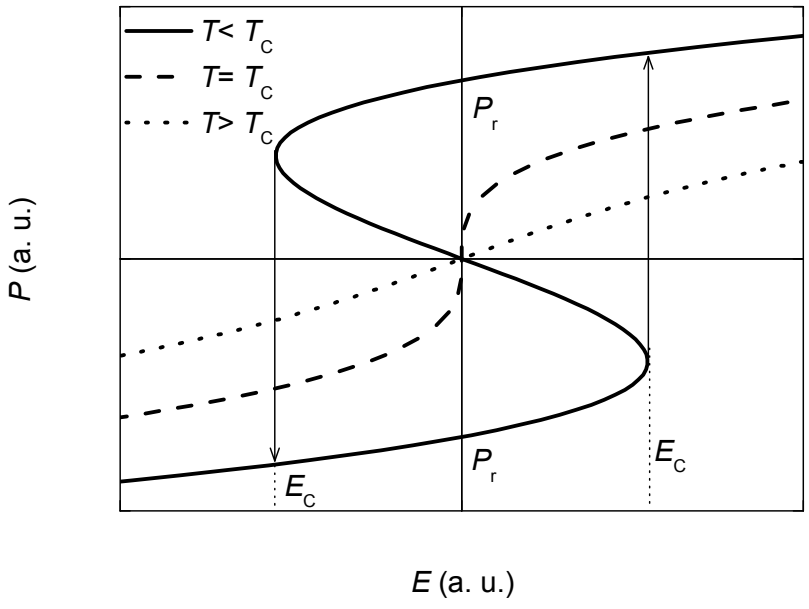

Figure 2.5.2. Theretical dependence of spontaneous polarization on external electric field at different temperatures around the T_C

Near T_C the potential barrier, which separates states with different polarization directions is so low, that even a low electric field can remove the barrier. The switching of polarization in electric field is associated with an occurrence of a phase transition in the crystal. In the case $T < T_C$ the

polarization dependence corresponds to an unstable condition where a jump of a polarization occurs. The value of polarization in absence of external electric field is called a remanent polarization P_r and the electric field necessary to change the direction of polarization is called a coercive electric field E_C (Fig. 2.5.2). The ferroelectric polymers shows a $P(E)$ hysteresis under special conditions by application of a poling field higher than E_C at a temperature below T_C.

Two possible directions of spontaneous polarization mean that ferroelectric crystals split into homogeneous spontaneous polarization fields - ferroelectric domains with different directions of polar axis. In fact, all anisotropic properties of ferroelectric crystals, measured in alternating electric field, depend on the dynamics of domain walls. The movement of domain walls causes dielectric relaxation dispersion in the radio frequency range. In case when the electric field frequency is low - ferroelectric hysteresis.

From the relation of dielectric susceptibility to the polarization, $X_{22} = \partial P_2 / \partial E_2 = \partial(\partial F / \partial E_2) / \partial E_2 = a \cdot \partial \eta / \partial E_2$, it becomes possible to find the dependence of dielectric constant on temperature from Eq. (2.5.2):

$$\frac{\partial \eta}{\partial E_2} = \frac{a}{\alpha(T - T_C) + 3\beta\eta}, \tag{2.5.8}$$

$$\frac{a}{\alpha(T - T_C)}\bigg| T > T_C \quad \text{and} \quad \frac{a}{2\alpha(T - T_C)}\bigg| T < T_C . \tag{2.5.9}$$

Assuming that $\varepsilon_{22} \approx 1 + X_{22} \approx X_{22}$, we obtain:

$$\varepsilon_{22} = \frac{a^2}{\alpha(T - T_C)}\bigg| T > T_C \quad \text{and} \quad \varepsilon_{22} = \frac{a^2}{2\alpha(T - T_C)}\bigg| T < T_C . \tag{2.5.10}$$

It can be seen that the dielectric constant of a crystal along the polar axis depends on temperature according to the Curie-Weiss law at $T > T_C$. Near the temperature of the phase transition the dielectric constant may increase significantly due to increase of induced polarization [54, 71, 72].

It is also possible to find temperature dependence of piezoelectric strain coefficient near T_C. Deformation of the crystal may be expressed through the thermodynamical potential as:

$$S_{xx} = -\frac{\partial F}{\partial \sigma_{xx}} = r \cdot \eta^2 \quad , \tag{2.5.11}$$

where

$$\partial F = \partial F_0 + \frac{1}{2}\alpha(T - T_c)\eta^2 + \frac{1}{4}\beta\eta^4 - a\eta E_2 - r\sigma_{xx} - g\sigma_{xx} - c\eta E_x\sigma_{xy} \quad . \tag{2.5.12}$$

Here r and c are constants and g_1 is electrostriction coefficient. If no strain at $T < T_C$ is applied to the crystal ($\sigma = 0$) and E_2 is 0, according to Eq. (2.5.2) the order parameter is:

$$\eta^2 = \frac{\alpha(T - T_c)}{\beta} \quad . \tag{2.5.13}$$

When $E_2 \neq 0$:

$$\frac{\partial \eta}{\partial E_y} = \frac{a}{\alpha(T - T_c) + 3\beta\eta_0^2} \tag{2.5.14}$$

Assuming the equilibrium value of η as η_0- $\Delta\eta$, where $\Delta\eta$ is a change of the order parameter and η_0 is the equilibrium value of η at $E_2 = 0$. Having in mind that for converse piezoelectric effect $S_{ij} = d_{kij}.E_k$, where d_{kij} is a piezoelectric strain constant we obtain:

$$d_{12} = \frac{ra}{\beta^{1/2}}\left[\alpha(T - T_c)\right]^{-1/2} \quad . \tag{2.5.15}$$

2.6 Dynamics of relaxational polarization

Relaxational polarization is characteristic for order-disorder crystals and, as a consequence, for ferroelectric semicrystalline polymers of order-

disorder type at frequencies below 10^{12} Hz. After the frequency electronic and atomic polarizations occur. This type of polarization is due to permanent dipoles or dipoles induced by an electric field. If the electric field is alternating, the electric displacement field lags behind the electric field and relative permittivity can be expressed in a complex form:

$$\varepsilon^* = \varepsilon' - j\varepsilon'' . \qquad (2.6.1)$$

Polarizability of dipoles is frequency dependent and the dielectric loss ε'' appears due to inability of polarization process of a polymeric system to follow the change of the oscillating applied electric field resulting in heat dissipation. At lower frequencies the dipoles have enough time to align with respect to the field before it changes its direction but if the relaxation time of dipoles in a polymeric system is smaller than the rate of oscillating electric field, no minimum loss is expected. The maximum of ε'' occurs when the frequency of applied electric field is at resonant with the oscillating system. When the frequency of the field increases the previously oscillating dipoles remain freezed with no contribution to the dielectric constant.

A model relating dielectric properties with the relaxation time is the Debye model. It is applied for analysis of relaxational behaviour involving damping of electric field in the system and is valid for a system with a single relaxation time:

$$\varepsilon^*(\omega) = \varepsilon_\infty + \frac{\Delta\varepsilon}{1 + i\omega\tau} , \qquad (2.6.2)$$

where ε_∞ is a contribution from all higher frequency processes, like electronic and ionic contribution, ω is the cyclic frequency, τ is the relaxation time of dipoles to return to the original position and $\Delta\varepsilon$ is the relaxation strength. The relaxation strength corresponds to the contribution of polarization mechanism to the static dielectric permittivity ε_0. The higher ε_∞ is, the higher is the ε''.

Many polymers are highly entangled between chains, thus the dipole relaxation time in different environments will vary due to the different mobility. Meanwhile dipolar interaction between each other can affect the whole polarization. Therefore, the whole polarization will be a sum of many polarization processes with different relaxation times. In this case frequency dependences of dielectric permittivity may be analysed employing Cole-Cole formalism (Eq. 2.6.3), Cole-Davidson (Eq. 2.6.4) or Havriliak- Nagami (Eq. 2.6.5) formalisms [54, 74, 75]:

$$\varepsilon(\omega) = \varepsilon_{\infty} + \frac{\Delta\varepsilon}{1+(i\omega\tau)^{1-\alpha}}, \tag{2.6.3}$$

$$\varepsilon(\omega) = \varepsilon_{\infty} + \frac{\Delta\varepsilon}{\left[1+i\omega\tau\right]^{\gamma}}, \tag{2.6.4}$$

$$\varepsilon(\omega) = \varepsilon_{\infty} + \frac{\Delta\varepsilon}{\left[1+(i\omega\tau)^{1-\alpha}\right]^{\gamma}}. \tag{2.6.5}$$

The parameter α defines the width of the distribution of relaxation times. When extending Eq. (2.6.3) to Havriliak- Negami formalism the mean relaxation time τ_{AV} (or the most probable relaxation time) must be taken into account:

$$\left\langle \ln \tau_{AV} \right\rangle = \ln \tau + \frac{\Psi(\gamma) + Eu}{1-\alpha}, \tag{2.6.6}$$

where Eu is Euler constant ($Eu \approx 0.5772$) and $\Psi(\gamma)$ is the Digamma function of γ coefficient which describes the asymmetry of spectra. Both α and γ vary between 0 and 1. The asymmetric function of Cole and Davidson was derived after a superposition of Cole-Cole functions and the Havriliak-Negami function was derived after a superposition of Cole-Cole and Cole-Davidson functions [74, 76].

The temperature dependence of the relaxation time may be treated as a property of polymer segmental motion due to the temperature dependent

segmental friction. Therefore, the temperature dependence of relaxation times may be also analysed in terms of an analogous model. Many experiments led to the Arrhenius law (Eq. 2.6.7) and the empirical Vogel-Fulcher (VF) law (Eq. 2.6.8):

$$\tau = \tau_0 e \frac{E_{Ar}}{k_B T} \tag{2.6.7}$$

and

$$\tau = \tau_0 e \frac{E_{VF}}{k_B (T - T_{VF})} , \tag{2.6.8}$$

where k_B is the Boltzmann constant, τ_0 is the attempt relaxation time approached with $T \rightarrow \infty$, and T_{VF} is the onset temperature of a process as cooling rate becomes infinitely slow. The apparent activation energy used in the VF equation E_{VF} relates to the activation energy used in the Arrhenius law E_{Ar}, as $E_{VF} = E_{Ar}(1- T/T_g)$, sometimes denoting an elastic shear energy around the local relaxation due to the change of an activation volume [77]. Arrhenius formalism typically is used to describe materials with almost independently relaxing dipoles. The Vogel-Fulcher formalism was originally developed for a temperature dependence of glass viscosity [78, 79] and describes behaviour of disordered materials as dipolar glass or amorphous materials. As we see, the means of dielectric spectroscopy are very important in investigation of polymer based materials. The function of frequency and temperature can be used to elucidate intermolecular cooperative motions and hindered dielectric rotations. If a polymer contains some fillers the interfacial interaction can restrict the polymer mobility. The dielectric loss maxima can provide information about various relaxation mechanisms upon the change of temperature and frequency. When temperature is increased polar groups are more free to orient with regard to the changing electric field and after ε^* reduces due to a hindering thermal motion. The free space in the polymer matrix is necessary for the segmental

movement. In order to compare the temperature behaviour of different materials the frequency should be fixed.

Dielectric spectroscopy can also provide some useful information on the ratio of the rigid amorphous phase to the amorphous part in semicrystalline polymers. A change in loss modulus value compared to polymer can reveal a change in content of mobile amorphous phase due to a change of the amount of rigid amorphous phase (RAP), reduces chain mobility [62, 67]. The RAP progressively mobilizes with increasing temperature and therefore can gradually loose its character as a separate phase.

The results of frequency and temperature behaviour can also confirm the presence of the α_c relaxation which appears at higher temperature than the glass transition temperature. As an example Figure 2.6.1 presents a temperature dependence of the real and imaginary parts of the complex dielectric permittivity of PVDF in a wide temperature range at various frequencies.

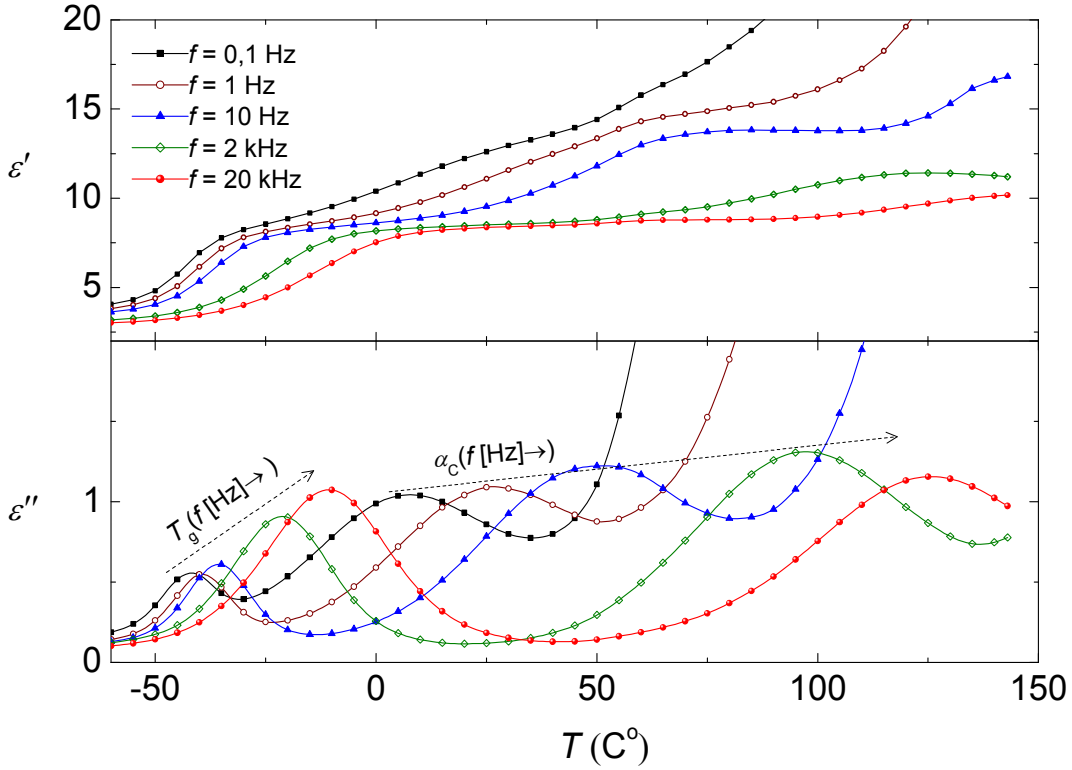

Figure 2.6.1. Temperature dependence of the complex dielectric permittivity for pure PVDF on heating at different frequencies (0.1 Hz- 20 kHz).

It is clearly seen from the temperature behaviour of the imaginary part that all curves have two expressed anomalies. The first one at low temperature is attributed to the glass transition (T_g) of PVDF and the second one is usually attributed to the α_c relaxation. The α_c relaxation varies greatly on the frequency scale. The frequency dependence of losses can be schematically represented as in the following Figure 2.6.2.

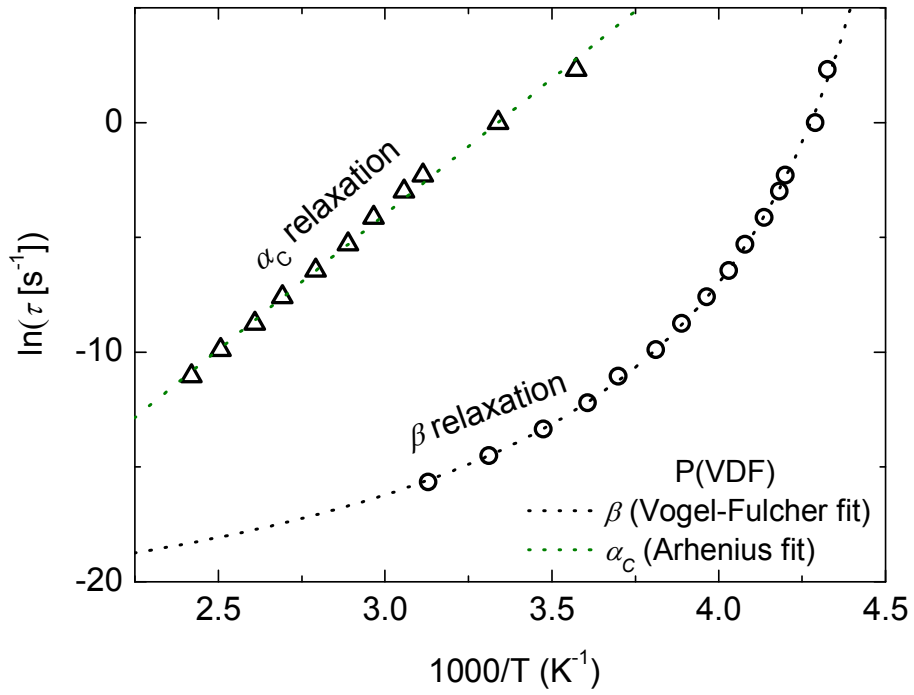

Figure 2.6.2. Temperature dependence of the relaxation time of the dielectric loss maximum for pure PVDF. Lines are the best fit according to the Arrhenius and Vogel–Fulcher law.

The frequency behaviour of the α_c relaxation can be best analysed in terms of the Arrhenius model and the β relaxation is well-described by the Vogel- Fulcher equation. The exponential shift of α_c relaxation can be logically explained by absence of the freezing temperature as in the case of the β

relaxation (T_g). The α_c relaxation is present until the crystalline part starts to melt.

2.7 Ultrasonic spectroscopy

In polymers, rubbers and plastics sound absorption depends strongly on the composition and structure of the material. The determining contribution to the absorption of sound is made by relaxation processes with a wide spectrum of relaxation times. Upon a propagation of ultrasonic waves coils of molecules are continuously folded and unfolded. There are two principal causes of ultrasonic wave attenuation are scattering and absorption [4, 80]. In non-homogeneous materials (polycrystalline aggregates) three scattering regimes are defined by the ratio of mean grain size to the wavelength λ. When $\lambda >> \pi \cdot a$, where a is a mean particle width, the scattering regime is called Rayleigh scattering is proportional to f^4. In the stochastic phase scattering regime ($\lambda \approx \pi \cdot a$) the ultrasonic attenuation is proportional to f^2. For the diffusion scattering regime ($\lambda << \pi \cdot a$) α does not depend on the frequency:

$$\alpha = \frac{c_d}{a} \qquad (2.7.1)$$

where c_d represents geometric factors as density and elastic anisotropy factors [80].

It is convenient to use acoustic waves of higher than 10^6 Hz frequency for the dynamics of elastic and electromechanical material properties. The ultrasonic and hypersonic waves are coherent phonons of known frequency, phase and wave number which strongly interact with the crystal thermal phonons. The interaction characteristics include the altered wave velocity and

attenuation, which provides information about the dynamics of phase transitions. The method of ultrasound and crystalline region interaction allows exploration of lattice dynamics in the frequencies below 10^9 Hz in crystals related to ferroelectrics. In case of Brillouin scattering experiments the frequency range does not exceed 10^{10} Hz (hypersound). Acoustic wave induced relaxations cause instantaneous long-range changes of the order parameter. As a consequence, an acoustic wave dispersion and attenuation takes place here.

Acoustic wave attenuation and velocity are dependent on the wave vector orientation with respect to the crystallographic axes. The velocity and acoustic wave attenuation vary anomalously at the Curie point. An ultrasound modulation of phonon frequency and distribution causes wave attenuation and dispersion of the wave velocity.

If a plane wave of a moderate amplitude and a cyclic frequency $\omega = 2\pi f$ propagates within a crystal, the mechanical stress σ, the strain S and the order parameter η vary as:

$$\eta(\boldsymbol{r},t) = \eta_0 \cdot e^{i(\omega t - \boldsymbol{k}\boldsymbol{r})}, \tag{2.7.2}$$

$$\sigma(\boldsymbol{r},t) = \sigma_0 \cdot e^{i(\omega t - \boldsymbol{k}\boldsymbol{r})} \tag{2.7.3}$$

and

$$S(\boldsymbol{r},t) = S_0 \cdot e^{i(\omega t - \boldsymbol{k}\boldsymbol{r})}. \tag{2.7.4}$$

Here t is a time variable, $\boldsymbol{r}$ is a position vector identifying a location in space in Cartesian coordinates and $\boldsymbol{k}$ is a complex wave vector due to the acoustic wave attenuation:

$$\boldsymbol{k} = \frac{\omega}{V^*} = \frac{\omega}{V} - i\alpha. \tag{2.7.5}$$

Here V^* is the acoustic wave velocity expressed by the complex frequency dependent elastic constant c^* and density ρ:

$$V^* = \sqrt{\frac{c^*}{\rho}}\,. \tag{2.7.6}$$

From Eq. (2.7.5) and Eq. (2.7.6) follows:

$$\frac{\omega}{V} - i\alpha = \omega\sqrt{\frac{\rho}{c^*}}\,. \tag{2.7.7}$$

Let's assume that τ is the soft mode relaxation time. For temperatures close to but below the phase transition temperature T_C in ferroelectric materials, ω can be compared to the inverse relaxation time of polarization, so that dispersion can affect the value of $c^*(\omega)$ [22]. Therefore, from the Landau-Khalatnikov theory if the acoustic wave interacts only with the soft ferroelectric relaxation mode in the ferroelectric phase:

$$c^* = c_\infty - \frac{c_\infty - c_0}{1 + i\omega\tau}, \tag{2.7.8}$$

where c_∞ is the elastic constant at high frequencies ($\omega\tau >> 1$) and c_0 is the value of c^* in the low temperature phase. If the attenuation is relatively small ($\alpha V/\omega << 1$), then according to the general theory of elasticity from Eq. (2.7.7) and Eq. (2.7.8):

$$V^2 = V_\infty^2 - \frac{V_\infty^2 - V_0^2}{1 + \omega^2\tau^2} \text{ and } \alpha = \frac{\omega^2\tau}{2V^3}\cdot\frac{V_\infty^2 - V_0^2}{1 + \omega^2\tau^2}\,. \tag{2.7.9}$$

According to the phenomenological Landau- Khalatnikov theory the relaxation time can be expressed as [22, 71, 81]:

$$\tau = \frac{\tau_0}{T_C - T} \tag{2.7.10}$$

where τ_0 is a prefactor with dimension s·K. In the phase transition region the ultrasonic velocity dispersion occurs simultaneously with the maximum

ultrasonic attenuation [22, 71, 72]. In the case of low frequencies $\omega\tau$<<1 it appears difficult to observe experimentally any velocity dispersion below the phase transition due to a very narrow temperature range:

$$V = V_0 = \sqrt{\frac{c_0}{\rho}} \quad \text{and} \quad \alpha = \omega^2 \tau \frac{V_\infty^2 - V_0^2}{2V^3}. \tag{2.7.11}$$

When the condition $\omega\tau$>>1 the polarization cannot vary with electric field and remains constant. The sound attenuation also remains independent on the frequency:

$$V = V_\infty = \sqrt{\frac{c_\infty}{\rho}} \quad \text{and} \quad \alpha = \frac{1}{\tau} \frac{V_\infty^2 - V_0^2}{2V^3}. \tag{2.7.12}$$

2.8 Importance of PDMS and P(VDF-TrFE) as a composite matrix

Polydimethylsiloxane (PDMS) is an organic polymer, which was commercialized in the United States in the early 1940s, and was used with other commercial silicones as additives in solvent-based coatings to prevent surface defects, such as scattering [82]. Since then the interest of PDMS has been growing in chemical and biological applications due to its long service life, optical transparency, mechanical compliance, chemical stability, bio-compatibility, and ease of fabrication [39, 83]. Most of the modern silicone insulators for high voltage are PDMS based polymers. PDMS as a flexible organic macromolecule with –(Si-O)$_n$- backbone exists in a semicrystalline state [84]. The unique properties of PDMS come from the bond in the backbone,

similar to that of the C-C backbone. A high equilibrium flexibility imparts properties such as relatively low melting temperature point of PDMS (~ 233 K). The glass transition, so called pseudo second order transition, is observed within the polymer's amorphous region [85]. When the temperature of static glass transition is approached the polymer goes from a rubber-like to a hard glass-like state [86]. This temperature for PDMS (T_g= 148 K) is one of the lowest among polymers [87]. The polymer matrix is extensively studied due to its industrial versatility.

One of the first ferroelectric polymers appeared to be polyvinilidenefluoride (PVDF), after it was established that substantial piezoelectric and pyroelectric activity could be generated in synthetic polymer films polarized by a strong DC electric field [26].

The macroscopic properties of PVDF mainly depend on the sequence of molecular groups in the chain. This ordered packing of chain molecules results in growth of crystalline lamellae with unique electromechanical properties. Crystallization and melting temperatures of PVDF and its based copolymers are dependent on so-called head-to head ($-CF_2-CF_2-$) and tail-to-tail ($-CH_2-CH_2-$) defects up to 6% of the chain molecules. Certain defects can also influence formation of different crystalline phase of PVDF:

1 The non-polar α phase with alternating layers of helix molecules, whose dipole moments are oriented in opposite directions. Sometimes the conformation is called as *trans-gauche-trans-gauche*' (tgtg') (Fig. 2.8.1).

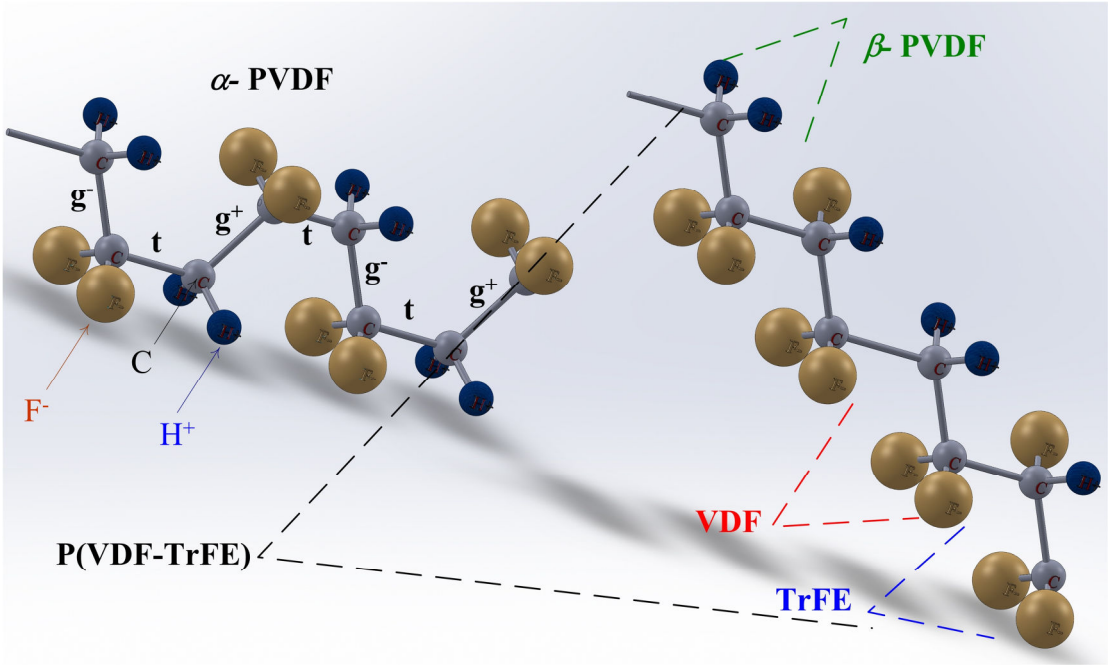

Figure 2.8.1. Structure of PVDF, P(VDF-TrFE) and its monomers

The *trans–gauche* state of conformation in the chain of PVDF means rotation about the bond linking two carbon atoms. If the angle of two planes joining the bonds is equal, the conformation is called *trans* state (*t*) and when the angle between the two planes is ±120°, the *gauche* plus (g^+) and minus (g^-), depending on the direction of rotation [3, 4].

2 One of the most studied ferroelectric polymers is PVDF in so called *β*-phase. However, it is difficult technologically to polarise it in this phase [25, 88, 89]. The *β* phase with its parallel stacking of planar zig-zag (tttt) chains is obtained from *α* phase material by stretching or by application of high electric fields. Here the -CF_2- groups create a strong permanent dipole moment.

3 In the polar *δ* phase the tgtg' chains are parallel with their dipole moments. The phase may be obtained in electric fields above from the *α* phase PVDF.

4 The γ phase is also polar of tttgtttg' chains packed parallel with their dipole moments.

5 The non-polar ε phase of antiparallel tttgtttg' packing.

Later, the neat organic PVDF copolymers, such as P(VDF-TrFE), have attracted intense scientific and technological attention due to their more stable ferroelectric state [1, 88, 90, 91]. The copolymers with the molar ratio of vinilidenefluoride and threefluorethylene 70/30 mol. %, having a high degree (more than 80 %) of crystallinity (ratio of the ordered molecules in the polymer to the randomly arranged molecules), are ferroelectric already in the as-grown state, which is responsible for its large electromechanical coupling [1, 88, 90-92].

A copolymerization of PVDF polymer together with vinylidene fluoride (VDF) monomer forms the planar zig-zag conformation of the β-phase molecules without stretching. Introduction of fluorine atoms into the polymer chain during polymerization process increases the unit cell size but hinders rotation of backbone defects necessary for formation of the paraelectric phase [93, 94]. This allows vinilidenefluoride/trifluoroethilene copolymer, P(VDF-TrFE), to crystallize in the ferroelectric phase with all-trans conformation regardless of the processing method [93-95]. P(VDF-TrFE) copolymer may exists in other two phases: paraelectric phases related to the α and the γ phases of pure PVDF.

The highest electromechanical properties of PVDF are found in films containing polar axes perpendicular to the surface (Fig. 2.8.2).

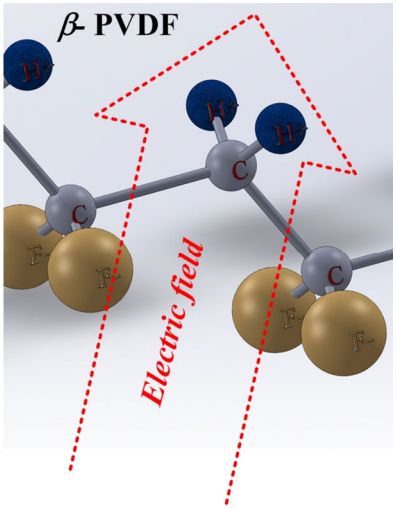

Figure 2.8.2. Orientation of β phase PVDF and P(VDF-TrFE) upon electric field

The advantages of the P(VDF-TrFE) based composites over conventional piezoceramics involve broad bandwidth, low acoustic impedance and good matching to human tissue, mechanical flexibility and the possibility of patterning the electrodes [7, 25, 26, 33, 35, 36, 63, 65, 70, 88, 91, 93, 95-105].

2.9 Fillers in nanocomposites

There are various types of nanoparticles used, as nanocomposite fillers, reported in the literature, e.g., metal nanoparticles, metal oxide nanoparticles, ceramic and polymer nanoparticles [5, 51, 106-108].

Metal oxide nanoparticles are one of the most versatile materials of diverse properties and functionalities. Zinc oxide (ZnO) nanoparticles have their own importance due to the broad area of applications starting from gas and chemical sensors, solar cells, electrical devices and finishing on cosmetics (protective sun lotions). ZnO is an attractive material with wide band gap (3.37 eV) for short-wavelength optoelectronic applications, i.e. blue to ultraviolet optoelectronics including laser developments. In addition, due to its non-

centrosymmetric crystallographic phase, ZnO shows the piezoelectric property, which is highly useful for the fabrication of devices nanocomposite based actuators [106, 107].

Another type of fillers for nanocomposites in electrical applications are fillers on a basis of lead zirconate titanate (PZT) ceramics. These fillers are in a contrast with its properties of the available polymer matrices. The electromechanical properties of $PbTiO_3$ ceramics may be more than ten times better than those of the piezoelectric polymer. The optimum property is determined by the type of interconnection between various fillers within a composite.

As the volume fraction of poled piezoelectric nanofillers is increased, the piezoelectric strain *d* coefficient (Eq. 3.3.1) of the composite increases. However loading of the piezoelectric fillers leads to a progressive increase of the electric permittivity in a low permittivity matrix, and as a consequence, the decrease in the piezoelectric voltage constant g_{ij}, which can be expressed through a change of the mechanical strain per unit S_i experienced by the change of the applied electric displacement D_j at a constant stress σ:

$$g_{ij} = \left(\frac{\partial S_i}{\partial D_j} \right)^{\sigma} \left[\frac{\mathrm{m}^2}{\mathrm{C}} \right]. \qquad (2.9.1)$$

Here *i* and *j* indices denote a direction of the applied electric displacement *D* and the induced strain *S*, respectively. Consequently there is an optimum particle loading as far as maximizing both *d* and *g* coefficients is concerned.
These two coefficients are considered to be a so-called “figure of merit” in comparising materials for various applications. The piezoelectric strain coefficient *d* perfectly represents the effectiveness of the transducer to act as transmitter, and the voltage constant *g* shows how effectively the transducer acts as a receiver. Fillers of high permittivity also make the poling of a polymer based nanocomposite difficult due to the high difference in the permittivities between the fillers and the polymer matrix. The applied electric

field is not equally distributed in such a composite, i.e. the local field is high in the polymer matrix and low is high in the fillers.

Various carbon nanomaterials as fullerenes, grapheme, carbon nanofibers and nanotubes are used as additives in conducting polymer nanocomposites [51, 52]. Different methods as arc catalytic chemical vapour deposition, discharge, laser ablation, are used for synthesis of carbon nanotubes [51, 109]. Carbon nanotubes (CNT) is a molecular form of carbon that has technologically promising and unique properties [52]. Carbon nanotubes are one-dimensional carbon nanostructure with tubular morphology of a graphite sheet, both ends of which are capped with fullerene hemispheres. Depending on the number of walls in carbon nanotubes, CNTs are named as single-walled carbon nanotubes (SWNTs), double-walled carbon nanotubes (DWNTs), and multi-walled carbon nanotubes (MWNTs). Each of these types has slightly different properties. The electrical conductivity of pure SWNT is higher than that of DWNT and MWNT. SWNT nanotubes are ductile and extremely stiff. It is the strongest known material with low density, which tensile strength varies from 50 GPa to 200 GPa. It exceeds the value of carbon fibres. Elastic modulus values vary in the order of 10^3 GPa. The structure of carbon nanotube is represented in Figure 2.9.1. The diameter of nanotubes is on the order of a nanometer (less than 100 nm). Each nanotube consists of a single molecule composed of millions of atoms. The length (L) of the nanotubes is on the order of thousands of times greater than the radius (R).

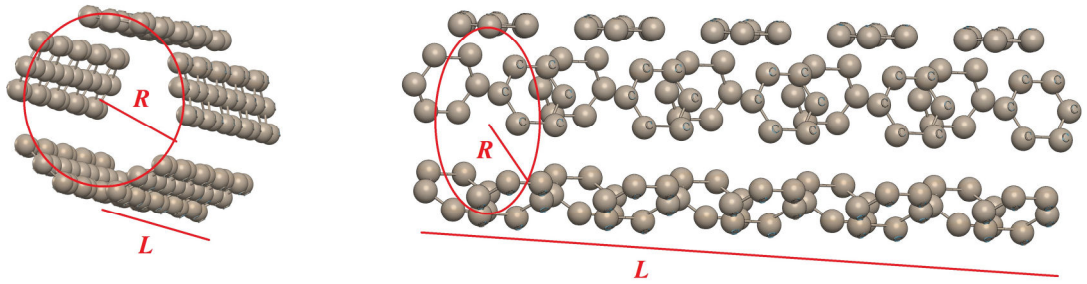

Figure 2.9.1. The structure of a carbon nanotube. Here R and L denote radius and length of a carbon nanotube

The nanotube can behave electrically as a metal or a semiconductor depending on its orientation. Due this property, it is anticipated to exploit CNT in liquid crystal displays in order to make the production cheaper and reduce power wastes [52].

Nanocomposites with a combination of piezoelectric ceramic fillers and fillers of carbon may act as passive “piezodampers” more effectively than traditional rubbers. Here the suppression of noise vibration is due to the electric properties of the fillers within a non-piezoelectric polymer [5].

3 Experimental

3.1 Means of dielectric spectroscopy

The complex dielectric permittivity was measured as a function of frequency (20 Hz-1 MHz) and temperature (100 K – 400 K) using a LCR meter HP4284A. Evaporated Al electrodes on the sample surface were used for electrical contacts. The equivalent electrical circuit was selected as the capacitance *C* and the tangent of losses:

$$tg\delta = \frac{\varepsilon''}{\varepsilon'}. \qquad (3.1.1)$$

From these quantities, according to the planar capacitor formula, complex dielectric permittivity was calculated as:

$$\varepsilon' = \frac{(C - C_0)\cdot d}{\varepsilon_0 S} + 1 \qquad (3.1.2)$$

and

$$\varepsilon'' = \varepsilon' tg\delta = \frac{C \cdot tg\delta - C_0 tg\delta_0}{C - C_0} + 1. \qquad (3.1.3)$$

Note, that C and $tg\delta$ are capacitance and loss tangent of the system with the sample, but C_0 and $tg\delta_0$ are capacitance and loss tangent of the empty system, d is the thickness of the sample, S is the area of the sample, ε_0 is the dielectric constant of vacuum.

In the frequency range of 1 MHz – 1 GHz the dielectric properties were studied by measuring the complex reflection coefficient r^* using a vector network analyzer Agilent 8714ET and a coaxial line [110]:

$$r^* = \frac{Z - Z_0}{Z + Z_0}, \tag{3.1.4}$$

where Z and Z_0 is the wave impedance of the transmission line (50 Ω) and Z is the impedance of the sample. Afterwards the capacitance was calculated through to the following relation between the complex admittance and the complex reflection coefficient:

$$Z^* = \frac{1}{j\omega C^*}, \tag{3.1.5}$$

Then the complex dielectric constant was calculated from the following equation:

$$\varepsilon' = \frac{\left(C^* - C_0{}^*\right) \cdot d}{\varepsilon_0 S} + 1, \tag{3.1.6}$$

where C and $C_0{}^*$ are complex capacitances of the filled and empty system.

Elmika 2400 scalar network analyser in combination with waveguides of various dimensions was used for dielectric spectroscopy investigation in GHz frequencies (8 GHz – 12 GHz; 27 GHz – 40 GHz; 35 GHz – 55 GHz). The complex reflection coefficient and phase are determined by automatized waveguide spectrometer. Several generators produced EM radiation (H_{10} mode) within the waveguides in the aforementioned frequency ranges. The

rod-shape sample inside the waveguide caused scattering of the radiation. The complex dielectric permittivity is found by solving the non-linear complex equation (Eq. 3.1.7) applying numerical optimization methods [54]:

$$\varepsilon^* = f(r,T). \qquad (3.1.7)$$

Here r and T are the complex reflection and transmission coefficients, respectively.

3.2 Means of ultrasonic specroscopy

Investigations of the ultrasonic wave attenuation and velocity at 10 MHz frequency in the composites were performed in the 300 – 420 K temperature range by the automatic pulse-echo method. The sample was placed between two ultrasonic waveguides lubricated with silicone oil to ensure acoustic contact for propagation of longitudinal waves between the sample and the waveguides (Fig. 3.2.1).

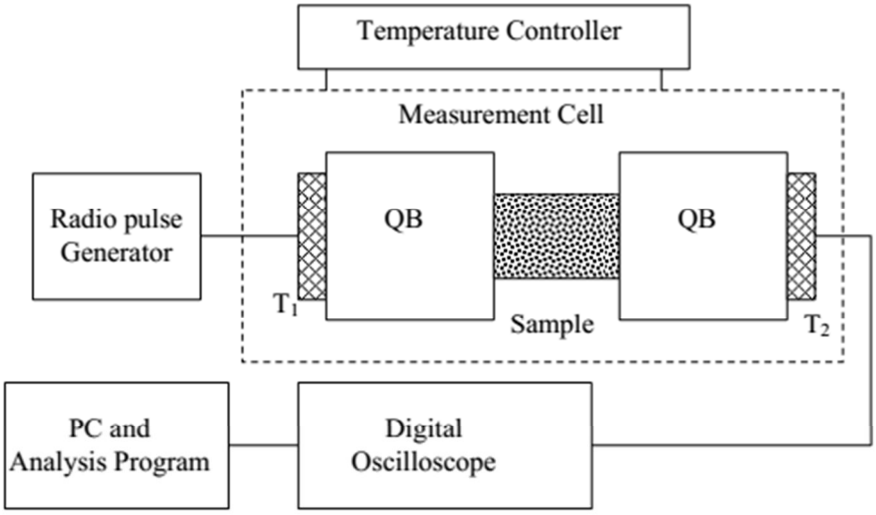

Figure 3.2.1 Block diagram of ultrasonic measurement assembly [111]

$LiNbO_3$ acoustic wave transducers placed at the end of the quartz buffers were used for transmitting and receiving the longitudinal acoustic wave. The velocity of the ultrasonic (US) longitudinal wave was calculated from the variation of the delay time in the mechanical system after subtracting the known part of the delay in the quartz buffers. Measurements were performed on heating and cooling at the rate of about 1 K/min. The temperature change was monitored by a Keithley Integra 2700 multimeter (Fig. 3.2.2) with a copper-constantan thermocouple adhered to the sample [7, 111].

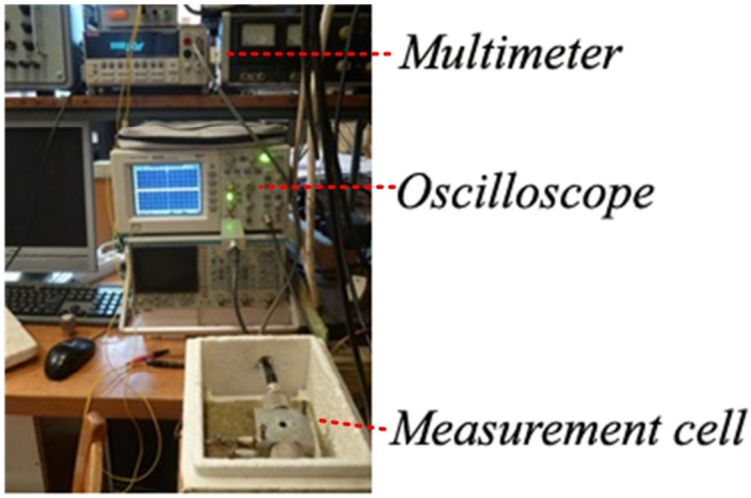

Figure 3.2.2. The measuring system of ultrasonic spectroscopy in bulk materials

Ultrasonically excited piezovoltage at 10 MHz frequency (AC voltage at f = 10 MHz) was measured by detecting the US wave on the composite attached to the buffer. The technique is the same as used in the automatic pulse-echo method when the receiving transducer is replaced by the thin plate of the polymer under investigation. Each measurement started at 390 K. In order to electrically polarize the sample, DC electric voltage of 300 V was applied to the polymer at 390 K and the sample was cooled to room temperature at the rate of about 1 K/min. At the room temperature the DC voltage was switched off and the sample was heated up to 390 K.

3.3 Means for ferroelectric characterisation

For ferroelectric and piezoelectric characterization of the samples TF Analyzer 2000E (aixACCT Systems) with a TREK 609E-6 4 kV voltage amplifier was used. All samples were deposited in a cell filled with a transformer oil in order to prevent electric arc. A bipolar triangle driving voltage applied to the samples was used to induce a ferroelectric loop and a mechanical displacement (Fig. 3.3.1).

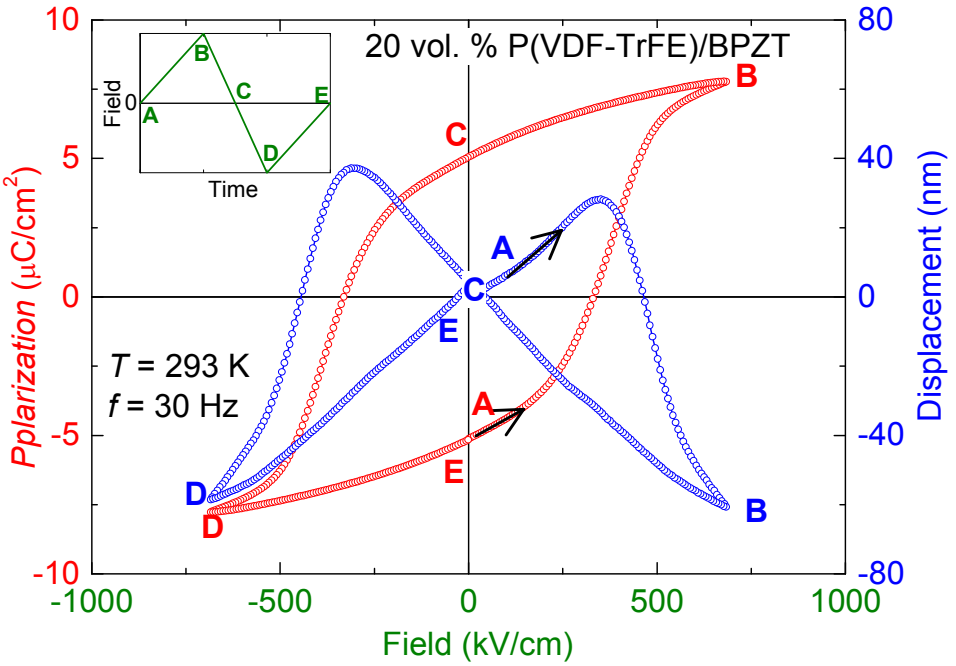

Figure 3.3.1. Ferroelectric loop and mechanical displacement versus electric field of 20 vol. % P(VDF-TrFE)/BPZT composite at f = 30 Hz and T = 293 K. The inset demonstrates schematic variation of the bipolar triangle driving voltage. Points A, B, C and D are to show instant value of polarization and displacement with respect to the electric field.

A pre-polarizing pulse was applied before each measurement to achieve a highly polarized state of the sample. At that the pulse used for pre-polarization of the film was followed by the driving voltage period used for polarization

measurements. The loops were obtained in both “clockwise” and “counter-clockwise” directions. There was a 1 s interval between polarizing pulse and driving voltage application. Afterwards, the polarization was calculated by integrating the measured current.

A beam interferometer was directed onto the contacting electrode allowing measurement of the mechanical displacement. The piezoelectric strain coefficient, parallel to direction of polarization (d_{33}), was derived from the linear dependence of the displacement on the applied voltage:

$$d_{33} = \frac{mechanical\ strain}{applied\ voltage}\left[\frac{m}{V} or \frac{C}{N}\right]. \qquad (3.3.1)$$

The butterfly curve and the hysteresis loop corresponding to the bipolar excitation signal are shown in Fig. 3.3.1. The hysteresis loop starts in the negative relaxed remanent polarization state (A) and turns into the positive saturation (B). When the voltage equals to zero the polarization reaches the positive remanent polarization state (C). Following the curve it turns into the negative saturation (D) and then back to the remanent polarization state (E).

3.4 Other techniques

Dynamical mechanical analysis (DMA) measurements were carried out using the tensile mode of Q800 dynamic mechanical analyser (TA instruments) in the temperature range 220 K to 400 K. The tests were performed for rectangular samples with 10 mm width and 20 mm length between clamps. The

isothermal experiments were conducted every 5 K. At each temperature a frequency of 1 Hz and 10 Hz was applied.

Thermal analysis was performed by a differential scanning calorimeter (DSC) Mettler Toledo 822e. The heating and cooling rates during DSC measurements were 10 K/min. The samples were annealed at two different temperatures, at about 390 K and melting temperature (415 K). Afterwards, the samples were cooled down to room temperature and heated for several times to 390 K and 415 K. The degree of crystallinity was determined from the ratio of the melting peak to the heat of fusion for P(VDF-TrFE) (38 J/g) [103].

Additionally, measurements of the thermally-stimulated discharge current (TSDC) were performed. Non- metallized films of neat P(VDF-TrFE) and P(VDF-TrFE)/CNT composites with 20 mm diameter were attached onto copper plates with a conductive double-side adhesive tape. According to some previous investigations, such conductive tapes prevent unwanted charge injection from the electrodes [112]. A corona triode poling of +12 kV constant voltage was applied at elevated temperature (353 K). In spite of various defects, during the process of corona charging, samples with only one electrode and higher electric fields can be used in contrary to sandwich contacting methods [113]. In our case samples were cooled down to room temperature under an applied field during 30 minutes. The needle-to-grid distance and the grid-to-sample distance were 43 mm and 5 mm, respectively. The highest surface potential was limited by the grid voltage of 2.5 kV [113]. The charge transport from the needle to the surface of the samples was performed at atmospheric pressure, as expected, mainly by cations [113]. In order to investigate orientation motion of dipoles and separate them from space charges relaxations, upon heating in the films, the TSDC measurements were carried out in open circuit (OC) mode [70, 114, 115]. In order to separate displacive currents (heterocharges) from currents of charges trapped on the sample surface, or in the near surface region (homocharges) [70, 99] upon heating, a glass spacer of 1 mm thickness as an isolating gap was placed on the surface of the

sample. This method allows charges drifting to the back electrode. In order to avoid stray currents, originated from unstable excessive charges, all samples were short-circuited after poling. This method facilitates a redistribution of the mobile charges and, as a result, the whole field in the bulk becomes zero [70, 98, 99, 102]. The TSDC currents were measured at the heating rate of 10 K/min. Afterwards the processes of polarization and TSDC measurement were performed again.

The morphology of the prepared film was examined using a scanning electron microscope (SEM) TOPCON model SM-300. For the SEM test, the film samples were cooled down in liquid nitrogen for 5 minutes and then fractured in the middle. The hollow samples were coated with gold before examination. The surface of fractured sample border was examined at various magnifications.

3.5 Materials

The ZnO nanoparticles with a size specification of 30–100 nm were purchased from Alfa Aesar, Chicago, Illinois. Fractions of ZnO with aggregate sizes of 30 nm were extracted by centrifugation (3,000 g force) from suspensions in isopropanol and used as fillers. Dow-Corning supplied the polydimethylsiloxane, Sylgard, as a two part material. The procedure of embedding ZnO fillers into PDMS polymer matrix was performed in several steps. Firstly, the ZnO nanoparticles were dispersed in isopropanol solvent and sonicated to break up large agglomerates. The ultrasonic processor used in these studies was a Cole Parmer High Intensity 750 W Ultrasonic Processor (20 kHz frequency), which is a horn type ultrasonic source that allows for submersion of the ultrasonic horn into the sample, providing more efficient transfer of energy to the sample. Afterwards, the suspension was mixed with

uncured PDMS. The isopropanol solvent was removed by vacuum. The mixture of PDMS and nanoparticles was cured at 60 ^{o}C for several hours and at 40 ^{o}C overnight. Such procedure allows preparing nanocomposites with satisfactory dispersion of nanoparticles as confirmed by an inspection in an optical microscope and by uniform photoluminescence of the composites under UV excitation as observed in the Olympus IX71 inverted fluorescence microscope. The latter characterization was possible based on fluorescence of ZnO nanoparticles under UV light. Composites with 1 wt. %, 2 wt. %, 5 wt. % and 10 wt. % of ZnO in PDMS were prepared.

A copolymer with a molar ratio 70/30 of VDF to TrFE, produced by polymerization from solution (dimethylsulfoxide/acetone mixture), was used as the composite matrix. As the filler, a carbon nanotube (CNT) powder was used. Synthesis of carbon nanotubes (CNTs) was carried out by chemical precipitation from the gas phase during pyrolysis of methane. The temperature of the synthesis was 900 ^{o}C at the constant pressure of 1.3 bar in a chamber with a flow of a gas mixture consisting of argon, hydrogen and methane. The total flow of the gas mixture was 750 cm^3/min. The duration of the process lasted 60 minutes. Subsequently, the resulting material was subjected to a liquid-phase treatment at elevated temperatures (in solutions of HCl, H_2O_2 and HNO_3/H_2SO_4 mixture) in combination with ultrasonic method of separation. These operations make it possible to purify CNTs from impurities and catalyst residues, and also to achieve formation of polar groups with C=O bond on the surface of CNT walls. Geometry parameters of CNTs were evaluated with the help of scanning electron microscopy (SEM): the mean diameter value was 20 nm and the length varied from 1.0 to 1.5 μm. To produce samples of a composite based on P(VDF-TrFE) and containing carbon nanotubes, a filler suspension was prepared in a solvent which was subsequently mixed with a polymer solution. Dispersion of the suspensions was carried out in the ultrasonic bath at temperatures not exceeding 10 °C with the ultrasonic power of 30 W/cm^2 during 60 minutes. The concentration of the filler in the matrix

was varied from 1 vol. % to 2 vol. %. More information on filler matrix preparation can be found elsewhere [6].

As the filler, also a $(Pb_{0.75}Ba_{0.24}Sr_{0.01})(Zr_{0.53}Ti_{0.47})O_3$ (BPZT) powder with the average particle size ~0.5 μm of lognormal distribution was used. The concentration of the filler in the P(VDF-TrFE) matrix was varied from 10 vol. % to 50 vol. %. Films had thickness varying from 20 to 50 μm depending on the concentration of the filler: 20 μm in case of neat P(VDF-TrFE), 30 μm in case of 10 vol. % BPZT and 20 vol. % BPZT, 40 μm in case of 30 vol. % BPZT and 50 μm in case of 50 vol. % BPZT. Both scanning electron microscopy and atomic force microscopy measurements (Fig. 1 and Fig. 3 in [18]) confirmed homogeneous dispersion of the BPZT grains in the polymer matrix without formation of agglomerates.

4 Experimental results

4.1 PDMS/ZnO

Temperature dependences of real (ε') and imaginary (ε'') parts of the complex dielectric permittivity ($\varepsilon^* = \varepsilon' - i\varepsilon''$) at 1 MHz frequency for all investigated composites and pure PDMS are shown in Fig. 1.

The temperature dependence of the complex dielectric permittivity exhibits an anomalous behaviour at low temperatures (close to 175 K). This behaviour is attributed to the dynamic glass transition, usually referred as a primary α

relaxation, due to a relatively large-scale cooperative motion of many backbone segments in amorphous phase of PDMS [116, 117].

The slope of the dielectric permittivity temperature dependence strongly decreases with the concentration of nanofillers in the temperature region 175 K – 260 K (Fig 4.1.3a). The similar behaviour of the real part of the dielectric permittivity of pure PDMS has been previously observed by H. Adachi et. al., [118] J. Ouyang et. al. [119] and was attributed to a subsequent growth of spherulites in the amorphous region. Hence, our cooling rate is slow enough (1 K/min) and enables the crystal nucleation within the polymer. From our results (Fig. 4.1.1a) it is obvious that the presence of ZnO nanoparticles strongly affects the crystallization rate and decreases the slope of $\varepsilon'(T)$.

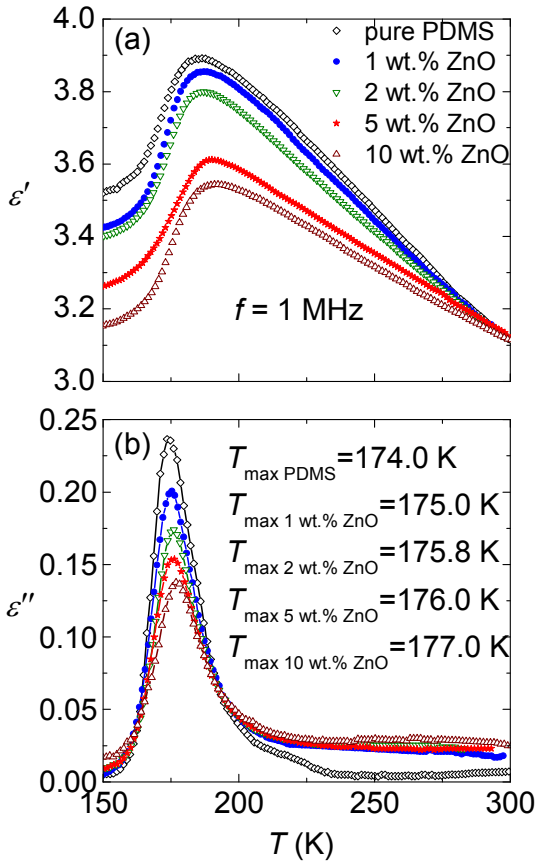

Figure 4.1.1. Temperature dependence of the complex dielectric permittivity for pure PDMS and for composites with 1 wt. %, 2 wt. %, 5 wt. % and 10 wt. % ZnO inclusions on cooling at 1 MHz frequency.

It is clearly visible that the peak of the dielectric loss maximum (T_{max}) is shifted towards higher temperatures with increasing the concentration of ZnO particles (Fig. 4.1.1b). This shift is related to the shift of the dynamic glass transition temperature and will be discussed later.

The dielectric dispersion and the peak of dielectric losses have been observed close to the temperature of the glass transition in all investigated composites. Figure 2 shows the frequency dependence of the imaginary part of the dielectric permittivity for 5 wt. % ZnO in PDMS close to the glass transition temperature T_g. The curves of losses show a relaxation peak in the frequency range of 1 kHz – 1 MHz. The dielectric dispersion is caused by the α relaxation in PDMS, which origin is related to the local segmental dynamics [118, 120].

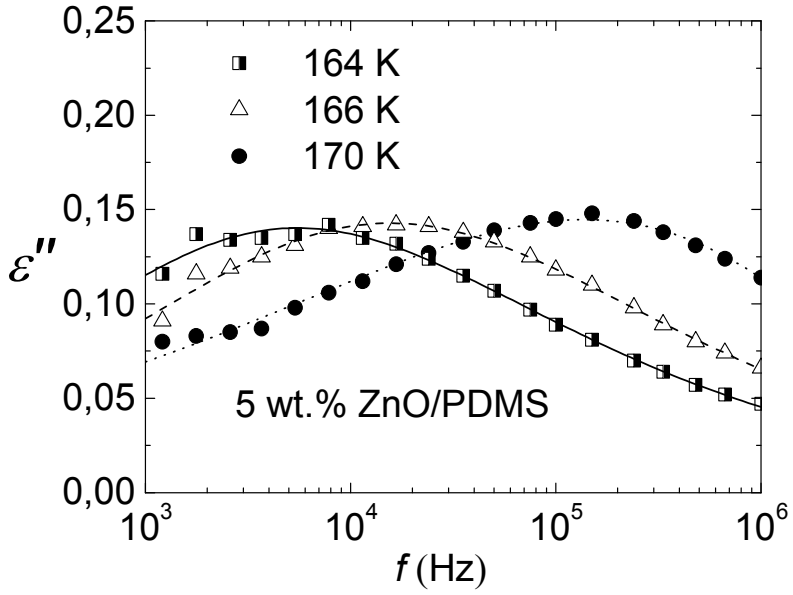

Figure 4.1.2. Frequency dependence of the imaginary part of the dielectric permittivity for 5 wt. % ZnO in PDMS at different temperatures close to T_g (160 -180 K). Symbols denote the experimental data. The curves are calculated according to the Cole- Cole spectral function (Eq. (4.1.3)).

In Fig. 4.1.3 experimental dependences of the longitudinal wave velocity and the ultrasonic wave attenuation on temperature and the concentration dependence of the ultrasonic wave attenuation (inset) are demonstrated.

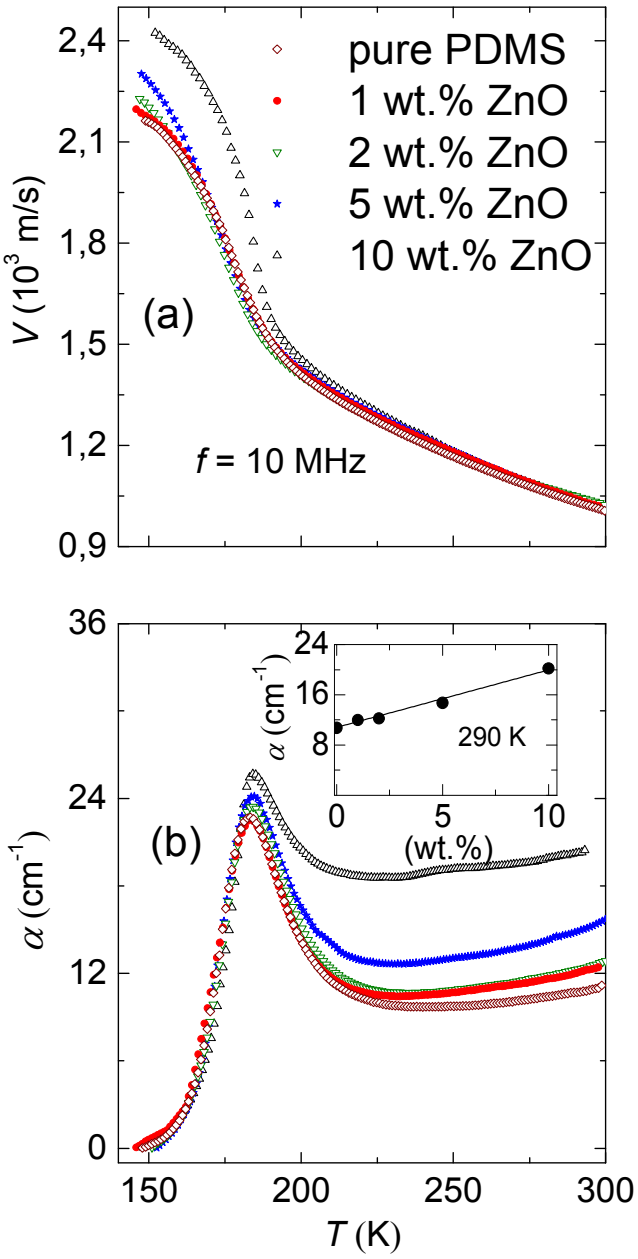

Figure 4.1.3. Temperature dependences of the ultrasonic velocity (a) and the ultrasonic wave attenuation (b) for the composites on cooling.

It is clearly observed that at low temperatures the ultrasonic velocity is noticeably dependent on the loading of ZnO nanofillers (Fig. 4.1.3a). The

larger concentration of ZnO nanoparticles embedded in the polymer matrix the higher velocity values are observed in the composites. It might be due to the large difference between elastic coefficients of zinc oxide and polymer material [42, 116, 117].

The peak corresponding to the maximum ultrasound wave attenuation within the composites is extended rightwards, depending from the concentration of ZnO (Fig. 4.1.3b). This is consistent with our observation in the dielectric behaviour of the composites (Fig. 4.1.1) and could be due to the crystallization process, which is affected by specific interactions between the filler and the polymer matrix [41, 117]. This suggests that the molecular mobility of the polymer matrix is affected by the presence of embedded nanoparticles. ZnO fillers reduce the flexibility of PDMS backbone and, as a consequence, more heat is needed for the transition from the glassy to the soft state.

An experimental dependence of the ultrasonic attenuation on ZnO content in PDMS nanocomposites is depicted on inset in Fig. 4.1.3b. The attenuation of ultrasonic wave within the composite at room temperature linearly depends on the concentration of ZnO nanofillers. Similar results are obtained earlier in PDMS/OLC composites [121]. To explain such dependence, we assume that adding ZnO nanoparticles to PDMS increases the dynamic heterogeneity in the composite, that is an important factor for the ultrasonic attenuation.

The numerical prediction of the scattering- attenuation induced by identical randomly distributed particles was previously predicted by C. M. Sehgal et. al. [122]. The attenuation in inhomogeneous medium was considered by scattering from closely-packed and independent elements. The contribution of the scattering to the attenuation may be expressed as:

$$\alpha = \frac{4\overline{\mu^2}k^4a^3}{\left(1+k^2a^2\right)\left(1+9k^2a^2\right)}, \qquad (4.1.1)$$

where $\overline{\mu^2} = (1-\eta)\left(1-\eta-\eta\frac{V_f^2}{V_m^2}\right)\frac{(V_f-V_m)^2}{V_f^2}$ is a mean velocity fluctuation in polymer based composite [123], η is a filler volume fraction in the composite, k is a wavenumber, a is the average size of the filler, V_f and V_m are sound velocities in the fillers and the polymer matrix, respectively, $k=2\pi f/V_m$. Considering ZnO (a = 30 nm) as the scattering particles and taking into account ZnO properties published in Ref. [42], negligible attenuation values were obtained (~10^{-3} m^{-1}) according to the Eq. (4.1.1). Therefore, the scattering and the attenuation could be induced by the larger particles in the composite matrix. We assume that the scattering may be caused by spherulites within the semicrystalline PDMS structure, they were previously investigated in other semicrystalline polymer [124, 125]. The spherulites may cause a "quasiresonant" ultrasound absorption, with attenuation maximum at $ka=\pi$. The size of spherulites can be up to few hundred microns [124]. According to this assumption, the value of attenuation can be calculated close to the experimentally observed one (~ 10 cm^{-1}). Although, the ratio of the acoustic wavelength (200 μm) and the ZnO particle size (30 nm) is very high, such rigid particles can cause an additional mechanical wave attenuation by the oscillatory deformation and the interfacial interaction with the polymer matrix [126]. A model considering absorption and multiple scattering effects has been proposed for ultrasonic frequencies in fiber-reinforced polymer [127]. A thermal hysteresis was observed in the temperature dependences of the ultrasonic wave velocity (Fig. 4.1.4a) and the attenuation (Fig. 4.1.4b).

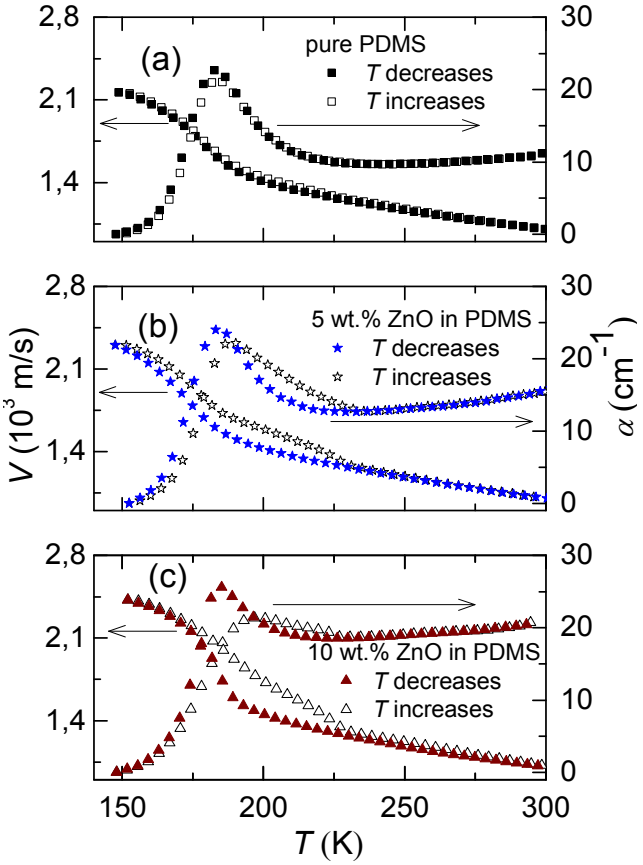

Figure 4.1.4. Temperature dependences of the ultrasonic velocity (left), the ultrasonic wave attenuation (right) for pure PDMS (a) and composites with 5 wt. % (b) and 10 wt. % (c) of ZnO inclusions. Solid symbols: on cooling, open symbols: on heating.

A similar thermal hysteresis was also observed in the temperature dependence of the imaginary part of the complex dielectric permittivity [128]. The hysteresis is caused by the first order phase transition (crystallization/melting), which was previously observed on heating by the differential scanning calorimetry in PDMS [41, 128]. The nanocomposites crystallize during slow cooling (at cooling rates not higher as 1 K/min) [129]. Upon heating, due to chain rearrangements and the decrease of the melt viscosity, PDMS also crystallizes from the amorphous phase [129]. A complex melting occurs in heating cycle in PDMS range 220-230 K in good agreement with previous investigations of PDMS polymer [130]. ZnO nanoparticles can serve as nuclei, capable of the supporting crystal growth within the composite.

As the amount of nanoparticles affects the crystallite size and the degree of the crystallinity, the melting is also enhanced by the presence of ZnO nanoparticles resulting in the appearance of the hysteresis. The temperature dependences of the ultrasonic wave attenuation and the velocity are different on cooling and heating cycles (Fig. 4.1.4). The hysteresis becomes more pronounced for higher nanofiller concentrations.

The position of the dielectric losses maximum is frequency dependent (Fig. 4.1.5).

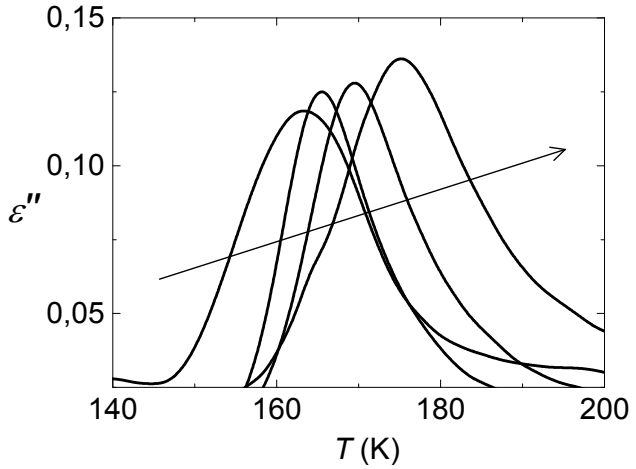

Figure 4.1.5.Temperature dependence of the losses at different frequencies (11.4 kHz – 1 MHz).

The peak increases and shifts to higher temperatures with the frequency. The shift can be characterized by the Vogel–Fulcher (VF) relation [78, 131]:

$$f = f_0 e^{\frac{-E_{VF}}{k_B(T_{\max} - T_{ref})}}, \qquad (4.1.2)$$

where f_0 is the frequency approached with $T_{\max} \to \infty$ and T_{ref} is the temperature of glass transition in the polymer as cooling rate becomes infinitely slow. Other parameters are similar as in Eq. 2.6.8.

Fig. 4.1.6a shows experimental and fitted values of frequency versus the dielectric loss maxima temperature according to the (VF) equation (Eq. (4.1.2)) for pure PDMS and the composites on cooling. The value for 10 MHz frequency is obtained from the previously described ultrasonic measurements.

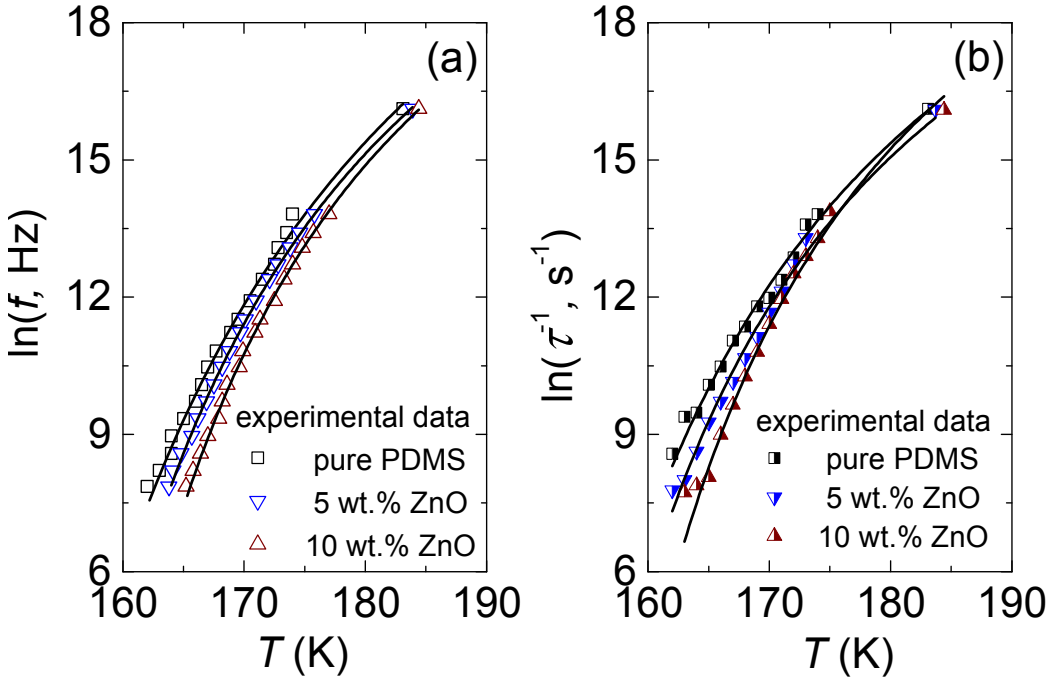

Figure 4.1.6. Measurements frequency versus the dielectric losses maximum temperature (a) and relaxation frequency $f_r=1/\tau$ obtained from the best fit of the Cole-Cole spectral function (b) for pure PDMS and composites with ZnO inclusions on cooling. Solid lines are the best fit according to the Vogel-Fulcher law (Eq. (4.1.2)).

Extracted parameters are listed in the Table 4.1.1.

Table 4.1.1. Vogel- Fulcher fit parameters of the relaxation time in PDMS/ZnO Nanocomposites

Material	f_0 (THz)	E_{VF} (meV)	T_{ref} (K)	E_{VF2} (meV)	T_{ref2} (K)	τ_0 (ns)
Pure PDMS	0.89	49	133.72	21	131.86	0.15
1 % PDMS/ZnO	0.89	47	136.98	21	134.00	0.14
2 % PDMS/ZnO	0.89	47	136.83	21	134.39	0.14
5 % PDMS/ZnO	0.89	45	137.46	20	137.40	0.14
10 % PDMS/ZnO	0.89	46	140.82	21	142.01	0.15

The frequency dependence of the imaginary part of dielectric permittivity was analyzed by the Cole-Cole spectral function (Eq. 2.6.3) [74] (CC):

The best fit is presented in Fig. 4.1.2 as solid lines. The α parameter, $\Delta\varepsilon$ and ε_∞ are almost temperature independent (in the range 160 K – 180 K). Obtained values of the relaxation time τ at various temperatures were converted to the relaxation frequency values f_r according to $f_r=1/\tau$. The temperature dependence of the relaxation frequency fit very well the VF equation (Fig. 4.1.6b). The values of f_0, E_{VF} and T_{ref} obtained by the VF fit of the relaxation time are consistent with those shown in Table 4.1.1.

It is clearly seen, that the glass transition temperature increases with the concentration of ZnO nanoparticles, while the concentration behaviour of the activation energy is less expressed. The increase of the glass transition temperature is due to the reduced mobility of the polymer backbone close to ZnO nanoparticles [83, 132, 133].

The ultrasonic attenuation peak can be described using the relaxation theory of elasticity [22] as in Eq. 2.7.9. In order to include the temperature dependence of the ultrasonic losses in acoustic bonds and buffers, a linear temperature dependence with two terms (A and α_0) can be added:

$$\alpha = \frac{\Delta V}{V^2}\frac{\omega^2\tau}{1+\omega^2\tau^2} + AT + \alpha_0 . \qquad (4.1.3)$$

where V and ΔV are the longitudinal ultrasonic velocity in the composite and its magnitude of downward step at a certain temperature, respectively. Parameters ω and τ are taken from Eq. 2.7.9. Here we assume that the relaxation time can be expressed by such VF relation:

$$\tau_u = \tau_0 e^{\frac{E_{F2}}{k_b(T-T_{ref2})}}, \qquad (4.1.4)$$

where τ_0 is the relaxation time, when $T\rightarrow\infty$.

Fits on the temperature-dependent ultrasonic wave attenuation for pure PDMS and 2 wt. % ZnO are plotted in Fig. 4.1.7 and extracted parameters are listed in the Table 4.1.1. As we see the deviation of fitted curves from the experimental ones is satisfactory.

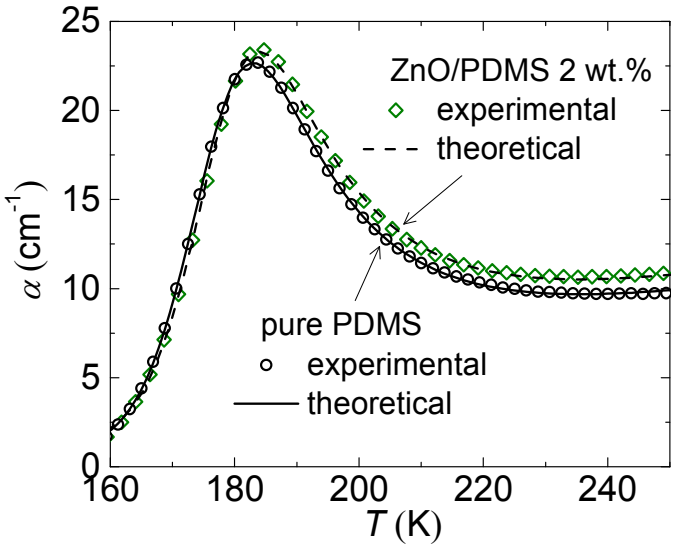

Figure 4.1.7. Temperature dependences of ultrasonic wave attenuation for pure PDMS and 2 wt. % PDMS/ZnO composites on cooling (solid lines are calculated according to Eq. (4.1.3)).

Obtained values of both of T_{ref} and T_{ref2} are very similar (Fig. 4.1.8).

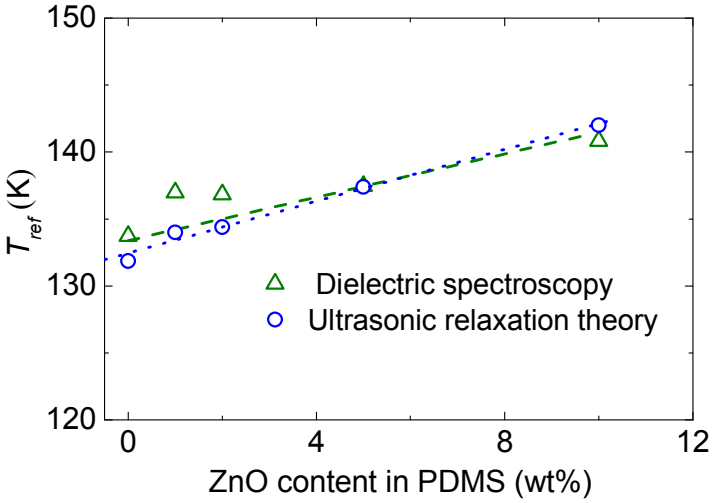

Figure 4.1.8. T_{ref} values obtained from dielectric spectroscopy and mechanical relaxation measurements (The lines are guide for eyes).

4.1.1 Summary

The effect of ZnO nanoparticles on PDMS/ZnO composite dielectric and mechanical properties has been studied. Our investigations show that the mechanical and dielectric losses in composites are strongly dependent on the concentration of ZnO, i.e. a composite containing higher concentration of fillers has a lower dielectric and higher mechanical loss peaks. Dielectric spectroscopic measurements in the PDMS/ZnO composites combined with ultrasonic measurements revealed the existence of the dielectric hysteresis between cooling and heating cycles and it is strongly dependent on the concentration of ZnO nanoparticles, acting as crystallization nuclei. The growth of spherulites (few hundred microns) can explain the increased scattering-attenuation in PDMS matrix for higher ZnO concentrations.The analysis of the dielectric losses maximum according to the VF law and the ultrasonic attenuation data shows that the glass transition temperature increases with increase of ZnO concentration in the composites. It has been shown that the ultrasonic and the dielectric relaxation processes can be described by VF law.

4.2 (PVDF-TrFE)/BPZT

4.2.1 Modelling and experiment of polarization reversal

The experimental ferroelectric hysteresis loops are presented in Figure 4.2.1.1.

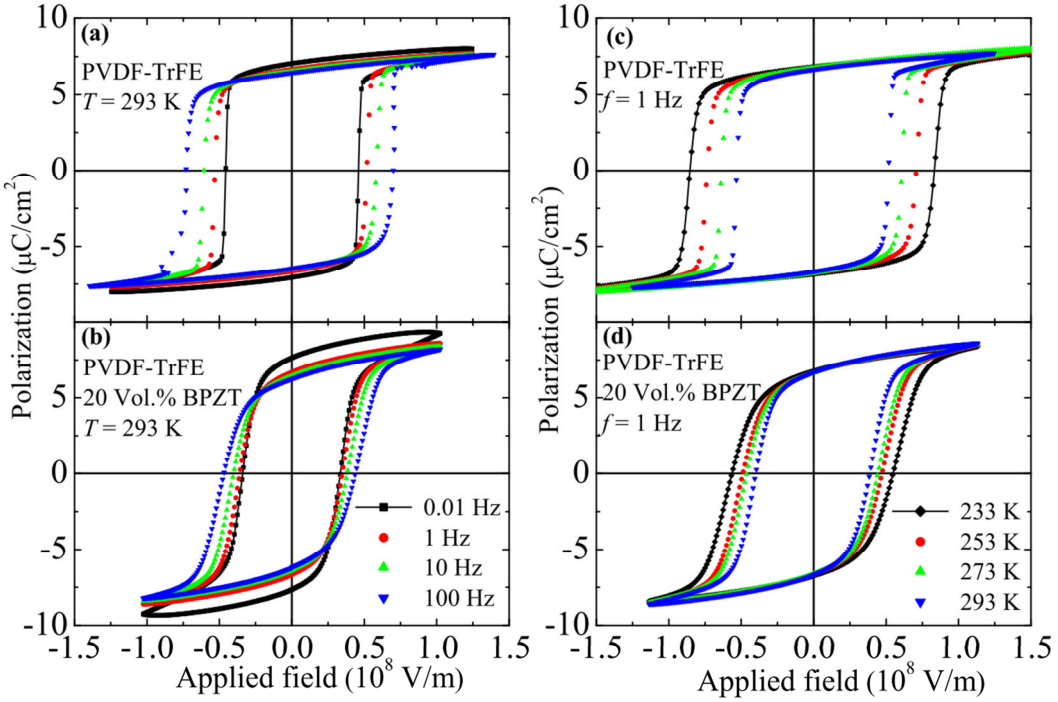

Figure 4.2.1.1. Ferroelectric loops of pure P(VDF-TrFE) ((a) and (c)) and P(VDFTrFE)-BPZT composite ((b) and (d)) at various frequencies at room temperature ((a) and (b)) and various temperatures at 1 Hz ((c) and (d)) [6].

The loops of the pure copolymer sample are close to be rectangular in shape, while they are tilted in the case of the composite. The tilting of near-coercive regions of the loops is connected with coercive field scattering that is dependent on the character of local interactions in the copolymer and on the character of inhomogeneities and their distribution in the composite. The slope of the saturated regions of the hysteresis loops is proportional to the dielectric permittivity.

The coercive field increases with both cooling and frequency increase. Such a behavior was expected and has been reported for many ferroelectric

systems. The hysteresis loops were slightly distorted due to the finite resistance of the samples at frequencies below 0.1 Hz (Figures 4.2.1.1a and 4.2. 1.1b). This means that the conductivity of the samples does not contribute to P-E loops and switching dynamics at higher frequencies, as the relaxation time of the free charge carriers is too long. At higher frequencies, a slight decrease of the remanent polarization with increasing frequency was observed.

Figure 4.2.1.2 demonstrates dependences of the coercive field and remanent polarization on frequency and temperature.

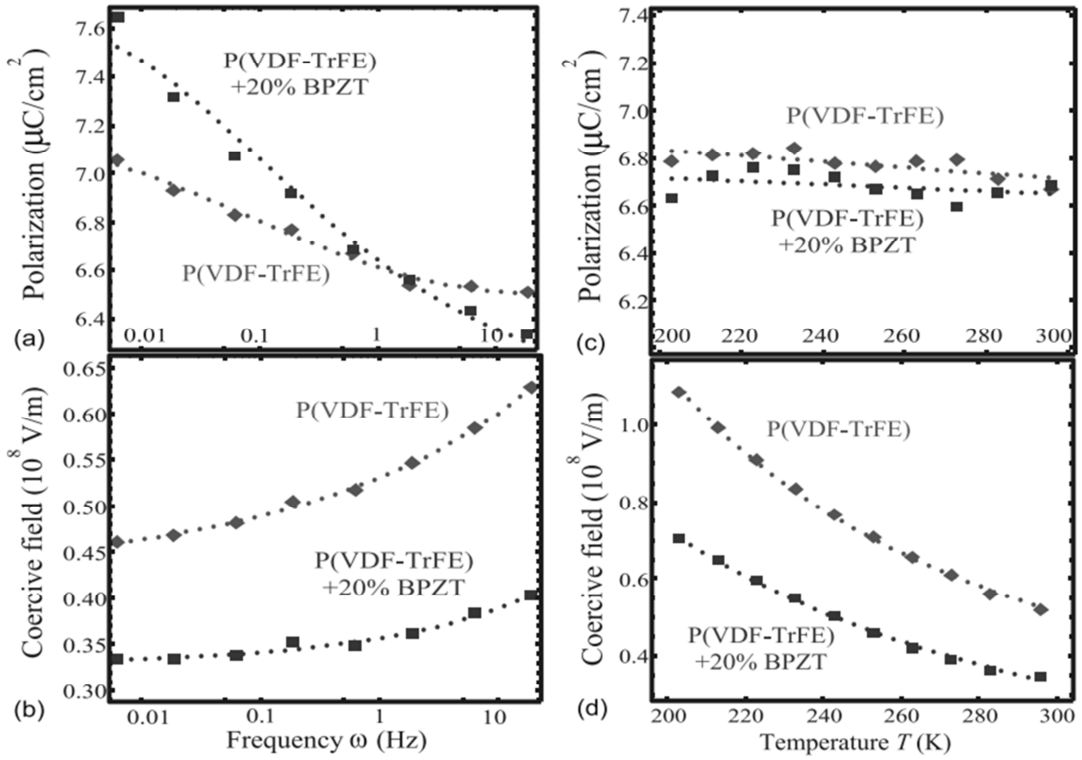

Figure 4.2.1.2. Experimental (symbols) and interpolated (dotted curves) frequency and temperature dependences of the remanent polarization ((a)and (c)) and coercive field ((b) and (d)) for P(VDF TrFE) and 20 vol. % P(VDF-TrFE)/BPZT. Data shown in panels (a) and (b) correspond to the room temperature. Data shown in panels (c) and (d) correspond to the frequency of 1 Hz [6].

The composite film demonstrates ferroelectric parameters noticeably different from those of the pure P(VDF-TrFE) film. It has the significantly smaller coercive field (by the factor of about 1.6–1.7) in the entire frequency and temperature range, where the measurements were carried out. The

remanent polarization of the composite sample is higher than that of P(VDF-TrFE) at frequencies below 1 Hz, but it becomes smaller at higher frequencies. As one can see from the comparison of Fig. 4.2.1.2a and Fig. 4.2.1.2b, the remanent polarization monotonically decreases and the coercive field monotonically increases with the increasing frequency at a fixed temperature for both copolymer and composite sample.

The experimentally observed increase of the coercive field with the increasing frequency shown in Fig. 4.2.1.2b was deduced from the Weiss model by Leschhorn and Kliem [134]. Dependences of the remanent polarization and coercive field on temperature are shown in Fig. 4.2.1.2c and Fig. 4.2.1.2d. For both materials, the remanent polarization slightly decreases in a non-monotonous fashion, while the coercive field exhibits a strong monotonous decrease with increasing temperature.

The frequency dependences of the polarization and coercive field can be approximated as:

$$P_r(\omega) = P_{\omega 0} + P_1 e^{-(C_{\omega P}\omega)^S} \tag{4.2.1.1}$$

and

$$E_C(\omega) = E_{\omega 0} e^{-(C_{\omega E}\omega)^Q}, \tag{4.2.1.2}$$

respectively. Similarly the temperature dependences of polarization and coercive field have been approximated as:

$$P_r(T) = P_0 + P_T\left(\frac{T}{T_C}\right) \tag{4.2.1.3}$$

and

$$E_C(T) = E_{T0}\left(1 - \frac{T}{T_C}\right)^{\gamma}. \tag{4.2.1.4}$$

Here $P_{\omega 0}$, $P_{\omega 1}$, P_0 and P_T are polarization amplitudes, S, Q and γ are dimensionless exponents, $E_{\omega 0}$ and E_{T0} are coercive field amplitudes, $C_{\omega P}$, $C_{\omega E}$ are factors and T_C is the Curie temperature. All fitting values are listed below in Table 4.2.1.1.

Table 4.2.1.1. Parameters used in the fitting of the experimental dependences $Ec(\omega)$, $Pr(\omega)$, $Ec(T)$ and $Pr(T)$ shown in Figure 4.2.2 [6]

Material	$P_{\omega 0}$ ($\mu C/cm^2$)	$P_{\omega 1}$ ($\mu C/cm^2$)	P_0 ($\mu C/cm^2$)	P_T ($\mu C/cm^2$)	S	$E_{\omega 0}$ ($10^8 V/m^2$)	E_{T0} ($10^8 V/m^2$)	$C_{\omega P}$ (Hz^{-1})	$C_{\omega E}$ (Hz^{-1})	Q	γ	T_C (K)
P(VDF-TrFE)	6.49	0.8	7.1	-0.517	0.3	0.417	2.42	1.33	$3.8 \cdot 10^{-5}$	0.180	1.5	431
20 vol. % P(VDF-TrFE)/BPZT	7.70	1.6	6.9	-0.304		0.328	1.63	1.00	$3.3 \cdot 10^{-5}$	0.312		434

It is also interesting to discuss properties of composites with smaller contents of ceramics inclusions. Preliminary results indicate that the noticeable changes of the remanent polarization and coercive voltage appear under the BPZT concentration increase over (10–15) vol. % only. Hysteresis loops' parameters for smaller concentrations look very similar to those obtained for pure PVDF. The changes appeared for more than (10–20) vol. % of BPZT are gradual. Concentrations of BPZT inclusions higher than 20 vol. % have not been studied yet, but here, we expect a strong cross-talk between the ceramic inclusions.

In order to describe polar properties of the P(VDF-TrFE)-based composites and explain the difference from the pure copolymer, we have adopted mean-field Weiss model and performed a weighted averaging over several independent parameters. The Weiss model has several advantages, because it provides a macroscopic description taking into account microscopic interactions between individual dipoles [6, 135]. For ferroelectrics, the intrinsic polarization reversal is a rather rare case. Averaging over the model parameters can include the hysteresis loop tilt originated from the domain steps reversal in the case of ergodic processes.

Within the framework of the Weiss model, ferroelectric polarization out-of-plane component P_3 dynamics is described by a dynamic relaxation-type equation:

$$\tau\left(P_3\right)\frac{dP_3}{dt}+P_3(t)=P_\infty(t) \tag{4.2.1.5}$$

supplemented by the initial conditions $P_3(0)= 0$ with following relations:

$$\tau\left(P_3\right)=\frac{\tau_0 e^{\frac{W_0}{kT}}}{2\cosh\left(\frac{p\left(E_a+\alpha P_3+\beta P_3^3\right)}{kT}\right)}\ , \tag{4.2.1.6}$$

$$P_\infty(t)=n\cdot p\cdot\tanh\left(\frac{p}{kT}\left(E_a+\alpha P_3+\beta P_3^3\right)\right). \tag{4.2.1.7}$$

Here, P_∞ is the equilibrium polarization, τ is the relaxation time, W_0 is the activation energy, n is the total density of dipoles, p is the dipole moment, constants α and β describe strength of linear and nonlinear interaction between dipoles. E_α has the meaning of an electric field "acting" on the polymer P(VDF-TrFE) matrix that includes both external and depolarization contributions originated from BPZT particles boundaries.

Table 4.2.1.2. Effective Weiss model parameters for pure P(VDF-TrFE) and composite P(VDFTrFE) with 20 vol. % of BPZT [6]

Material	τ_0 (s)	$\Delta\tau$ (s)	$\Delta\tau_{min}$ (s)	α (V·m/C)	$\Delta\alpha$ (V·m/C)	p (C·m)	W_0, J	n (m^{-3})
P(VDF-TrFE)	$2\cdot10^{-11}$	$1\cdot10^{-9}$	$1\cdot10^{-13}$	$4.0\cdot10^{-9}$	$<0.05\cdot10^{-9}$	$15\cdot10^{-30}$	$5\cdot10^{-20}$	$1.9\cdot10^{-28}$
20 vol. % P(VDF-TrFE)/BPZT		$1\cdot10^{-8}$	$1\cdot10^{-13}$	$5.5\cdot10^{-9}$	$0.95\cdot10^{-9}$	$23\cdot10^{-30}$	$4\cdot10^{-20}$	$2.0\cdot10^{-27}$

Robels et al. have shown that the depolarization field effect can lead to the loop tilting for the case of unscreened dielectric particles in a dielectric matrix [136]. However, we mainly rely on the result that depolarization effects in a ferroelectric composites "particles/ultra-thin screening charge layer/ matrix" do not lead to the noticeable loop tilting [137]. There are two main physical

reasons for averaging: (a) local mesoscopic disorder inherent to pure P(VDF-TrFE) due to semi-crystallinity and coexistence of polar and nonpolar phases, and (b) local strains and screening charges concentrated around BPZT inclusions. Both these reasons demand a renormalization of Weiss model parameters, primarily α and S. Averaging over different values of the parameter, α (that corresponds to the polarization response to the electric field at the location of the dipoles), was carried out with weighted coefficients corresponding to the normal Gauss distribution. It has been found that the averaging over α leads to the transformation of the squared polarization hysteresis loop into the tilted one [6]. Averaging over the characteristic relaxation times, τ, was performed according to the Gaussian distribution. Generally, the hysteresis loop shape changes appeared under the increasing frequency are very similar for the averaging over α or S. However, the S-averaged dependences demonstrate a slower growth with the increase in frequency. Effective parameters are listed in Table 4.2.1.3.

Table 4.2.1.3. Effective parameters for averaging on α and τ of P(VDF-TrFE) with 20 vol. % of BPZT [6]

Averaging on	Fit parameters						
α	τ_0 (s)	α_{min} (V·m/C)	α_{max} (V·m/C)	α (V·m/C)	p (C·m)	W_0, J	n (m^{-3})
	$2\cdot10^{-11}$	$4.0\cdot10^{-10}$	$4.95\cdot10^{-10}$	$4.75\cdot10^{-10}$	$2.3\cdot10^{-30}$	$5.91\cdot10^{-20}$	$1.85\cdot10^{-28}$
τ	τ_0 (s)	τ_{min} (s)	τ_{max} (s)	α (V·m/C)	p (C·m)	W_0, J	n (m^{-3})
	$2\cdot10^{-11}$	$1\cdot10^{-13}$	$1\cdot10^{-10}$	$1\cdot10^{-10}$	$4.65\cdot10^{-30}$	$5.8\cdot10^{-20}$	$1.25\cdot10^{-28}$

We assume a strong dispersion of the coupling constant α for 20 vol. % P(VDF-TrFE)/ BPZT. Following Kliem and Kuehn [135], the Curie temperature $T_C = \frac{n \cdot p^2 \alpha}{k}$ in the Weiss model. Since the parameters n and p are regarded constant, the relation leads to a strong dispersion of T_C. Actually, without

inclusions we have obtained that $\Delta\alpha < 0.05 \cdot 10^9$ Vm/C in the pure P(VDF-TrFE) and $\Delta\alpha = 0.95 \cdot 109$ Vm/C in the 20 vol. % P(VDF-TrFE)/ BPZT.

The physical manifestation of such a dispersion should be a variation of T_C in the PVDF-TrFE regions close to inorganic inclusions due to the local disorder created by the latter. In particular, inhomogeneous elastic fields that exist around BPZT particles lead to the additional dispersion of α due to the e.g. electrostriction mechanism [137]. Experimentally, the dispersion of T_C can result in a broadening of the peak on temperature dependence of the dielectric permittivity. Nevertheless, no significant difference between the width of the dielectric permittivity maximum for the pure and composite films has been observed.

In other words, the strong dispersion of the mean field constant, $\Delta\alpha = 0.95 \cdot 10^9$ Vm/C, for the case of composite is closely related to the local increase of the dielectric susceptibility, which takes place at the nanoscale in the vicinity the BPZT inclusions. Further, it effectively becomes macroscale due to the long-range nature of the inhomogeneous elastic and electric fields occurring at the interfaces between the polymer matrix and ceramic inclusions. Nothing similar happens in the pure P(VDF-TrFE) polymer, where $\Delta\alpha < 0.05 \cdot 10^9$ Vm/C.

Averaged polarization hysteresis loops for the pure polymer and composite samples calculated at room temperature and different frequencies of applied voltage are shown in Figures 4.2.1.3a and 4.2.1.3c, respectively.

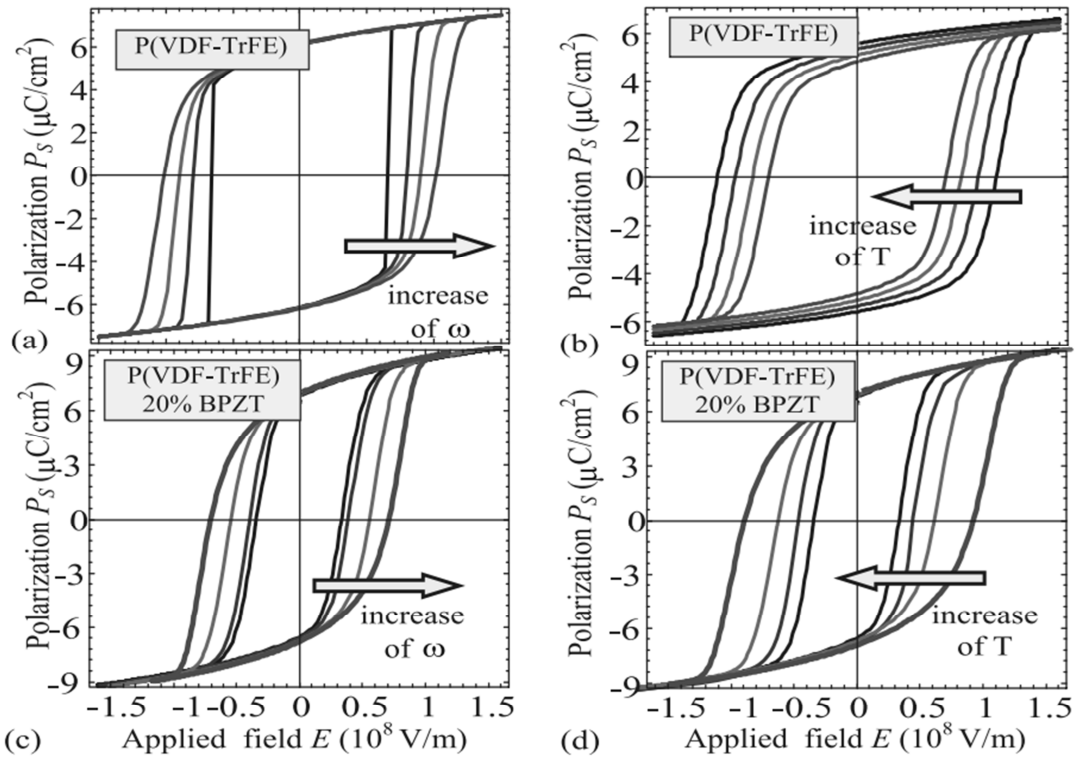

Figure 4.2.1.3. Averaged polarization hysteresis loops of PVDF-TrFE ((a) and (b)) and P(VDF-TrFE) with 20 vol. % of BPZT ((c) and (d)). Loops (a) and (c) are calculated at temperature 300 K for frequency values ω = 0.001, 1, 10, and 50 Hz. Loops (b) and (d) are calculated at frequency ω = 50 Hz for different temperatures T = 290 K, 295 K, 300 K and 305 K. Effective parameters are listed in Table 4.2.3 [6].

The loops of the P(VDF-TrFE) copolymer have almost rectangular shape, and their tilt increases slowly with the frequency, while the composite loops are more tilted and their shape is more sensitive to the frequency changes. The trend is in a qualitative agreement with the experimental data (compare Figs. 4.2.1.3a and 4.2.1.3c with Figs. 4.2.1.1a and 4.2.1.1b). The averaged polarization hysteresis loops of the pure polymer and the composite calculated at different temperatures and fixed frequencies of applied voltage are shown in Figures 4.2.1.3b and 4.2.1.3d, respectively. The loops of P(VDF-TrFE) have almost rectangular shape, and their width decreases with the temperature, while the composite loops are noticeably tilted and their width is more sensitive to

the temperature changes. For both materials, the coercive field and remanent polarization monotonically increases with increasing frequency (Fig. 4.2.1.4a and Fig. 4.2.1.4b). At the same time, the remanent polarization monotonically decreases with the increase in the temperature (Fig. 4.2.1.4c and Fig. 4.2.1.4d).

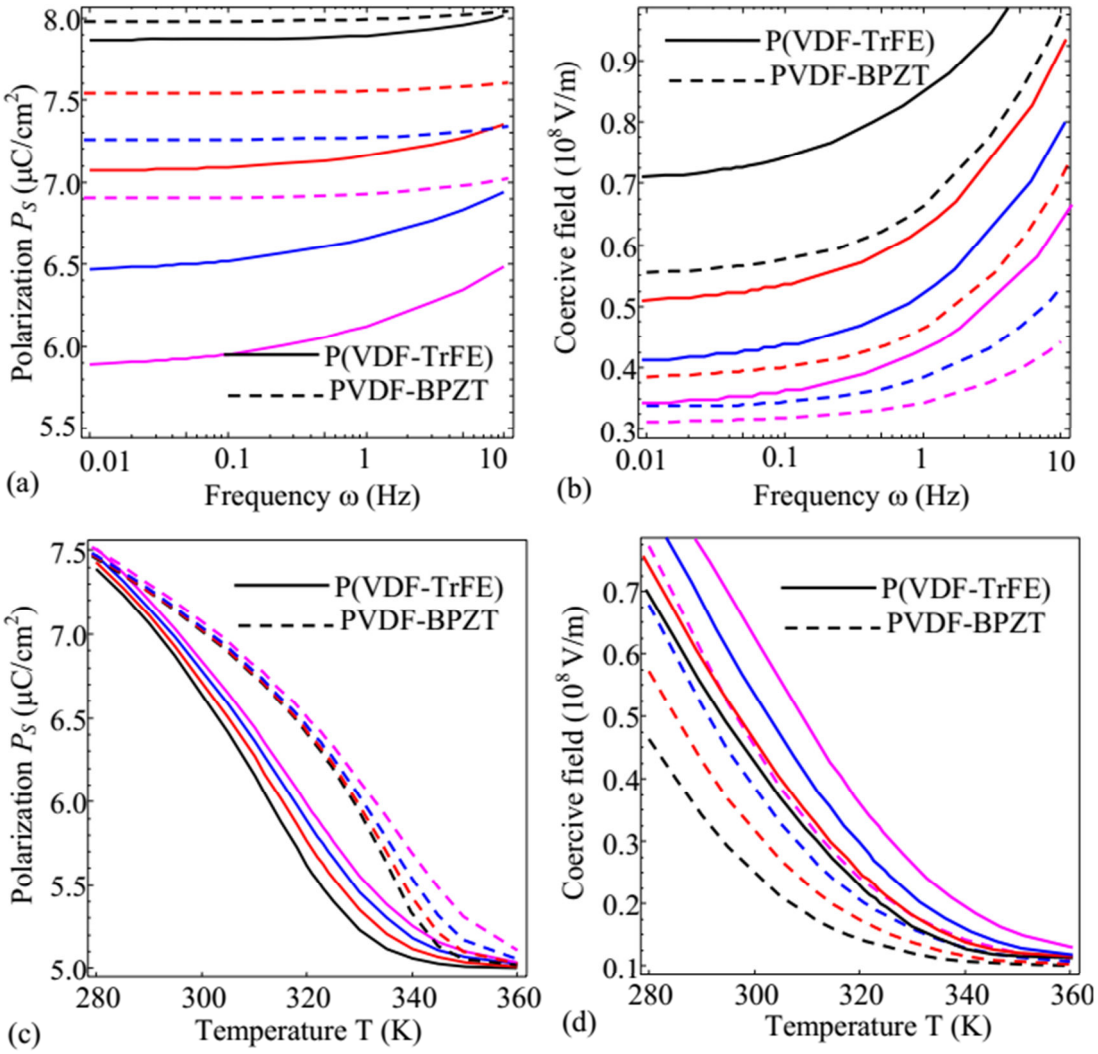

Figure 4.2.1.4. Remanent polarization (a,c) and coercive field (b,d) dependences vs. frequency ω (Hz) (a,b) and temperature T (c,d). Different curves (black, red, blue and magenta) in the plots (a,b) correspond to the temperatures T= 280 K, 300 K, 310 K and 320 K. (c,d) Different curves (black, red, blue and magenta) in the plots (c,d) correspond to the frequencies ω=100 Hz, 300 Hz, 600 Hz, 1000 Hz. Other parameters are listed in the Table 4.2.3.

In a qualitative agreement with the experiment, the coercive field of the composite is smaller than that of the copolymer. The coercive field

demonstrates exponential growth upon cooling; the trend is in an agreement with the experiment (compare Fig. 4.2.1.3d with Fig. 4.2.1.1d). This is unlike the remanent polarization, which changes according to a more complicated law. The main difference appears in the frequency dependence, where the simulated results demonstrate more sharp changes with the frequency than the experimental results.

There are two most important experimental facts that should be taken into account when explaining the differences between polarization reversal in copolymer and the composite. First, BPZT has at least one order of magnitude larger dielectric permittivity (two orders close to room temperature) [138, 139]. Second, according to previous results, the inclusions are modifying properties of P(VDF-TrFE) in their immediate vicinity [2].

The first fact means that the electric field inside the inclusions is close to zero. This was demonstrated by simulations for the case of ferroelectric inclusions in an epoxy resin matrix [140]. Those results showed that the effective dielectric properties are related only to enhancement of the average local field in the low permittivity matrix. The same should take place in our case, if the distortions of molecular chains and its consequences are also negligible from the total energy point of view. As a result, the effective coercive field would be smaller, since absence of the field in some parts of the composite would lead to its enhancements in the others, if the total voltage is conserved. Furthermore, the observed reversed polarization of the composite would remain the same, as inclusions at the surface would act in the similar way as very high-ε dielectric particles due to the zero electric field inside them. Dielectric inhomogeneities formed here are responsible for the inhomogeneity of the electric field both under forming the polar state and under polarization reversal.

4.2.1.1 Summary

Ferroelectric based composites of copolymer P(VDF-TrFE) matrix and ceramic BPZT inclusions reveal enhanced ferroelectric properties promising for advanced applications in sensorics. We observed experimentally that BPZT inclusions provide increasing remanent polarization at low frequencies, significantly decreasing coercive field (factor 1.6), and a tilt of the ferroelectric hysteresis loops in the composite. To simulate the observed effects, we modified the mean field Weiss model by introducing the averaging over the dipole interaction constants and relaxation time spectrum. We showed theoretically that the changes of the hysteresis loops' shape and characteristics of the composite originate from the increase in the dielectric susceptibility due to the strong dispersion of the dipole interaction constant α. This is closely related to the local increase of the susceptibility arising in the vicinity of the BPZT micro-inclusions. Further, it effectively becomes macroscale due to the long-range nature of the inhomogeneous elastic and electric fields occurring at the matrix-inclusion interfaces.

4.2.2 Dielectric, ferroelectric and piezoelectric investigation

Investigation of dielectric spectroscopy for P(VDF-TrFE)/BPZT composites with various volume fractions of fillers was performed over wide frequency and temperature ranges, i.e. 20 Hz- 40 GHz and 110 K- 400 K, respectively (Fig. 4.2.2.1(a) and Fig. 4.2.2.1(b)).

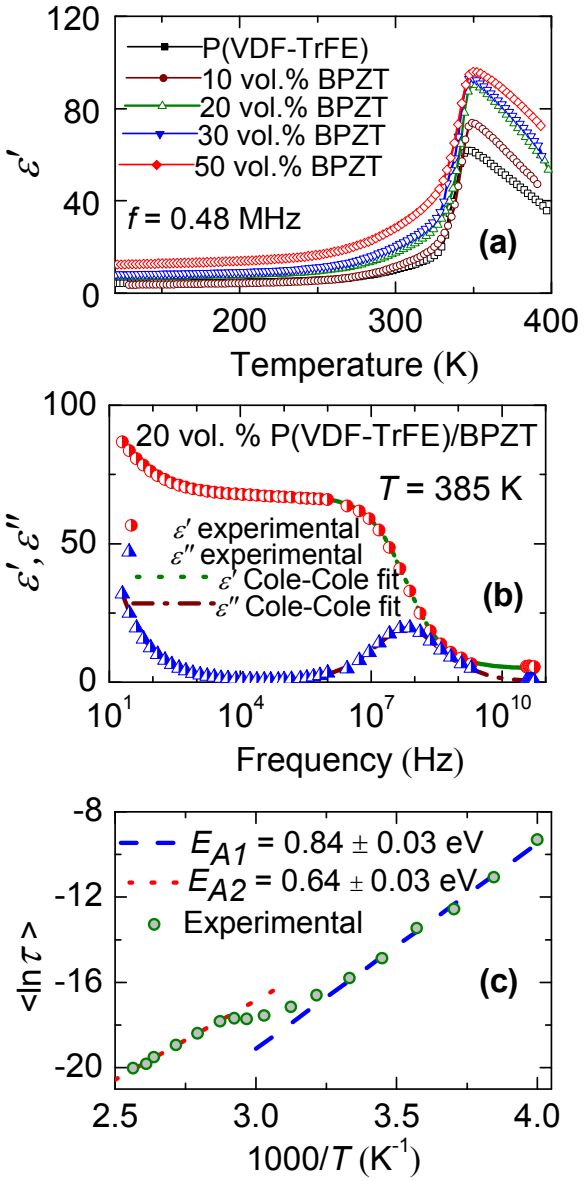

Figure 4.2.2.1. Temperature dependences of the real part of the complex dielectric permittivity for the neat P(VDF-TrFE) and the P(VDF-TrFE)/BPZT composites on cooling at 0.48 MHz (a). Frequency dependence of the real and imaginary parts of the complex dielectric permittivity for 20 vol. % P(VDF-TrFE)/BPZT obtained at 385 K on cooling (b). Temperature dependence of the mean dielectric relaxation time for 20 vol. % P(VDF-TrFE)/BPZT (c).

The frequency and temperature dependences of dielectric permittivity in P(VDF-TrFE)/BPZT composites have been analysed employing Cole-Cole formalism [74] (Eq. 2.6.3) (Fig. 4.2.2.1(b)). The best fit of experimental curves to Eq. (2.6.3) is presented in Fig. 4.2.2.1c as solid lines. The relaxation time derived from Eq. (4.2.2.1) is considered as the most probable mean relaxation time ($<\ln \tau_{AV}>= \ln \tau$)[76].

It is found, that the temperature dependence of the mean dielectric relaxation time may be discussed by two Arrhenius plots separated in the point of paraelectric-ferroelectric phase transition (Eq. 2.6.7) [77, 78]. The activation energy fit parameters for dielectric relaxation in P(VDF-TrFE) based composites obtained from the best fit in two temperature regions are listed in Table 4.2.2.1. As seen from the Table 4.2.2.1, no significant change of the activation energy on the filler volume fraction has been observed. Similar results for pure P(VDF-TrFE) were obtained by N. Koizumi et al. [19].

Table 4.2.2.1. Arrhenius fit Parameters of Dielectric Relaxation in P(VDF-TrFE) based composites

Material	E_{A1} (eV)[a]	E_{A2} (eV)[b]
P(VDF-TrFE)	0.82±0.01	0.58±0.01
10 vol. % BPZT	0.83±0.03	0.58±0.02
20 vol. % BPZT	0.84±0.03	0.64±0.03
30 vol. % BPZT	0.84±0.02	0.60±0.03
50 vol. % BPZT	0.87±0.02	0.52±0.02

[a] E_{A1} is the activation energy of a material in a ferroelectric phase

[b] E_{A2} is the activation energy of a material in a paraelectric phase

The dielectric dispersion of the imaginary part of the complex dielectric permittivity has been observed for the composite below room temperature and is presented in Fig. 4.2.2.2(a).

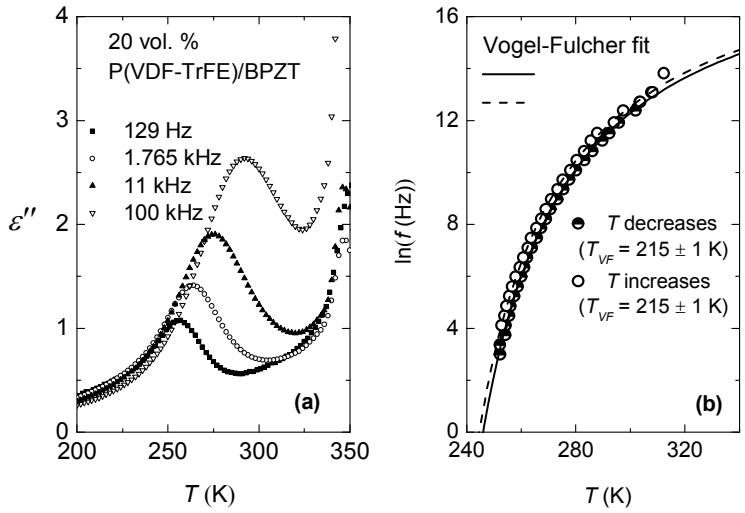

Figure 4.2.2.2. Temperature dependence of the dielectric losses at different frequencies (129 Hz – 0.1 MHz) on cooling (a), measurements frequency versus the dielectric losses maximum temperature for 20 vol. % P(VDF-TrFE)/BPZT composite on cooling and heating (b). Solid lines are the best fit according to the Vogel-Fulcher law (Eq. (4.1.2)).

The anomaly shows dipolar-glass-like behaviour attributed to the glass transition of the polymer matrix [7, 9, 38]. The peak increases and shifts to higher temperatures with increasing the frequency. These results are consistent with those presented elsewhere [9, 19, 38, 141, 142]. The temperature behaviour of dielectric losses has been discussed employing Vogel-Fulcher formalism (FV) both on cooling and heating cycles (Fig. 4.2.2.2(b)) (Eq. 4.1.2) [77, 78].

It is found that the Vogel-Fucher temperature (T_{VF}) attributed to the static glass transition temperature is not dependent on adding the fillers and remains equal to 215 K (Fig. 4.2.2.2(b)).

Figure 4.2.2.3(a) shows temperature dependences of real part of the effective dielectric permittivity for the neat P(VDF-TrFE) and P(VDF-TrFE)/BPZT composites on cooling at 480 kHz frequency. The values of ε' were normalized with respect to the absolute values of the neat polymer matrix ($\varepsilon'_{\text{matrix}}$). The dependence of the ratio of composite's real part of the effective permittivity to the matrix's permittivity remains almost constant in the

temperature range below the Curie temperature of P(VDF-TrFE). Therefore, only this temperature range will be considered in the further study.

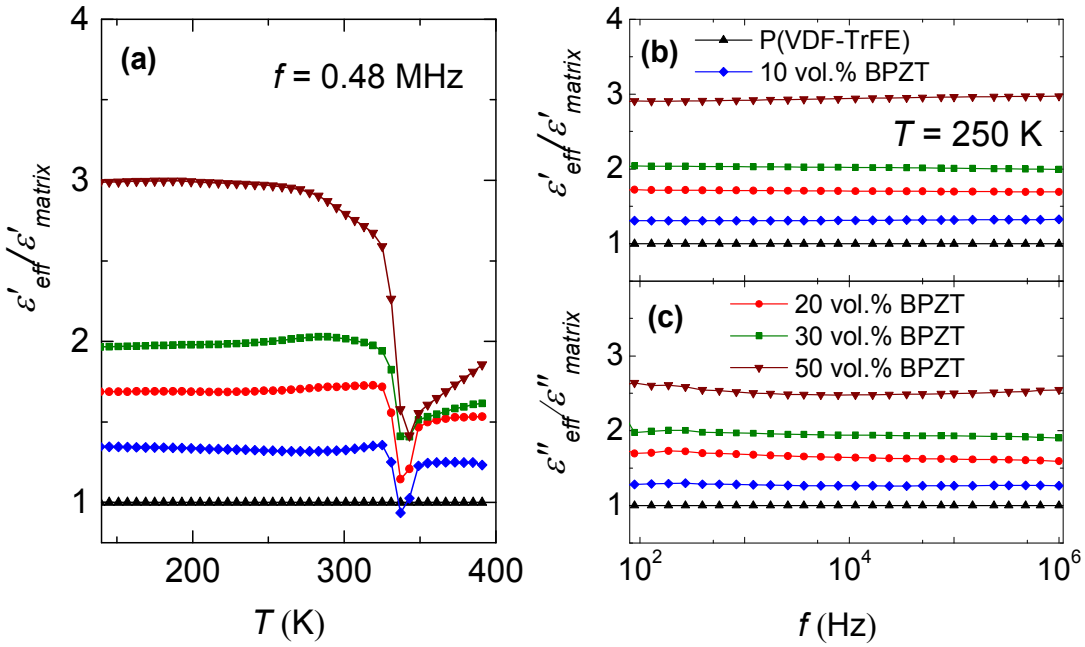

Figure 4.2.2.3. Temperature dependence of the normalized real part of the complex dielectric permittivity for the neat P(VDF-TrFE) and P(VDF-TrFE)/BPZT composites on cooling (0.48 MHz) (a). Frequency dependence of the normalized real (b) and imaginary (c) parts of the complex dielectric permittivity for the neat P(VDF-TrFE) and P(VDF-TrFE)/BPZT composites (T = 250 K). All values of ε' and ε'' were normalized with respect to the absolute values of the neat P(VDF-TrFE).

It is known, that the effective dielectric constant in composite materials is dependent on the geometry of embedded fillers [143, 144]. The BPZT inclusions in our composites had a spherical shape with the average particle size ~0.5 μm [2, 6]. It is clearly seen that the ratio of the effective permittivity of the composite to the matrix permittivity remains the same in a wide frequency range (Fig. 4.2.2.3(b) and Fig. 4.2.2.3(c)). Therefore, one frequency (0.48 MHz) and one temperature (250 K) will be considered in a temperature range below T_C for the neat P(VDF-TrFE) and the P(VDF-TrFE)/BPZT composites. Based on this approach, the dependence of the effective permittivity $\varepsilon^{\alpha}_{eff}$ was

analysed in terms of Lichtenecker effective medium approximation model [145, 146].

$$\varepsilon_{eff}^{\alpha} = V_h \varepsilon_h^{\alpha} + (1 - V_h)\varepsilon_l^{\alpha} \quad (4.2.2.1)$$

where ε^{α}_h and ε^{α}_l are the relative dielectric constants of the high-dielectric phase (BPZT fillers) and low-dielectric phase (PVDF-TrFE copolymer), respectively, V_h is the volume fraction of the high dielectric phase and α is a parameter that determines the type of mixing rule. As the fillers' concentration in the composite is small (V_h) the model between the serial ($\alpha = -1$) and homogeneous ($\alpha = 0$) distribution of particles within the composite has been applied ($-1<\alpha<0$). According to the electrodynamic boundary condition between the BPZT fillers inside the polymer matrix $\mathbf{D}_{BPZT} = \mathbf{D}_{P(VDF\text{-}TrFE}$, where **D** is the dipolar displacement, and considering that the dielectric permittivity of inclusions is much higher than of the polymer matrix($\varepsilon_h >> \varepsilon_l$), the Eq. (4.2.2.1) simplifies and becomes dependent only on the fillers' volume fraction and α:

$$\frac{\varepsilon_{eff}}{\varepsilon_l} = (1 - V_h)^{\frac{1}{\alpha}} \quad (4.2.2.2)$$

As the fit parameters α in Eq. (4.2.2.2) do not depend on temperature below T_C, therefore the dependence of effective permittivity for low concentrations can be analysed by a single fit. It is clearly seen from Figure (4.2.2.4) that the model (solid lines) can be applied for lower concentrations of BPZT fillers in P(VDF-TrFE)/BPZT composites.

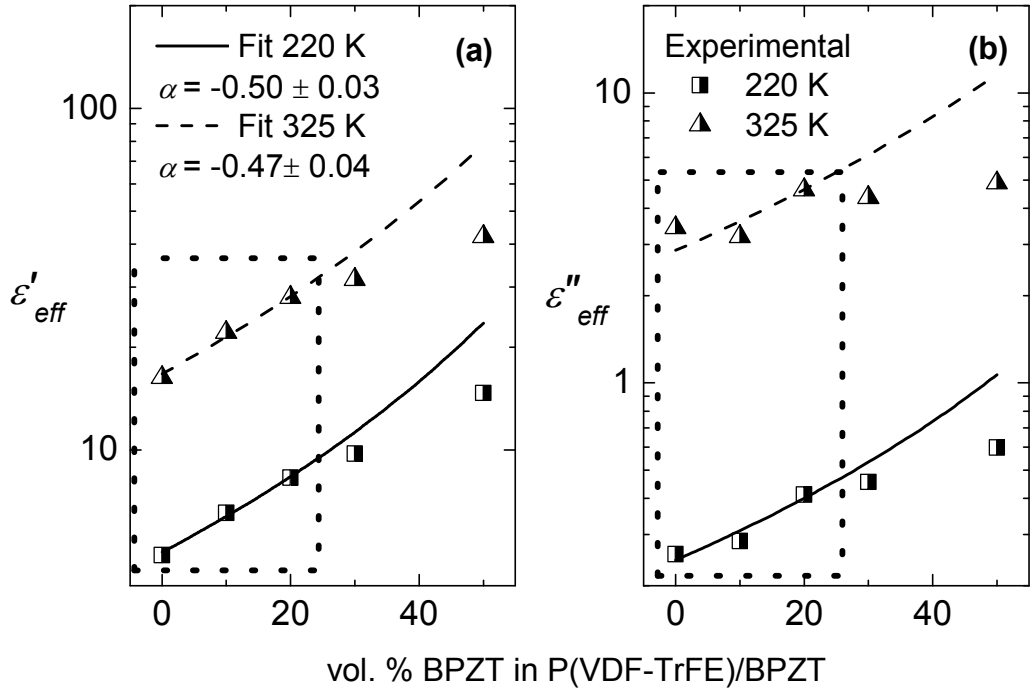

Figure 4.2.2.4. Dependence of the real (a) and imaginary (b) parts of effective dielectric permittivity on the concentration of BPZT on cooling at 220 K and 325 K. Solid lines are calculated according to Eq. (4.2.2.2).

A possible model for particle distribution within P(VDF-TrFE)/BPZT composites below 20 vol. % of BPZT is presented in Figure (4.2.2.5).

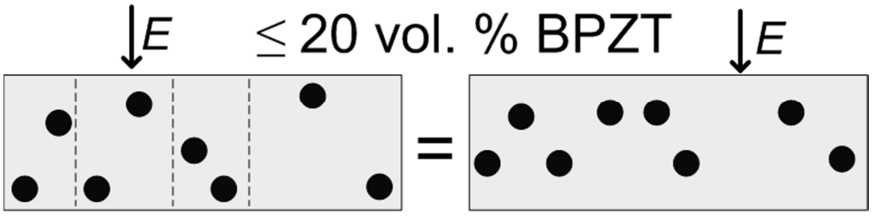

Figure 4.2.2.5. A possible Lichtenecker model of filler distribution within the composite film for concentrations below 20 vol. % BPZT. The arrows denote the direction of electric field polarization.

Although the behaviour of composites with higher concentrations of inclusions cannot be analysed by the model due to unknown distribution of

particles within the copolymer. In the case of concentrations above 30 vol. % the distribution of fillers can be different within the bottom and the upper parts of the composite film, i.e. can percolate on the bottom.

In order to perform a more detailed elucidation of the proposed model the impact of filler concentration on the shape of ferroelectric hysteresis loop was also studied. Because of a good agreement between the experimental values and Lichtenecker's model (with an approach of a high difference between dielectric permittivity of BPZT fillers and P(VDF-TrFE) copolymer) only concentrations below 20 percent of volume fraction of BPZT are considered in further discussions of ferroelectric characterization. The decrease of positive (E_C+) and negative (E_C-) coercive electric fields can be clearly observed in Figure 6(a).

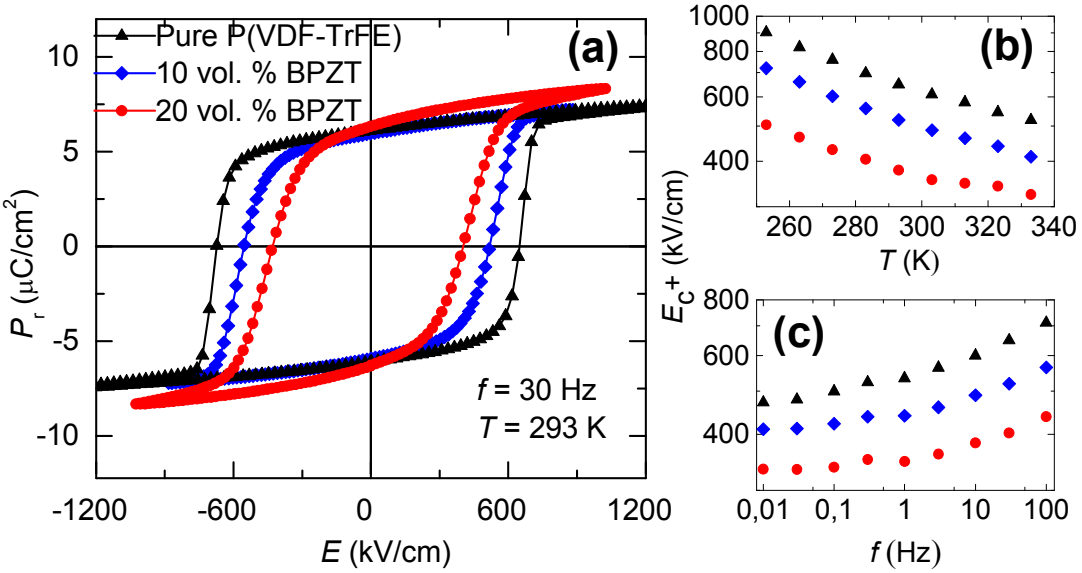

Figure 4.2.2.6. Ferroelectric loops of pure P(VDF-TrFE) and P(VDF-TrFE)/BPZT composites at f = 30 Hz and T = 293 K (a), temperature (b) and frequency (a) dependences of coercive electric field of pure P(VDF-TrFE) and P(VDF-TrFE)/BPZT composites.

It is seen that the ratio between the E_C+ of the composites and the polymer matrix remains the same in broad temperature and frequency ranges (Fig.

4.2.2.6(b) and Fig. 4.2.2.6(c)). The dependence of the reciprocal ratio of coercive field between the pure P(VDF-TrFE) and its based composites is shown in Figure 4.2.2. 7.

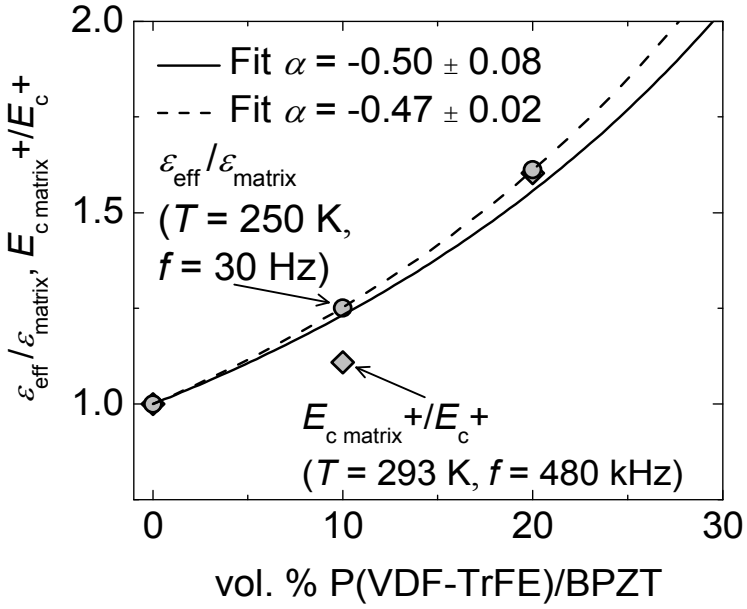

Figure 4.2.2.7. Concentration dependences for the ratio of effective dielectric constant of P(VDF-TrFE)/BPZT composites to the ε_{eff} of P(VDF-TrFE) and reciprocal ratio of positive coercive electric field of P(VDF-TrFE)/BPZT composites to E_C+of P(VDF-TrFE) (blue and red symbols, respectively). Solid lines are calculated according to Eq. (4.2.2.2).

The dependence of the coercive electric field on the BPZT concentration in the composites is also analysed by an analogous model considering that the coercive electric field of the polymer matrix $E_{\text{C matrix}}$ is much higher than the coercive electric field of the inclusions $E_{\text{C BPZT}}$ ($E_{\text{C matrix}} >> E_{\text{C BPZT}}$). It is clearly seen that the dependences of $\varepsilon_{eff}/\varepsilon_{\text{matrix}}$ and $E_{\text{C matrix}}/E_{\text{C}}$ ratios have similar fit parameters (Fig. 4.2.2.7). This can be explained by considering the boundary condition with absence of charges in the interface between BPZT fillers and the polymer matrix, i.e. $\varepsilon_l\varepsilon_0\boldsymbol{E}_l = \varepsilon_h\varepsilon_0\boldsymbol{E}_h$. Here indices l and h have the same meaning as in Equation (4). The higher dielectric permittivity (ε_h) the fillers

have, the higher electric field is concentrated in the polymer matrix of the composite ($\boldsymbol{E_l}$).

To be compared, P(VDF-TrFE) based composites with fillers of low dielectric permittivity ($LiNbO_3$) have also been studied. Temperature dependence of the normalized real part of the complex dielectric permittivity for the neat P(VDF-TrFE) and P(VDF-TrFE)/$LiNbO_3$ composites on cooling are presented in Fig. 4.2.2.8a. Frequency dependences of the normalized real and imaginary parts of the complex dielectric permittivity at $T = 250$ K are also shown (Fig. 4.2.2.8a and Fig. 4.2.2.8b). All values of ε' and ε'' were normalized with respect to the absolute values of the neat P(VDF-TrFE). As we see, the aforementioned Lichtenecker's model cannot be applied to analyse the temperature and frequency dependences of copolymer based composites with fillers of dielectric constant, that is of the same order as ε of P(VDF-TrFE). It follows, that the model can only be applied upon an approach of a high difference between dielectric permittivity of the fillers and the copolymer matrix.

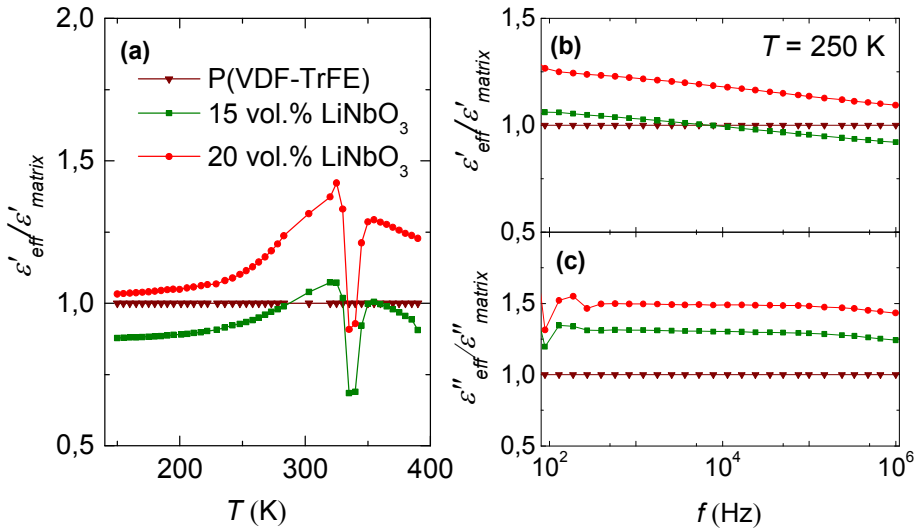

Figure 4.2.2.8.Temperature dependence of the normalized real part of the complex dielectric permittivity for the neat P(VDF-TrFE) and P(VDF-TrFE)/$LiNbO_3$ composites on cooling (0.48 MHz) (a). Frequency dependence of the normalized real (b) and imaginary (b) parts of the complex dielectric permittivity for the neat P(VDF-TrFE) and P(VDF-TrFE)/ $LiNbO_3$ composites (T = 250 K). All values of ε' and ε'' were normalized with respect to the absolute values of the neat P(VDF-TrFE).

Piezoelectric strain coefficients at various temperatures also were calculated from measuring the displacement of the pre-polarized samples under bipolar triangle driving voltage.

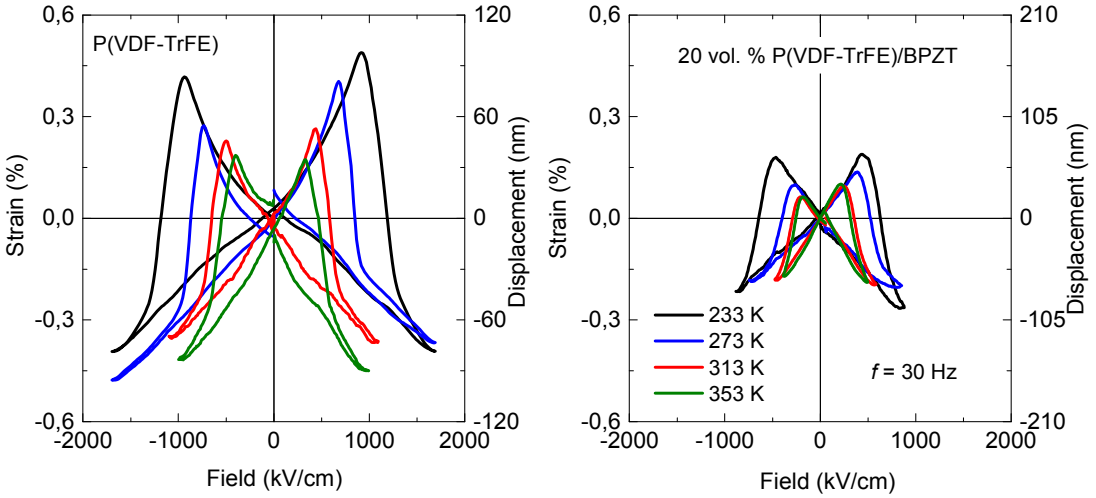

Figure 4.2.2.9. Strain and mechanical displacement dependence on electric field of P(VDF-TrFE) and 20 vol. % P(VDF-TrFE)/BPZT composites at different temperatures (233 K, 273 K, 313 K and 353 K)

No significant impact of concentrations below 20% volume fraction on piezoelectric coefficients in the composites was observed (Fig. 4.2.2.10a).

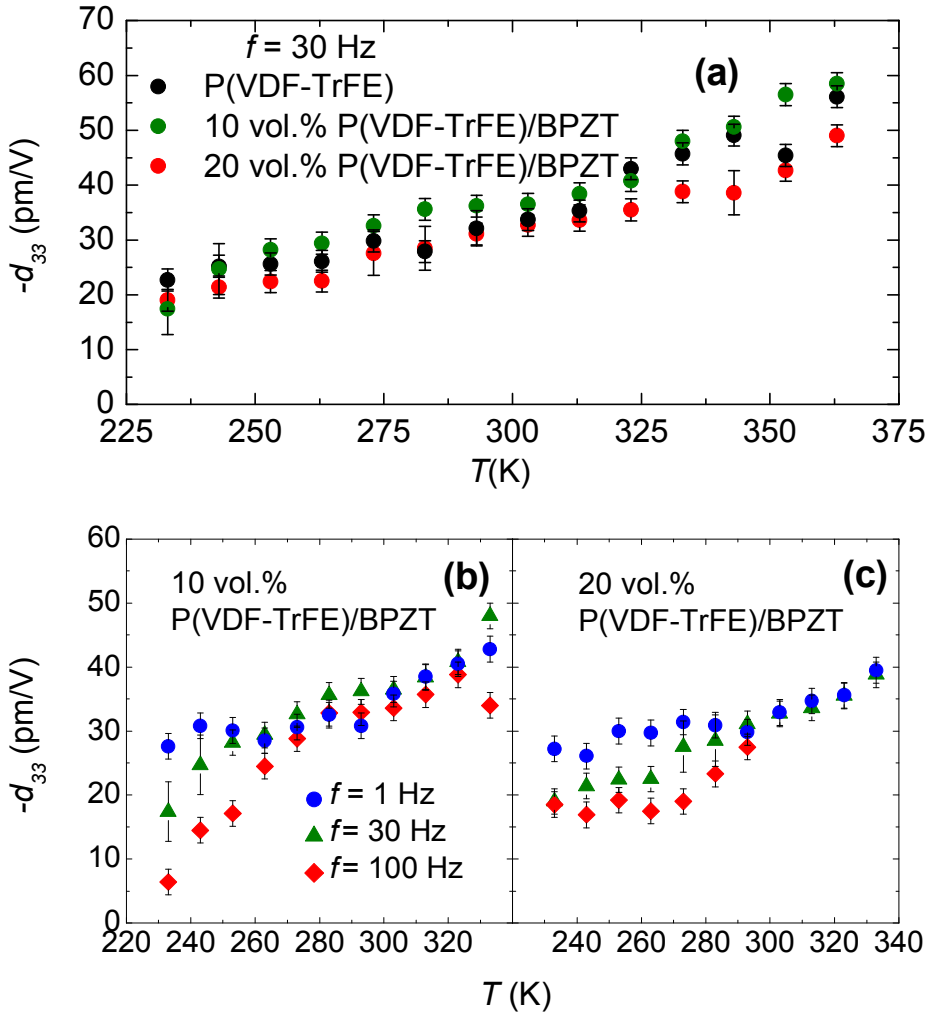

Figure 4.2.2.10. Temperature dependence of piezoelectric strain coefficients of the neat P(VDF-TrFE) and P(VDF-TrFE)/BPZT composites (f = 30 Hz) (a). Temperature dependence of piezoelectric strain coefficient of the neat 10 vol. % P(VDF-TrFE)/ BPZT (b)and 20 vol. % P(VDF-TrFE)/BPZT (c) composites at various frequencies.

This could be explained by the previously discussed model, i.e. the high dielectric permittivity of inclusions in comparison to the low ε of the matrix results in a big difference of voltage distribution within the composites. As the displacement directly depends on the voltage, no significant change is observed. From the above results, it appears that the applied external electric field is mainly distributed in the polymer matrix, meanwhile, the BPZT particles remain unpolarized.

Moreover, a frequency dependence of the piezoelectric strain coefficients in the composites below room temperature was observed (Fig. 4.2.2.10(b) and Fig. 4.2.2.10(c)) and is attributed to the dielectric dispersion of the imaginary part of the complex dielectric permittivity in the composite (Fig. 4.2.2.2a). The anomaly showing dipolar-glass-like behaviour is attributed to the shift of dynamic glass transition of the polymer matrix on the frequency [9, 38, 142].

4.2.2.1 Summary

We have studied the ferroelectric, the dielectric and the piezoelectric properties of P(VDF-TrFE) polymer matrix with fillers of high dielectric permittivity. Our investigations show that the complex dielectric permittivity (ε^*) of P(VDF-TrFE)/BPZT composites with smaller filler concentrations ($\leq$ 20 vol. %) obeys the Lichtenecker's mixing rule ($\alpha < 0$). The composites containing a higher concentration of the fillers have high dielectric loss peaks, related to the dielectric anomalies of the glass and ferroelectric-paraelectric phase transitions. Embedding BPZT fillers to the P(VDF-TrFE) polymer matrix increases the effective dielectric permittivity and decreases the coercive electric field (E_c) of the composite according to the electrodynamic boundary conditions. Since the permittivity of the polymer is much lower than of the permittivity of the fillers, the proposed mixing rule can also be applied to explain the passive behaviour of ceramic particles in the composites. Also, we have demonstrated the frequency dependence of the piezoelectric coefficients below room temperature, which, we assume, is related to the glass transition of the polymer matrix.

4.2.3 Ultrasonic spectroscopy

It is known that when P(VDF-TrFE) films are annealed at temperatures higher than their melting temperature, T_m, with having the highest chain mobility and cooled down, the recrystallization, even with the same molar ratio, drastically affects the morphology of the copolymer [34, 105, 147, 148]. Moreover, annealing for a long period may considerably increase T_m of the polymer matrix [34]. Both effects may result in changes of Young's modulus, piezoelectric properties and the ferroelectric Curie temperature, T_C [14, 33, 36, 37, 149]. Therefore, in order to retain the structure invariant, it was necessary not to exceed T_m during heating of the samples.

In Fig. 4.2.3.1, an experimental temperature dependence of the longitudinal wave velocity in the neat P(VDF-TrFE) polymer is presented. It is clearly seen that the dependence is comprised of two step-like regions. The first one, at lower temperature, is related to the paraelectric-ferroelectric phase transition of the crystallized part of the polymer [1, 34, 38, 90-92]. The second region, at higher temperatures, corresponds to melting of the P(VDF-TrFE) sample. A rapid increase of the ultrasonic velocity above T= 420 K is explained by the change in the thickness of the compressed sample due to a decreasing polymer viscosity.

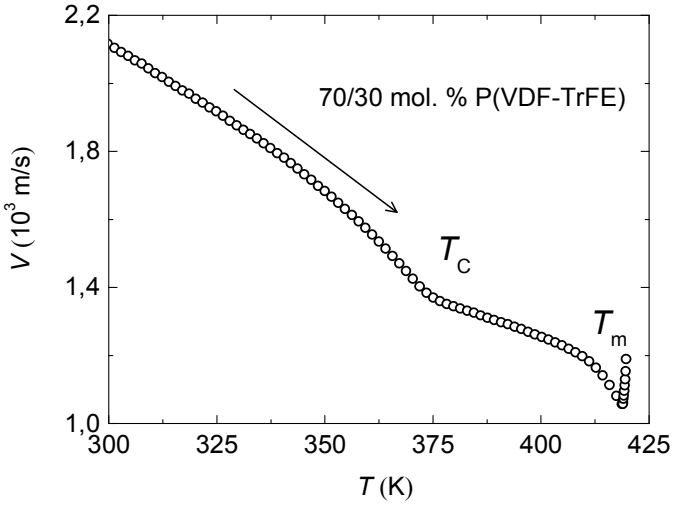

Figure. 4.2.3.1. Temperature dependence of ultrasonic velocity in the pure P(VDF-TrFE) copolymer

DSC measurements of the neat P(VDF-TrFE) also show a set of anomalies that are attributed to the first order ferroelectric phase transition (at T_{C1} on cooling and T_{C2} on heating), melting at T_m temperature on heating, and crystallization at T_{Cr} on cooling (Fig. 4.2.3.2).

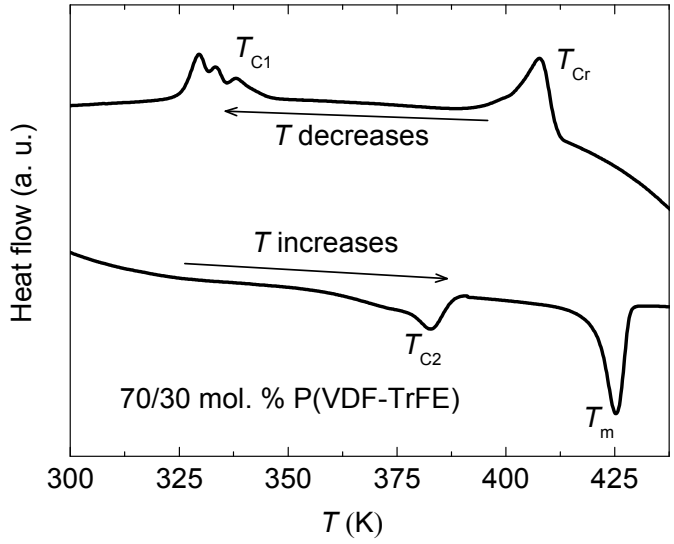

Figure. 4.2.3.2. Results of differential scanning calorimetry measurements of the P(VDF-TrFE) copolymer

In addition to the main peak at T_{C2}, a broad shoulder at lower temperatures can be seen in the DSC thermogram of the copolymer on heating (Fig. 4.2.3.2). Various mechanisms related to this phenomenon were discussed by R. L. Moreira et al. [33, 36, 37]. It can be attributed to the presence of the conformational TrFE-dependent intra-chain defects with fast mobility or, possibly, to existence of an intermediate phase. Furthermore, three satellite peaks are observed on cooling near T_{C1} (Fig. 4.2.3.2). They probably indicate the existence of the intermediate crystalline γ-phase with trans-gauche (T_3GT_3G')- like conformation and its transformation to the ferroelectric β -phase, resulting in precedence of the low-temperature β-phase already above T_{C1}. Another explanation relates these peaks to an increasing amount of imperfect crystallites on cooling after the sample was heated over T_m [33, 36, 37]. In order to remove internal stresses and retain the same morphology, all samples were annealed up to 390 K prior to the ultrasonic or dielectric measurements.

Figures 4.2.3.3 and 4.2.3.4 present attenuation of ultrasonic wave for the neat P(VDF-TrFE) and the P(VDF-TrFE)/BPZT composite with 10 vol. % of BPZT, respectively.

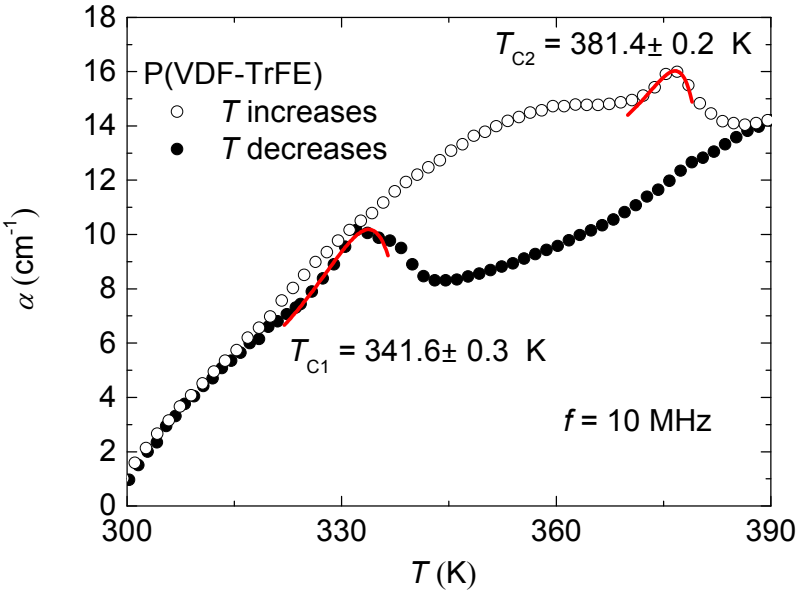

Figure 4.2.3.3. Temperature dependences of ultrasonic attenuation for the neat P(VDF-TrFE). The fitting curves are shown by red colour. T_{C1} and T_{C2} denote the values of Curie temperature on cooling and heating, respectively, which were derived from the best fit with Eq. 4.1.3.

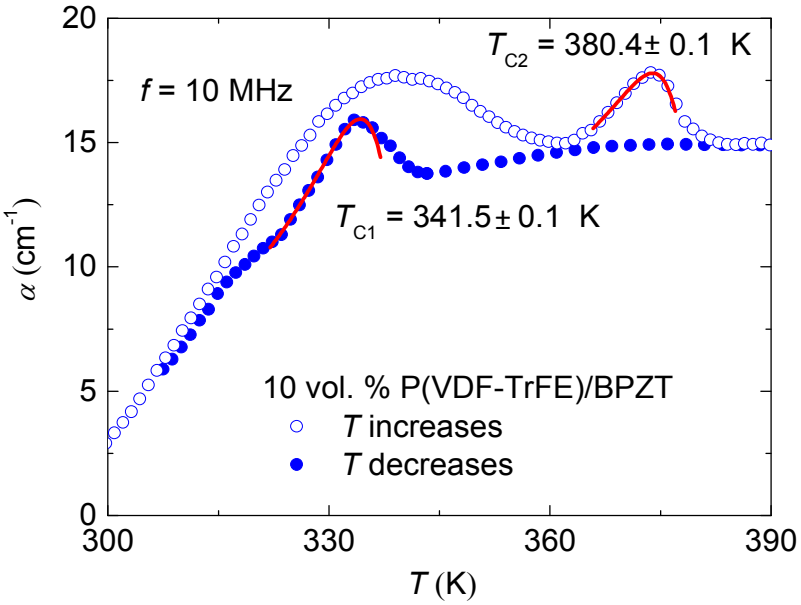

Figure 4.2.3.4. Temperature dependences of ultrasonic attenuation for the 10 vol. % P(VDF-TrFE)/BPZT composite. Fitting curves are shown by red colour. T_{C1} and T_{C2} denote the values of Curie temperature derived from the best fit with Eq. 4.1.3.

Temperature dependence of attenuation of longitudinal US waves propagating in the samples show two pronounced anomalies: a broad peak attributed to the glass transition at T_g and a sharper peak at Curie temperature T_C. The same transition temperatures are revealed by dielectric measurements (Figure 4.2.3.5). The existence of a shoulder above the main attenuation maxima (on cooling) can be a manifestation of either the intermediate crystalline γ-phase or an increasing amount of imperfect crystallites that are responsible for the complicated exothermic peak structure seen in DSC thermograms (Fig. 4.2.3.2) [33, 36, 37].

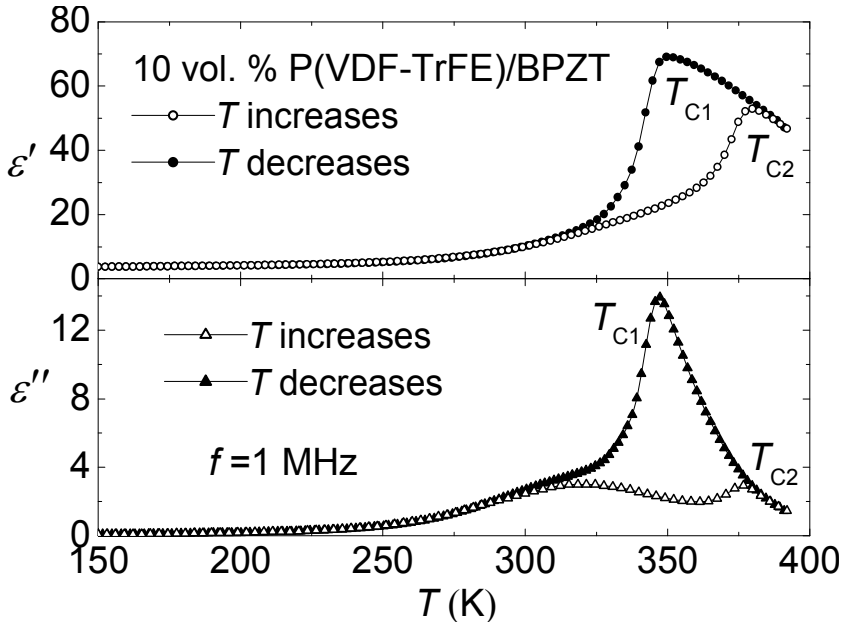

Figure 4.2.3.5. Temperature dependence of the complex dielectric permittivity for the 10 vol. % P(VDF-TrFE)/BPZT composite measured on heating and cooling at 1 MHz frequency.

Broadband dielectric spectroscopy revealed a dipolar-glass-like behaviour of the dielectric loss peaks (Fig. 4.2.3.6), which is known as β-relaxation process related to semicrystalline morphology of the P(VDF-TrFE) matrix [38, 150, 151]. On the contrary, in non-ferroelectric polymers like polydimethylsiloxane (PDMS) this dynamic glass behaviour, referred to as the primary α-relaxation, is due to relatively large-scale cooperative motion of

many backbone segments in the amorphous phase [117, 152]. Strong dielectric dispersion of the imaginary part of the dielectric permittivity is observed in the P(VDF-TrFE) based composites below and above its Curie temperature, both on heating and cooling (Fig. 4.2.3.6). At the same time, no significant anomaly can be seen in the real part of the dielectric permittivity, which indicates that the β-relaxation process has a weakly polar nature [9].

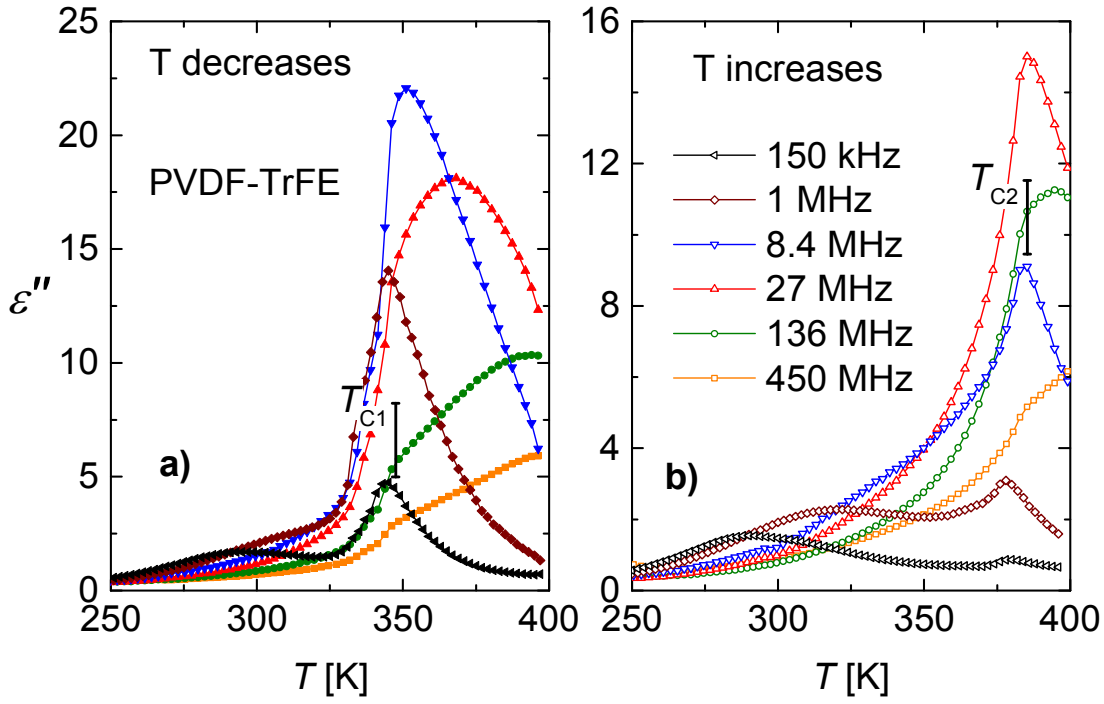

Figure 4.2.3.6. Temperature dependences of the imaginary part of the dielectric permittivity (dielectric losses) for the neat P(VDF-TrFE) on cooling (a) and heating (b) at different frequencies (150 kHz- 450 MHz).

In addition to the broad frequency dependent glass transition peak, the relatively sharp maximum, corresponding to the ferroelectric-paraelectric transition, is observed at lower frequencies at T_{C1}= 345 K on cooling (Fig. 4.2.3.6a) and T_{C2}= 377 K on heating (Fig. 4.2.3.6b). Meanwhile, it seems that this transition-related loss maximum gradually broadens and shifts towards higher temperatures on increasing the frequency. We assume that this is

explained by a dynamic nature of the aforementioned glass transition that also occurs in a vicinity of T_C. As it should be, the loss maximum related to the dynamic glass of the polymer matrix transition also increases with the increasing frequency. For a certain frequency, the anomalies, related to the glass transition and to the ferroelectric- paraelectric transition, superimpose, resulting in the highest values of ε'' of the copolymer. For even larger frequencies, the broad maximum, related to the glass transition, shifts above the Curie temperature.

The ultrasonic attenuation peaks, related to ferroelectric phase transition, are described using the relaxation theory of elasticity [22] (Eq. 4.1.3). Here, we assume that the relaxation time can be expressed from the phenomenological Landau- Khalatnikov theory [22, 81] (Eq. 2.7.10). In our case, the condition $\omega\tau > 1$ was fulfilled in a wide temperature rang far below T_c in the samples with a comparatively long polarization relaxation time prefactor ($\tau_0 = 8 \cdot 10^{-8}$- $1.3 \cdot 10^{-7}$ s·K), that slightly increases with adding the BPZT fillers (on heating $\tau_{0P(VDF\text{-}TrFE)} = 8 \cdot 10^{-8}$ s·K, $\tau_{0\ 10\ vol.\ \%\ P(VDF\text{-}TrFE)/BPZT} = 1.0 \cdot 10^{-7}$ s·K). The phase transition temperatures obtained from the best fit of experimental curves to Eq. 4.1.3 (Fig. 4.2.3.3 and Fig. 4.2.3.4) are consistent with those observed in the dielectric and DSC measurements of the investigated composites (Fig. 4.2.3.7 and Fig. 4.2.3.8).

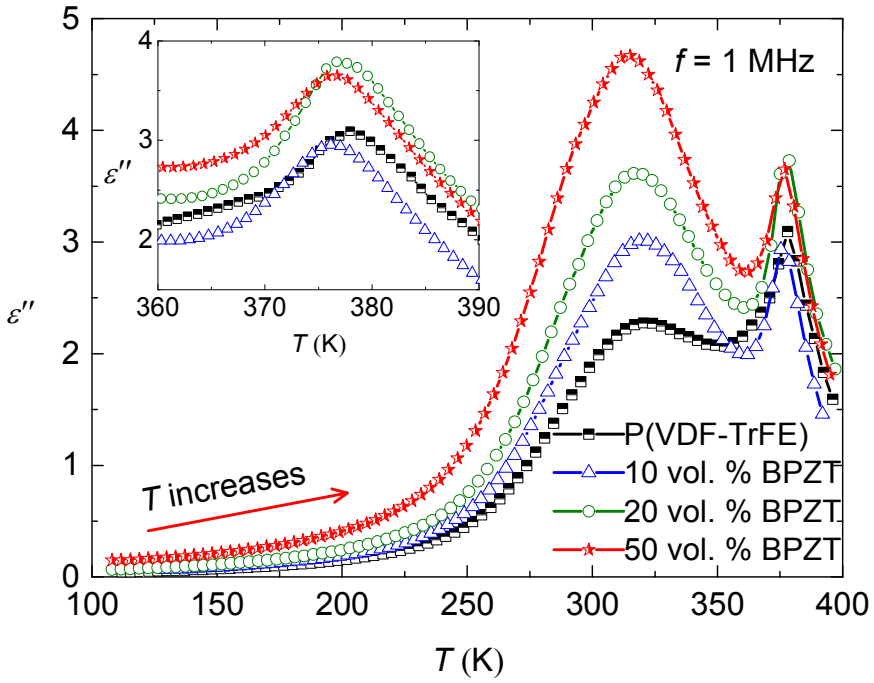

Figure 4.2.3.7. Temperature dependences of ε'' of the neat P(VDF-TrFE) copolymer and the P(VDF-TrFE)/BPZT composites (1 MHz). The inset demonstrates an enlarged view of the dielectric losses near Curie temperature.

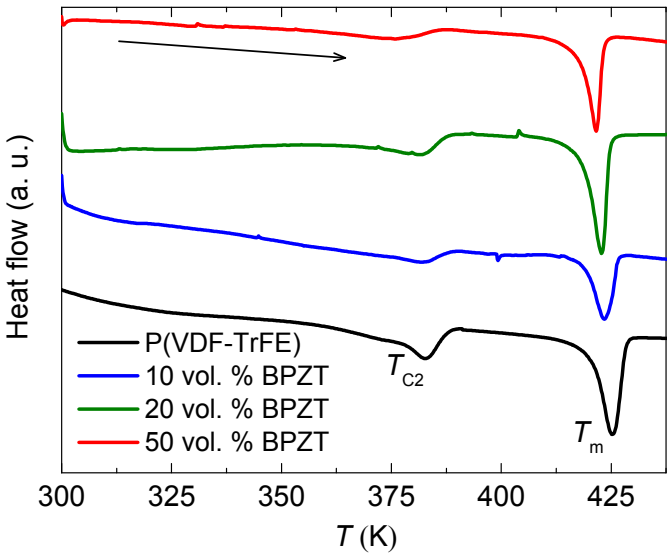

Figure 4.2.3.8. DSC curves for the P(VDF-TrFE) copolymer and the P(VDF-TrFE)/BPZT composites measured on heating.

We found that the addition of the BPZT filler results in a significant increase of the dielectric loss peak at both the dynamic glass transition temperature, T_g, and Curie temperature, T_C. It is supposed that, in the studied composites, the large increase of the dielectric susceptibility is due to the long-range nature of the inhomogeneous elastic and electric fields occurring at the interface (interface width ~40 nm) between the matrix and inclusions [2, 6]. Furthermore, the peak of the dielectric loss maximum associated with the Curie temperature is shifted toward lower temperatures with increasing concentration of BPZT particles (see the inset of Figure 4.2.3.7). This is in a good agreement with the results of the DSC measurements (Fig. 4.2.3.8), where the peak related to the ferroelectric- paraelectric transition also shifts toward lower temperatures for samples containing a larger amount of filler. For the sample with 50 vol. % of PBZT, the DCS peak at the Curie temperature is smeared out. Nevertheless, the shift of T_{C2} to lower temperatures is noticeable. These results are consistent with those obtained from the best fit of the ultrasonic relaxation measurements that also show a decrease of the ferroelectric transition temperature in the composite samples (Fig. 4.2.3.3 and Fig 4.2.3.4). We assume that the change of the Curie temperature with the filler content can be related to defects created by BPZT particles within the polymer, as was discussed above when explaining the additional peaks in the DSC curves [33, 36, 37, 149]. Also, a decrease of the melting temperature in the composites is demonstrated (Fig. 4.2.3.8).

The temperature dependences of the ultrasonic velocity and the piezovoltage, measured on cooling and heating, are presented in Figure 4.2.3.9. As the amplitude of the piezovoltage depends on the intensity of the ultrasonic wave exiting the sample, the value of piezovoltage U/U_{300} was normalized to unity with respect to the absolute amplitude obtained at T = 300 K. After the sample was depolarized at T = 390 K, a constant electric field was applied. Note that the constant electric field could be removed at temperatures higher that room temperature without significant change of the signal.

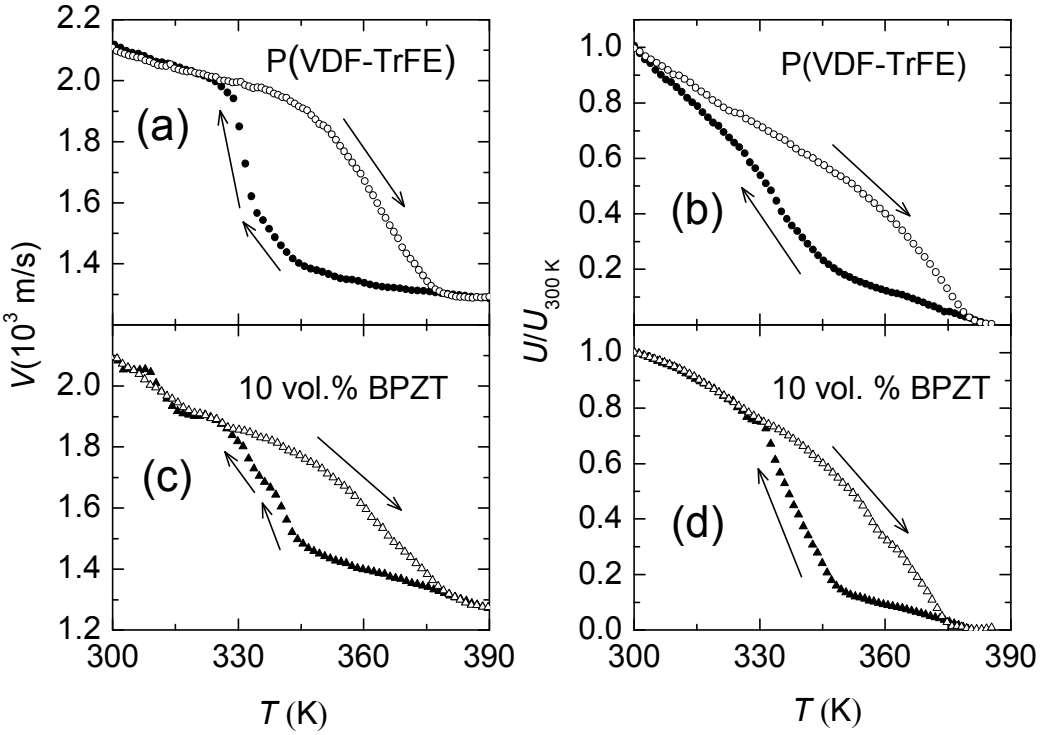

Fig. 4.2.3.9. Temperature dependences of the ultrasonic velocity (left), the piezovoltage (right) for the pure P(VDF-TrFE) (a and b) and the composite with 10 vol. % of BPZT inclusions (b and d). Solid symbols: on cooling, open symbols: on heating.

The piezovoltage in the pre-polarized samples vanishes above room temperature, which is close to T_C obtained from previously described ultrasonic attenuation experiments. The temperature dependences of the velocity and the piezovoltage show large thermal hysteresis. To analyse the anomaly of the ultrasonic velocity, a contribution of a square polarization term AP^2 to the real part of the elastic constant must be added [22], where A is a constant and P is the spontaneous polarization. As the ultrasonic velocity is determined by the complex elastic constant, it correlates to the temperature dependence of the piezovoltage, which is also related to P. The value of the ultrasonic velocity at room temperature is similar to that of neat P(VDF- TrFE) presented elsewhere [24].

One can note that the temperature dependences of the ultrasonic velocity changes slope on cooling in the temperature range 330 K – 340 K. We assume that this is caused by an increase of gauche defects in the polymer matrix responsible for several auxiliary ferroelectric phase transitions observed by means of X-ray diffraction and differential scanning calorimetry [33, 37, 148, 149]. However, the change of the slope is less apparent in the temperature dependence of the ultrasonic piezovoltage.

4.2.3.1 Summary

The effect of BPZT filler on ultrasonic, piezoelectric and dielectric properties of P(VDF-TrFE)/BPZT composites has been studied. Our investigations show that observed anomalies of the ultrasonic velocity and the ultrasound-induced piezovoltage in the composite samples are related to the ferroelectric-paraelectric phase transitions of the copolymer. It is shown that the ultrasonic attenuation maxima at the ferroelectric phase transition can be well described by the relaxation theory of elasticity, and the relaxation time in the ferroelectric phase is expressed by the Landau-Khalatnikov theory. It was shown that the polarization relaxation time prefactor τ_0 slightly increases with increasing BPZT concentration in the composites. A large thermal hysteresis, typical for the first order ferroelectric phase transition, was observed in both temperature dependences of ultrasonic velocity and piezovoltage in the investigated composites. The dielectric spectra of the P(VDF-TrFE)/BPZT composites show that the dielectric losses of the composites strongly depend on the concentration of BPZT. The composites containing a higher concentration of the fillers have high dielectric loss peaks, related to the superposition of dielectric anomalies of the glass and ferroelectric-paraelectric

phase transitions. Both the Curie and melting temperatures decrease with the addition the BPZT filler.

4.2.4 P(VDF-TrFE)/CNT

It is known that fillers (liquid crystals LC, CNT) dispersed in a polymer matrix, can induce relaxation peaks that can be observed by means of differential scanning calorimetry or dielectric spectroscopy [153, 154]. Therefore, in order to check the composites for the presence of additional loss peaks, related to fillers, several samples of P(VDF-TrFE) 70/30 mol. % and P(VDF-TrFE)/CNT composites were selected to be measured in a wide temperature range (150 K – 400 K). The temperature dependences of the complex dielectric permittivity (ε^*) of the neat P(VDF-TrFE) and its composites with CNT show typical of the copolymer relaxation peaks related to the paraelectric-ferrolelectric phase transition on cooling at T_{C1} and heating at T_{C2} (Fig. 4.2.4.1.) [36, 37, 153]. Therefore, all other investigations with P(VDF-TrFE)/CNT composites were performed in temperature range above room temperature.

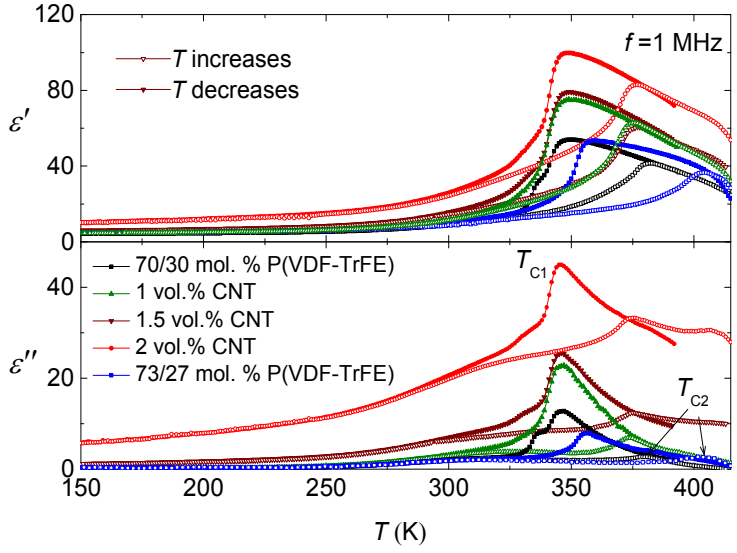

Figure 4.2.4.1. Temperature dependence of the complex dielectric permittivity for the neat P(VDF-TrFE) and its composites measured on heating and cooling at 1 MHz frequency.

Besides the main maximum related to the ferroelectric-paraelectric phase transition another step-like anomaly is observed at lower temperature in $\varepsilon^*(T)$ dependences for the P(VDF-TrFE) copolymer with 70/30 mole fractions of both components. However, for the P(VDF-TrFE) 73/27 mol. % sample this anomaly is absent. These results are consistent with those presented elsewhere [36, 37] and can be explained by the existence of an intermediate polar γ or non-polar ε phase, probably, of orthorhombic conformation [36, 37]. The γ phase has a conformation in between that of the α (paraelectric) and β (feroelectric) phases and is hardly experimentally accessible [25, 33, 34, 36, 37, 88, 89, 93, 95], although it may serve in precedence of the main ferroelectric phase on cooling [7, 37]. Another explanation was proposed by R. Gregorio jr. et al. [35] considering the existence of two types of paraelectric and ferroelectric phases with different Curie temperatures.

It is noteworthy that both the real and imaginary parts of ε^* increase with adding the CNT fillers. The increase of ε^* is mostly pronounced in the sample with 2 vol. % of CNT and can be particularly referred to the increase of mobile charges within the composites [154, 155]. Such heterogeneous systems comprised of two constituents of significantly different electrical conductivity also can cause the low frequency Maxwell- Wagner relaxation due to blocking of charges at the interface of the filler and matrix [155, 156]. Figure 4.2.4.2 presents values of the real part of complex conductivity σ' for P(VDF-TrFE) based composites at different frequencies and CNT concentrations derived from the results seen in Fig. 4.2.4.1 at 270 K according to relation $\sigma' = j \cdot \omega \cdot \varepsilon_0 \cdot \varepsilon''$, where j, ω, ε_0, ε'' units are explained in Chapter 2.6. It is clearly seen how the conductivity in (PVDF-TrFE)/CNT composites is strongly dependent on CNT concentration. To be compared, values of σ' for 73/27 mol. % P(VDF-TrFE) are also shown in Fig. 4.2.4.2 and remain very similar to those of pure 70/30 mol. % P(VDF-TrFE) copolymer.

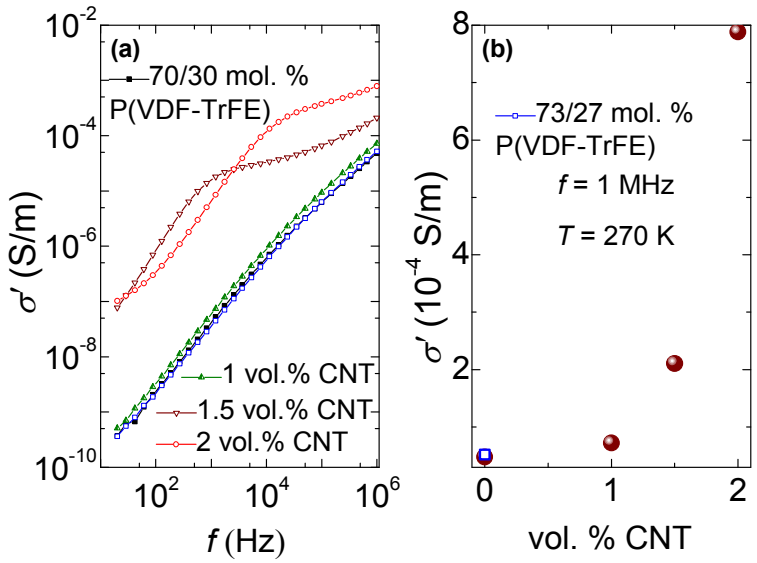

Figure 4.2.4.2. Frequency dependence of the real part of complex conductivity for the neat P(VDF-TrFE) and its composites measured on cooling at 270 K temperature (a), dependence of the real part of complex conductivity on CNT concentration for P(VDF-TrFE) based composites measured on cooling at 1 MHz frequency and 270 K temperature (b).

4.2.4.1 DSC and DMA results

To confirm results seen in Fig. 4.2.4.1 differential scanning calorimetry analysis of the P(VDF-TrFE) copolymer and P(VDF-TrFE)/CNT composites was performed in a wide temperature range and is presented in Fig. 4.2.4.1.3. It is known, that after being annealed at temperatures just below the melting point, P(VDF-TrFE) copolymers change its crystalline structure and crystallization degree (X_C) [34, 104, 105] and as a consequence may change its electromechanical properties [104]. Therefore, thermal analysis was performed the second time after cooling to room temperature at 5 K/min rate. Results obtained from the DSC analysis are presented in Table 4.2.4.1.1.

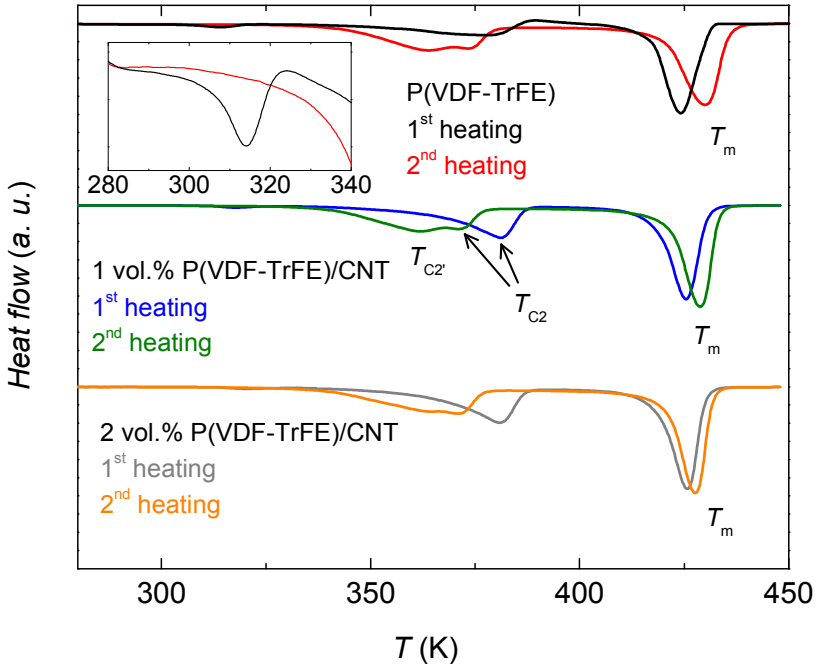

Figure 4.2.4.1.3. DSC curves of the P(VDF-TrFE) 70/30 mol. % copolymer and P(VDF-TrFE)/CNT composites. The second endotherm was performed after cooling the sample to room temperature at 5 K/min rate. The inset demonstrates an enlarged view of the DSC curve for the P(VDF-TrFE) in a temperature region of α_C relaxation.

Table 4.2.4.1.1. Melting temperature and degree of crystallinity of P(VDF-TrFE) and P(VDF-TrFE)/CNT composites obtained on first (T_{m1}, X_{C1}) and second (T_{m2}, X_{C2}) heating

Material	T_{m1} (K)	X_{C1} (%)	T_{m2} (K)	X_{C2} (%)
P(VDF-TrFE)	424.3	77.8	429.9	79.3
1 vol. % CNT	425.4	73.2	428.8	79.9
2 vol. % CNT	425.8	74.5	427.8	75.9

As seen, the degree of crystallinity of the pure P(VDF-TrFE) changes insignificantly in the slowly cooled samples (X_{C2}) and remains relatively high near ~80 %. By adding CNT to the polymer matrix X_C lowers just by several percent. Despite the increase of the overall X_C after slow cooling in all samples, an additional peak appears at $T_{C2'}$, corresponding to ferroelectric-paraelectric transition and manifesting the presence of newly formed

ferroelectric crystalline structure in addition to the β structure with the T_{C2} Curie temperature [34]. The shift of the main ferroelectric to paralelectric transition temperature T_{C2} is usually attributed to a worse arrangement of the crystalline region [35, 36, 105].

The inset in Fig. 4.2.4.1.3 demonstrates an enlarged view of the DSC curve for the P(VDF-TrFE) below $T_{C2'}$. It is clearly seen, that after the first heating the peak, observed at 315 K, vanishes. The α_C relaxation, which is usually related to molecular motions within the spherulites of the crystalline regions [63] or to thermo-mechanical slippage between crystallites [64, 157], can be observed in PVDF-based copolymers above the T_g. The size of spherulites in the crystalline region determines the strength and the frequency of the α_C relaxation, which, differently to the dynamic glass transition, cannot be described by Vogel-Fulcher formalism due to the absence of the vitrification temperature. Thus the relaxation is sometimes called a size dependent relaxation. More information can be found elsewhere [69]. This transition is very sensitive to processing conditions, applied heat history or physical aging, and disappears at higher temperatures above the glass transition temperature T_g [158]. It is important to mention, that the aforementioned peak was not observed in the composites containing CNT fillers. This may be explained by existence of another phase (T_m= 315 K), which conformation changes after the melted sample was cooled down to room temperature.

In order to have a deeper insight into the behaviour upon thermal cycling of peaks, corresponding to the ferroelectric phase transition, four different heating/cooling cycles for the sample of the neat P(VDF-TrFE) were performed. Figure 4.2.4.1.4 shows DSC thermograms. As can be seen from the endotherms in Fig. 4.2.4.1.4a, after the sample is annealed near T_m = 415 K, T_{C2} shifts to lower temperatures for further cycles, indicating a worse arrangement of the crystalline phase but a simultaneous increase of the overall crystallinity of the P(VDF-TrFE) copolymer [35, 36, 105]. It is well known that the

main peak at T_{C2} is very sensitive to the amount of conformational defects, dependent on the TrFE molar ratio, that appear during recrystallization of less perfect crystals [34, 36]. In this case, these mobile defects accompanying by inhomogeneous strain fields can serve as nucleation centres for paraelectric phase (PE) [34, 36]. The shoulder, seen in addition to the main peak at T_{C2} on heating (Fig. 4.2.4.1.4a), was previously discussed when explaining Fig. 4.2.4.1.3 [7, 36, 37]. Moreover, every cycle below 390 K shifts the peaks more down (dashed lines in Fig. 4.2.4.1.4a and Fig. 4.2.4.1.4b). The second and further thermal treatments do not change the crystallinity of the material until the temperature is below T_m [34, 36], but, probably, changes the amount of temperature dependent conformational defects [36]. These results are in a good agreement with that published elsewhere [33-37, 105] and fits the theory proposed by R. L. Moreira et al. [36].

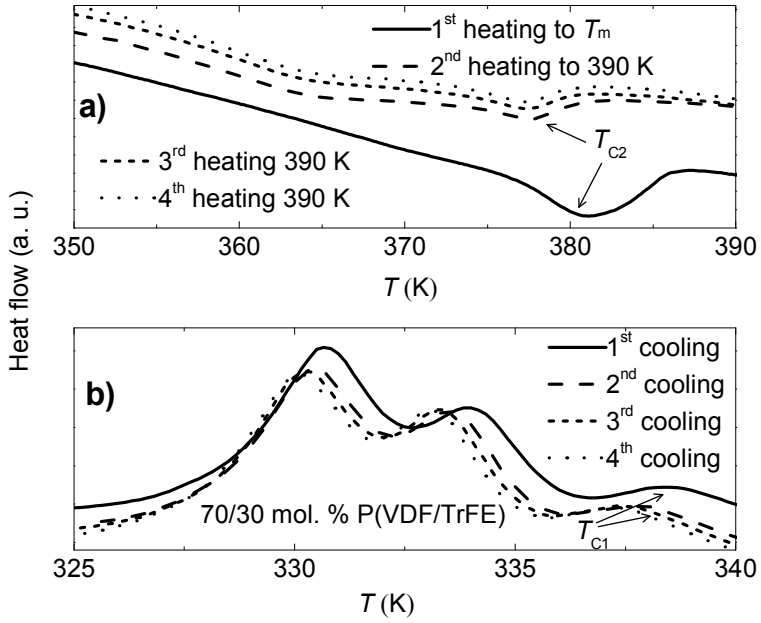

Figure 4.2.4.1.4. DSC curves for the P(VDF-TrFE) 70/30 mol. % copolymer measured on heating (a) and cooling (b).

Here, in Fig. 4.2.4.1.5 also shown that after the first cycle the DSC curve still has two peaks on cooling (black curve) and only after the sample is being

annealed below T_m, the third low temperature peak (blue curve) appears manifesting the existence of another less organized (many gauche defects) ferroelectric phase [35]. It is supposed, that the worse organised ferroelectric phase merges during annealing at temperatures above 403 K [36]. On the contrary, annealing at temperatures below 403 K may also cause a relaxation of the defects produced during the polymer formation when it was cooled down with freezing the mobile defects [35, 36].

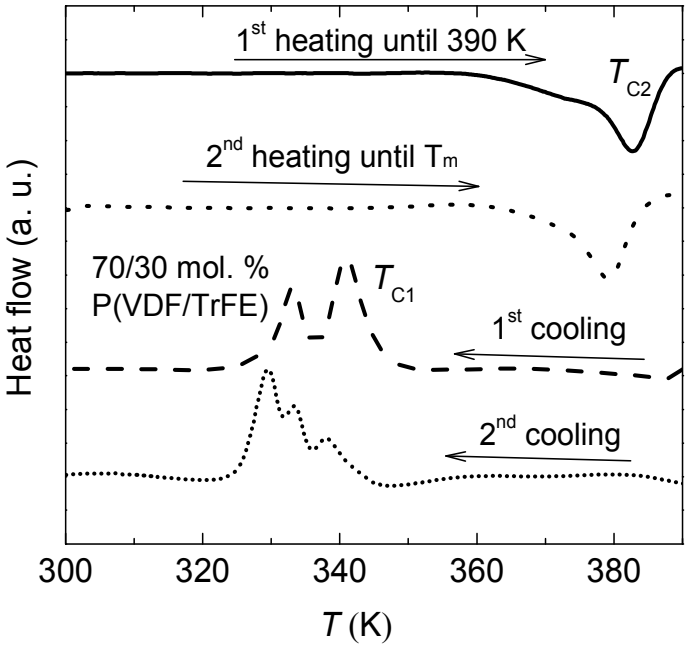

Figure 4.2.4.1.5. DSC curves for the neat P(VDF-TrFE) 70/30 mol. % copolymer.

Before the measurements of the ultrasonic attenuation for P(VDF-TrFE) and P(VDF-TrFE)/CNT composites were carried out, the damping factor $tg\delta$ (the ratio of loss modulus to storage modulus) had been measured in a wide temperature range. This was necessary to elucidate the amount mechanically induced relaxations at low frequencies and to confirm existence of the α_c relaxation in the neat P(VDF-TrFE) copolymer. Five peaks are clearly seen in Fig. 4.2.4.1.6. The first peak at 245 K is attributed to the glass transition of the

polymer matrix and called β relaxation [117]. Although the peak attributed to a motion of many backbone segments in the amorphous phase (α relaxation) and the peak corresponding to the relaxation in the crystalline region (α_c relaxation) are smeared out at 1 Hz, they are clearly seen at 10 Hz. We assume that the peaks observed at higher temperatures are due to the existence of two types of ferroelectric phases with different Curie temperatures.

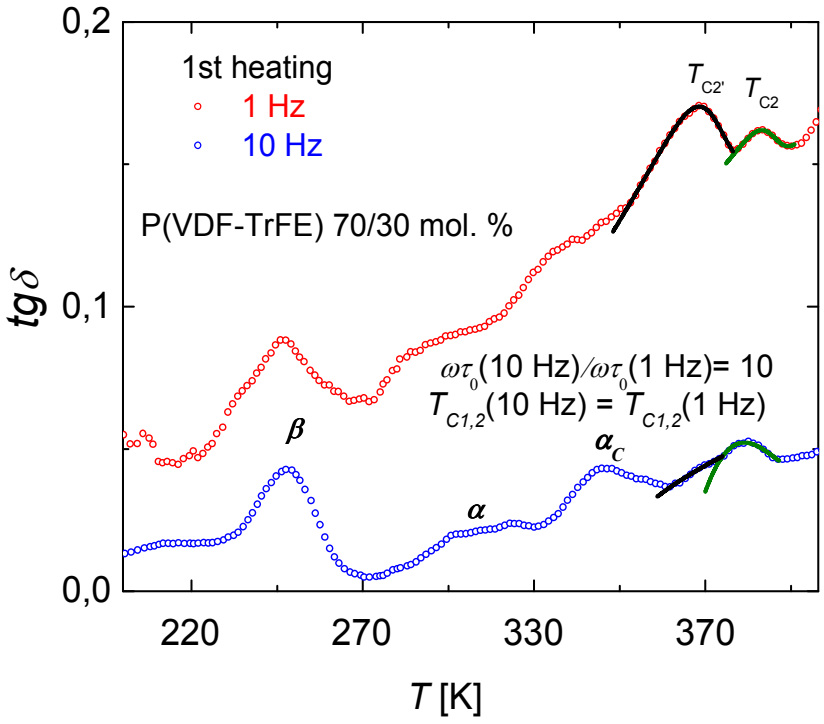

Figure 4.2.4.1.6. Dynamical mechanical analysis for the P(VDF-TrFE) 70/30 mol. % at 1 Hz and 10 Hz frequencies.

The temperature and frequency dependence of $tg\delta$ in the neat P(VDF-TrFE) was analysed employing the Cole-Cole formalism (CC) [21, 74] (Eq. 4.2.4.1.1 and Eq. 4.2.4.1.2):

$$tg\delta = -\frac{\mathrm{Im}\,E^*(\omega)}{\mathrm{Re}\,E^*(\omega)}\text{ , where} \qquad (4.2.4.1.1)$$

$$E^*(\omega) = E_\infty - \frac{E_\infty - E_0}{1+i\omega\tau} \qquad (4.2.4.1.2)$$

Here E_∞ and E_0 are the contributions of all higher and lower frequency processes, respectively, ω is the angular frequency and τ is the mechanical relaxation time, which, according to the phenomenological Landau-Khalatnikov theory [7, 22], in the vicinity of ferroelectric-paraelectric phase transition, can be expressed through the Curie temperature T_c and the polarization relaxation time prefactor (Eq. 2.7.10). The curves obtained from the best fit of experimental curves to Eq. (4.2.4.1.1) are shown in Fig. 4.2.4.1.6 as solid lines. The values obtained from the best fit are presented in Table 4.2.4.1.2.

Table 4.2.4.1.2. Cole-Cole fit parameters of DMA analysis in P(VDF-TrFE)

Frequency	$T_{C2'}$ (K)	$\tau_{0'}$ (s·K)	T_{C2} (K)	τ_0 (s·K)	E_∞- E_0
1 Hz	375.1	2.01	390.5	1.52	0.026
10 Hz	375.1	2.01	390.5	1.52	0.026

It is shown, that the attenuation maxima of the experimental curves at 1 Hz and 10 Hz can be well described by the best fit with similar values of temperature ($T_{C2'}$ and T_{C2}) and τ_0, indicating that these peaks correspond to ferroelectric-paraelectric transitions.

4.2.4.2 Ultrasonic studies

In order to carry out ultrasonic investigations on P(VDF-TrFE) samples with different X_C, they were annealed near 415 K (melting temperature, T_m of P(VDF-TrFE) [7, 34, 93, 105]) after the first heating at ultrasonic investigations. As seen from Fig. 4.2.4.2.7a, the curve of ultrasonic attenuation for P(VDF-TrFE) on the first heating has two anomalies, that are a broad lower temperature peak near T = 350 K and a narrow one near T = 375 K.

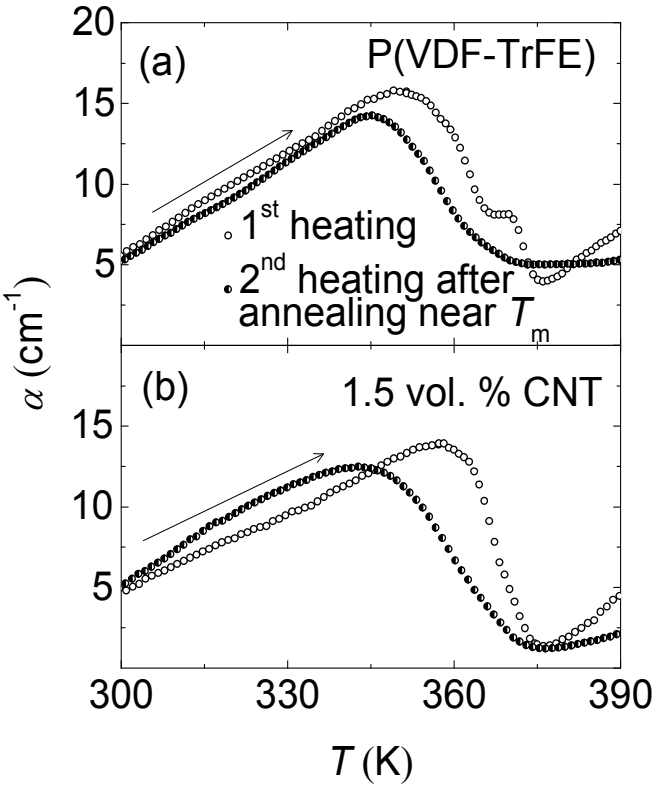

Figure 4.2.4.2.7. Temperature dependences of the ultrasonic attenuation (10 MHz) in (a) neat P(VDF-TrFE) and (b) 1.5 vol. % P(VDF-TrFE)/CNT composite before and after annealing near 415 K. Arrows show direction of temperature variation

The lower temperature peak is, probably, related to the dynamic glass transition of the polymer matrix and the high temperature peak is related to the ferroelectric- paraelectric phase transition of the crystalline region at T_{C2} [6, 7, 94]. The ferroelectric- paraelectric phase transition is of an order-disorder type with the polarization as the order parameter [36, 37]. Meanwhile, the peak referred to the ferroelectric- paraelectric phase transition of the crystalline region of the copolymer, is not observed in the composite sample (Fig. 4.2.4.2.7b). Such unusual behaviour of the ultrasonic loss peak can be explained by superposition of maxima related to the dynamic glass transition and ferroelectric- phase transition of the copolymer, both resulting in a broader maximum shifted to higher temperatures, as can be seen in Fig. 4.2.4.2.7b. After the samples were annealed once near 415 K, the ultrasonic anomaly

related to T_C shifted to lower temperatures (opaque dots in Fig. 4.2.4.2.7a and Fig. 4.2.4.2.7b).

Figure 4.2.4.2.8 presents the effect of thermal cycling on the ferroelectric phase transition of 1 vol. % P(VDF-TrFE)/CNT composite as investigated by means of pulse- echo method at 10 MHz frequency.

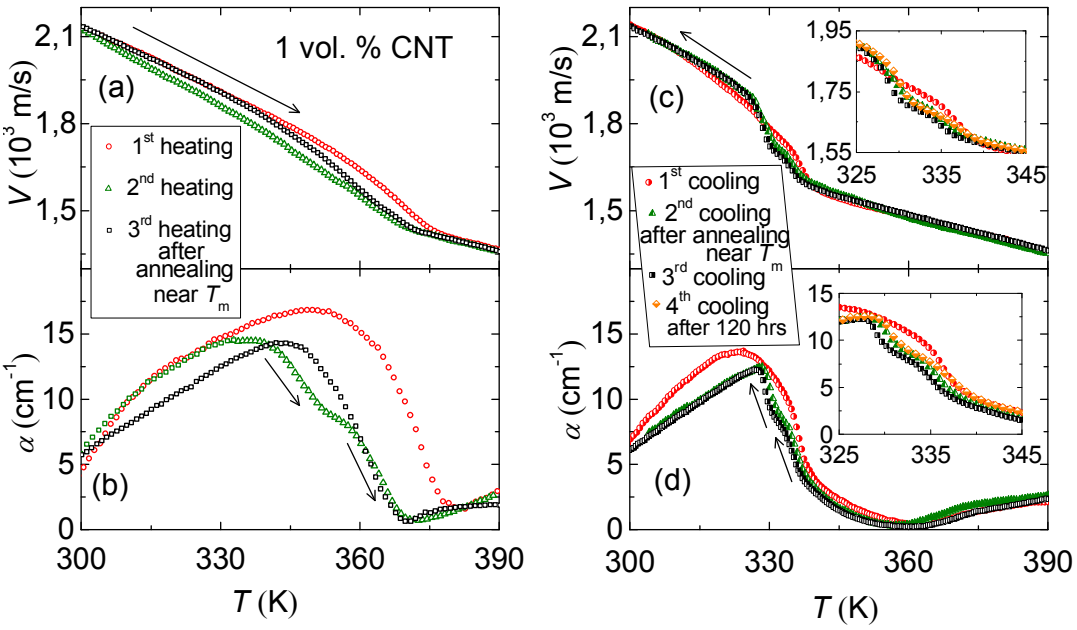

Figure 4.2.4.2.8. Temperature dependences of ultrasonic wave attenuation in 1 vol. % P(VDF-TrFE)/CNT composite before and after several thermal cycles. Arrows show direction of temperature variation

The temperature dependences of the ultrasonic wave velocity (Fig. 4.2.4.2.8a) also showed anomalies attributed to Curie temperature T_c and a structural relaxation also known as β - relaxation process [7, 33, 34, 36-38, 91]. In our case, the condition of maximum ultrasonic attenuation near T_c [22], is not fulfilled due to a comparatively long polarization relaxation time prefactor used in Eq. 2.7.10 [7, 22]. Therefore, there is no visible decrease of the velocity at $T< T_{C1}$ and $T< T_{C2}$. It is clearly seen that both curves of the ultrasonic velocity (Fig. 4.2.4.2.8a) and the attenuation (Fig. 4.2.4.2.8b) in the composite shift leftwards on heating after the first cycle. The shift of T_g and the Curie

temperature, and existence of the shoulder in the ultrasonic loss curve (Fig. 4.2.4.2.8b) can be related to the discussed mobile defects and the intermediate phase, respectively. Possible increase of the concentration of such defects responsible for the shift of T_C without changing the degree of crystallinity of the composite is also shown in Fig. 4.2.4.2.8 after the first heating below 390 K. Although, after the sample is annealed near T_m, the step- like temperature range of the ultrasonic wave attenuation vanishes on heating (Fig. 4.2.4.2.8b). The memory effects produced by annealing at 390 K were erased by annealing over the structural transition near 415 K. Hence, annealing at T> 403 K, can produce again gauche defects in the molecular chain, thereby increasing the overall crystallinity of the less packed composite and releasing the defects, allowing them to relax [34, 35]. Ultrasonic anomalies referred to the additional ferroelectric phase transition can be analyzed by the elastic relaxation theory with the increase of ferroelectric relaxation time (the Landau-Khalatnikov theory) [7].

For the investigation of ultrasonic wave attenuation in the P(VDF-TrFE)/ CNT composites on cooling, annealing was deliberately performed after the first cycle in order to show its strongest effect on the shape of the temperature dependence of ultrasonic attenuation near T_C (Fig. 4.2.4.2.8c and Fig. 4.2.4.2.8d). It is important to note, that further thermal cycles do not shift the loss peak significantly to lower temperatures since the structure is already perturbed and consists of imperfect crystalline regions after the annealing near T_m [34]. Moreover, after the samples were left for 120 hrs at room temperature, the anomalies on the curves of V and α shifted were to higher temperatures (insets in Fig. 4.2.4.2.8c and Fig. 4.2.4.2.8d). We assume, that relaxations of internal defects can be seen by US curve as explained elsewhere [33, 34]. The shift of the temperature dependences of the ultrasonic velocity and attenuation after 120 hours shows that we are able to see long relaxation time of conformational defects. All these mentioned anomalies of US attenuation and

DSC curves can also be seen on cooling in temperature dependences of the complex dielectric permittivity for P(VDF-TrFE)/CNT composites (Fig. 4.2.4.2.10).

4.2.4.3 Dielectric studies

The same tendency in all composites was observed by dielectric measurements on heating and is demonstrated in Fig. 4.2.4.3.9.

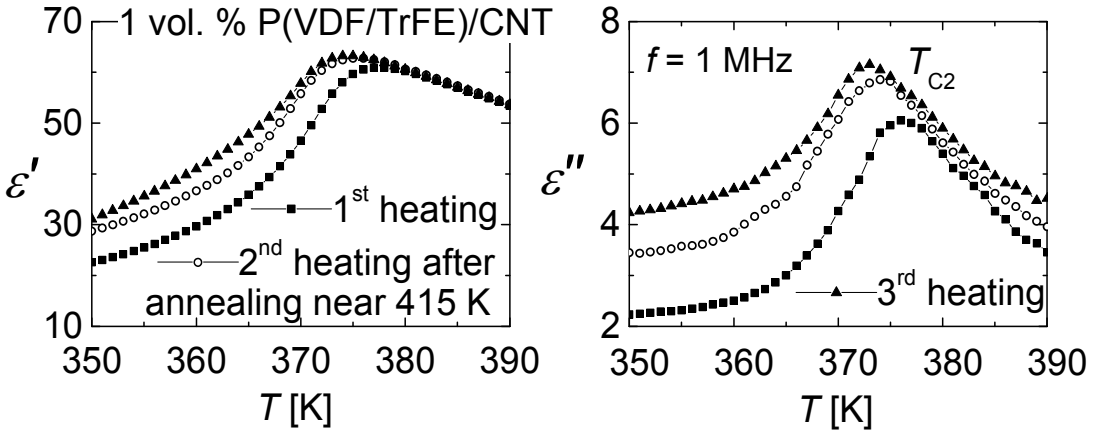

Figure 4.2.4.3.9. Temperature dependence of the complex dielectric permittivity in 1 vol. % P(VDF-TrFE)/CNT composite measured on heating at 1 MHz frequency after heating and annealing cycles.

The temperature dependences of the ultrasonic velocity and attenuation on cooling have changes of slope in the temperature range 330 K- 340 K. The region is clearly seen on cooling in both the real and imaginary parts of the complex dielectric permittivity for the neat copolymer and its composite (Fig. 4.2.4.3.10). It can be also explained by two assumptions, i.e. the intermediate γ phase according to L. R. Moreira et al. [36, 37], or two types of paraelectric-ferroelectric phase transitions of crystallites with different degrees of perfection according to R. Gregorio jr. et. al. [35]. Furthermore, the shoulder vanishes with the addition of CNT filler when the composite is cooled down

for the first time (Fig. 4.2.4.3.10b and Fig. 4.2.4.3.10d). The presence of CNT can impact the degree of crystallinity of the composite, thus resulting in a change of ε^* temperature dependence similarly as it was observed for PDMS/ZnO composites [152].

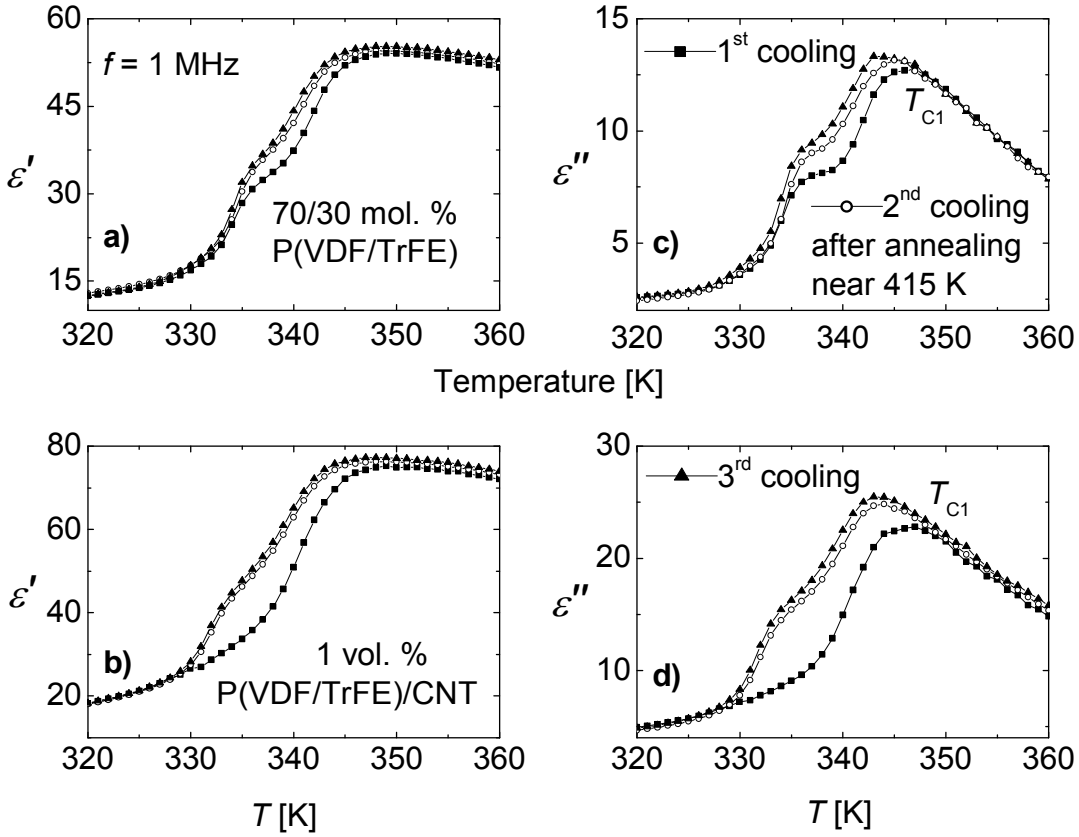

Figure 4.2.4.3.10. Temperature dependence of the complex dielectric permittivity in P(VDF-TrFE) (a and c) and 1 vol. % P(VDF-TrFE)/CNT (b and d) composite measured on cooling at 1 MHz frequency.

4.2.4.4 TSDC studies

In order to have a deeper insight on the impact of CNT fillers combined with thermal cycling on thermal processes in P(VDF-TrFE) copolymer, TSD currents in all samples were studied shortly after poling (Fig. 4.2.4.4.11a).

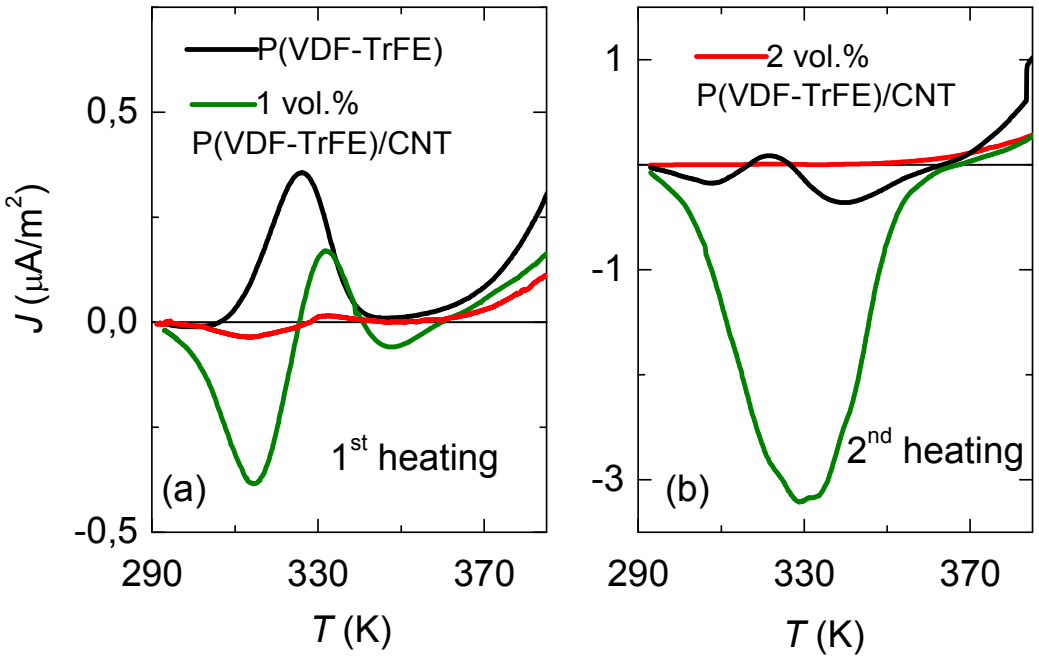

Figure 4.2.4.4.11. Temperature dependence of the TSD currents *J* in the neat P(VDF-TrFE) and P(VDF-TrFE)/CNT composites measured on the first (a) and the second (b) heating.

The neat P(VDF-TrFE) shows a positive TSDC peak at 325 K (Fig. 4.2.4.4.11a). The polarity of the measured current is of the same polarity regarding the initial corona charging of the sample. Due to that fact, the peak was attributed to a relaxation of space charges, injected during the process of corona discharge and, propagating to the grounded electrode after being detrapped upon the Poole-Frenkel effect [70, 113, 114]. The process of detrapping for bulk charges is probably caused by the α relaxation [70, 151, 159]. It is known, that the position and the size of TSDC signals is directly related to intrinsic relaxations [70]. This can explain the significant decrease of the peak after the second polarization (Fig. 4.2.4.4.11b). This is in a good agreement with the results of the DMA measurements, seen in Fig. 4.2.4.4.6. The neat copolymer also showed two negative peaks at 308 K and 339 K in the second TSDC measurement. It is clear from the direction of the peaks, that the peaks correspond to dipolar disorientation or ion displacement within the P(VDF-

TrFE) sample [70, 96, 101, 102]. The less thermally stable peak is referred to the component caused by a reorientation of aligned dipoles in amorphous phase [70, 101, 102]. Due to a high degree of crystallinity of the copolymer (Table 4.2.4.1.1) and a higher amplitude of the negative peak at 339 K, the TSD current can be related to the ferroelectric component in crystalline phase [101]. On the other hand, the composite containing 1 vol. % CNT showed similar to the aforementioned discharge behaviour already on the first TSDC heating. Here three peaks at 308 K, 322 K and 339 K were observed (Fig. 4.2.4.4.11a). Although, the temperatures were lower than those of the neat P(VDF-TrFE). As the electret component is accompanied by space and surface compensating charges [70, 100], a change of the trap depth of the bulk charges in polymer matrix [70] by presence of CNT fillers could explain lower temperature of the first two peaks. A strong electret component can also be explained by internal polarization due to charge separation within the dielectric and caused by conduction either between interfaces, such as domain boundaries (Maxwell-Wagner effect) [70, 99]. The smaller peak corresponding to the ferroelectric component can be explained by the effect of CNT fillers during formation of the crystalline phase, similarly as it was expected in PDMS/ZnO composites [152]. Figure 4.2.4.4.11b shows faster polarization in composites containing 1 vol. % CNT. Further polarisation cycles, that were not presented here, showed a saturation of the discharge peak, indicating its dipolar nature [70]. We assume, that compensating charges induce an additional mechanism at surfaces of crystallites in which charges and dipoles are mutually attracted, therefore producing high remnant polarisation, as reported elsewhere [99]. Although a high electret component can affect negatively stability of piezoelectric coefficients [100, 101]. Contributions of the electret and the ferroelectric components to formation of the single peak at 330 K still require more elucidation.

It is obvious that the conductivity of the samples strongly depends on the CNT fillers (Fig. 4.2.4.2). Therefore the lowest TSDC current was observed in

P(VDF-TrFE) sample containing 2 vol. % CNT (Fig. 4.2.4.4.11a and Fig. 4.2.4.4.11b). If CNT fillers percolate above a certain concentration, producing the rapid transfer of the bulk charge, so the polarization field, produced by the charges on and near the samples surface, decreases. If the field is lower than the coercive electric field of the material, we do not expect the ferroelectric polarisation. This assumption could explain the absence of the more thermally stable TSDC peak in 2 vol. % P(VDF-TrFE)/CNT composites.

An abrupt current increase for all samples at temperatures higher than 370 K was observed. According to some literature, the existence of the spontaneous current may be a result of electrochemical effects in the metal-polymer interface, and an effect of bulk electrical resistance as the polymer undergoes structural transitions, i.e. the ferroelectric to paraelectic phase transition [97].

4.2.4.5 SEM analysis

Figure 4.2.4.5.12 presents SEM images of 1 vol. % P(VDF-TrFE)/CNT composite at different magnification. Although spherutlites were not observed in the composite films, as it was shown in previous reports on spherulite size up to 5 μm [69], we assume that the size of spherulites is less than 1 μm. Nevertheless, it is clearly seen, that the distribution of CNT fillers in the polymer matrix is relatively good, as there no conglomerates of the fillers were observed at magnification of 10 000 times.

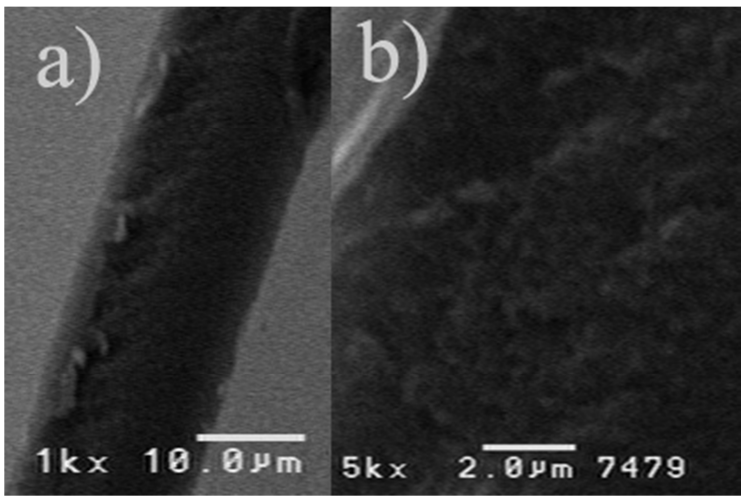

Figure 4.2.4.5.12. SEM images of 1 vol. % P(VDF-TrFE)/CNT composite at different magnification ((a) x1000, (b) x5000).

4.2.4.6 Summary

A complex investigation of the effect of thermal cycling and annealing on the crystallinity and ferroelectric phase transition of P(VDF-TrFE)/CNT composites by means of DSC, ultrasonic and dielectric spectroscopy was performed. The change of conformation of the crystalline region changes mechanical and dielectric properties of the composite, thus resulting in the change of the peaks related to the glass and ferroelectric- paraelectric transition anomalies. A change of the thermal hysteresis was observed in temperature dependences of the ultrasonic velocity, attenuation and complex dielectric permittivity of the investigated composites. Thermally stimulated discharge current measurements of the P(VDF-TrFE)/CNT composites combined with ultrasonic measurements revealed a strong dependence of the electret component on the presence of CNT nanoparticles. The small ferroelectric component can be explained by acting of CNT fillers as crystallization nuclei

for the non-ferroelectric phase and a subsequent growth of spherulites. Although previous investigations of composites with carbon fillers have shown an increase of spherulite size, it was suggested based on the SEM analysis that in our case the presence of the CNT fillers in the polymer matrix forms relatively tiny spherulites of different to β-crystalline phase of P(VDF-TrFE).

5 Conclusions

In the present work we have studied the effect of inorganic ZnO and BPZT fillers and organic CNT fillers on organic composite dielectric and mechanical properties. Following statements have been made:

1. In composites of non-piezoelectric PDMS with ZnO nanoinclusions the temperature dependent dielectric and mechanical relaxation anomalies are dependent on concentration of ZnO particles, i.e. a composite containing higher concentration of fillers has a lower dielectric and higher mechanical loss peaks. ZnO fillers act as nucleation centers in glass-crystalline state, or scattering centers in amorphous high temperature state of PDMS. Room temperature increase of ultrasonic attenuation in the strongly doped PDMS/ZnO composites is due to increased scattering centers for ultrasonic wave.
2. The complex dielectric permittivity and coercive electric field of P(VDF-TrFE)/BPZT composites with smaller filler concentrations (≤ 20 vol. %) obey Lichtenecker's effective medium approximation model. Since the permittivity of the polymer is much lower than of the permittivity of the fillers, the proposed mixing rule can also be applied to explain the passive behaviour of ceramic particles in the ferroelectric composites.
3. Both the Curie and melting temperatures of P(VDF-TrFE)/BPZT decrease with the addition the BPZT fillers.
4. In composites of (PVDF-TrFE) polymer with small amount of organic CNTs the dielectric and mechanical properties depend not only on the increased conductivity of composite determined by large conductivity of CNT, but also by CNTs acting as nucleation centers for a subsequent growth of spherulites. Such change of conformation in glass-crystalline-

amorphous polymer matrix results in the change of the loss maxima temperature anomalies related to the glass or ferroelectric- paraelectric transition.

6 References

[1] T.R. Dargaville, M.C. Celina, J.M. Elliott, P.M. Chaplya, G.D. Jones, D.M. Mowery, R.A. Assink, R.L. Clough, J.W. Martin, Characterization, performance and optimization of PVDF as a piezoelectric film for advanced space mirror concepts, SANDIA report, Sandia National Laboratories Albuquerque, New Mexico, 2005, pp. 1-49.

[2] M.V. Silibin, A.V. Solnyshkin, D.A. Kiselev, A.N. Morozovska, E.A. Eliseev, S.A. Gavrilov, M.D. Malinkovich, D.C. Lupascu, V.V. Shvartsman, Local ferroelectric properties in polyvinylidene fluoride/barium lead zirconate titanate nanocomposites: Interface effect, J Appl Phys, 114, pp. (2013).

[3] L.H. Sperling, INTRODUCTION TO PHYSICAL POLYMER SCIENCE, FOURTH EDITION ed., John Wiley & Sons, Inc., Hoboken, New Jersey, 844 2006.

[4] G. Strobl, The Physics of Polymers. Concepts for Understanding Their Structures and Behavior, Third Edition ed., Springer-Verlag, Berlin Heidelberg 518 2007.

[5] A.J. Moulson, J.M. Herbert, Electroceramics: Materials, Properties, Applications, Second Edition ed., John Wiley & Sons Ltd, West Sussex, 557 2003.

[6] M.V. Silibin, J. Belovickis, S. Svirskas, M. Ivanov, J. Banys, A.V. Solnyshkin, S.A. Gavrilov, O.V. Varenyk, A.S. Pusenkova, N. Morozovsky, V.V. Shvartsman, A.N. Morozovska, Polarization reversal in organic-inorganic ferroelectric composites: Modeling and experiment, Appl Phys Lett, 107, pp. (2015).

[7] J. Belovickis, V. Samulionis, J. Banys, M. Silibin, A. Solnyshkin, Y. Shilyaeva, K. Nekludov, S. Gavrilov, V. Rubanik Jr., V. Rubanik, V.V. Shvartsman, Ultrasonic spectroscopy of copolymer based P(VDF-TrFE) composites with fillers on lead zirconate titanate basis, Polymer Testing, 53, pp. 211- 216 (2016).

[8] Z.-g. Zeng, G.-d. Zhu, L. Zhang, X.-j. Yan, EFFECT OF CRYSTALLINITY ON POLARIZATION FATIGUE OF FERROELECTRIC P(VDF-TrFE) COPOLYMER FILMS, Chinese Journal of Polymer Science, 27, pp. 479−485 (2009).

[9] V. Bharti, Q.M. Zhang, Dielectric study of the relaxor ferroelectric poly(vinylidene fluoride-trifluoroethylene) copolymer system, Phys Rev B, 63, pp. (2001).

[10] E. Edqvist, E. Hedlund, Design and manufacturing considerations of low-voltage multilayer P(VDF-TrFE) actuators, J Micromech Microeng, 19, pp. (2009).

[11] T.J. Reece, S. Ducharme, A.V. Sorokin, M. Poulsen, Nonvolatile memory element based on a ferroelectric polymer Langmuir-Blodgett film, Appl Phys Lett, 82, pp. 142-144 (2003).

[12] G.W. Taylor, J.R. Burns, S.M. Kammann, W.B. Powers, T.R. Welsh, The energy harvesting eel: A small subsurface ocean/river power generator, Ieee J Oceanic Eng, 26, pp. 539-547 (2001).

[13] T. Okoshi, New Concept of Microporous Structure in Small-Diameter Vascular Prostheses, Artif Organs, 19, pp. 27-31 (1995).

[14] Y. Lianyun, L. Xinyu, W. Allahyarov, P. Taylor, Q. Zhang, L. Zhu, Novel polymer ferroelectric behavior via crystal isomorphism and the nanoconfinement effect, Polym Bull, 54, pp. 1709-1728 (2013).

[15] M. Kupnik, B.T. Khuri-Yakub, Sensor for measuring properties of liquids and gases, Issued patent US 8276433 B2, 2012.

[16] M. Dietze, M. Es-Souni, Structural and functional properties of screen-printed PZT-PVDF-TrFE composites, Sensor Actuat a-Phys, 143, pp. 329-334 (2008).

[17] P. Kumar, S. Singh, J.K. Juneja, C. Prakash, K.K. Raina, Dielectric behaviour of La substituted BPZT ceramics, Physica B, 404, pp. 2126-2129 (2009).

[18] D.A. Kiselev, M.D. Malinkovich, Y.N. Parkhomenko, A.V. Solnyshkin, A.A. Bogomolov, M.V. Silibin, S.A. Gavrilov, V.V. Shvartsman, D.C. Lupascu, The Microstructure and Local Piezoelectric Response in Polymer Nanocomposites with Different Ferroelectric Crystalline Additions, Mater. Res. Soc. Symp. Proc., 1556, pp. 1-5 (2013).

[19] N. KOIZUMI, N. HAIKAWA, H. HABUKA, DIELECTRIC BEHAVIOR AND FERROELECTRIC TRANSITION OF COPOLYMERS OF VINYLIDENE FLUORIDE AND TIUFLUOROETHYLENE, Ferroelectrics, 57, pp. 99-119 (1984).

[20] I. Alig, S. Tadjbakhsch, G. Floudas, C. Tsitsilianis, Viscoelastic contrast and kinetic frustration during poly(ethylene oxide) crystallization in a homopolymer and a triblock copolymer. Comparison of ultrasonic and low-frequency rheology, Macromolecules, 31, pp. 6917-6925 (1998).

[21] I. Alig, D. Lellinger, S. Agarwal, H. Oehler, Monitoring of photopolymerization kinetics and network formation by combined real-time near-infrared spectroscopy and ultrasonic reflectometry, React Funct Polym, 73, pp. 316-322 (2013).

[22] V. Valevichius, V. Samulionis, J. Banys, Ultrasonic dispersion in the phase transition region of ferroelectric materials, J Alloy Compd, 211– 212, pp. 369-373 (1994).

[23] K. Kruger, J. Petzelt, J.E. Legrand, Brillouin spectroscopic investigations of the ferroelectric phase transition in a Polyvinylidenefluoride- Trifluoretylene copolymer, Colloid & Polymer Sci, 264, pp. 791-797 (1986).

[24] H.Y. Guney, Elastic properties and mechanical relaxation behaviors of PVDF (poly (vinylidene fluoride)) at temperatures between-20 and 100 degrees C

and at 2 MHz ultrasonic frequency, J Polym Sci Pol Phys, 43, pp. 2862-2873 (2005).

[25] I. Katsouras, K. Asadi, M.Y. Li, T.B. van Driel, K.S. Kjaer, D. Zhao, T. Lenz, Y. Gu, P.M. Blom, D. Damjanovic, M.M. Nielsen, D.M. de Leeuw, The negative piezoelectric effect of the ferroelectric polymer poly(vinylidene fluoride), Nat Mater, 15, pp. 1- 8 (2016).

[26] H. Kawai, The Piezoelectricity of Poly (vinylidene Fluoride), Japanese Journal of Applied Physics, 8, pp. 975-976 (1969).

[27] Y. Wada, R. Hayakawa, A model theory of piezo- and pyroelectricity of poly(vinylidene fluoride) electret, Ferroelectrics, 32, pp. 115–118 (1981).

[28] T. Furukawa, J.X. When, K. Suzuki, Y. Takashina, M. Date, Piezoelectricity and pyroelectricity in vinylidene fluoride/trifluoroehtylene copolymers, J. Appl. Phys., 56, pp. 829–834 (1984).

[29] M.G. Broadhurst, G.T. Davis, Physical basis for piezoelectricity in PVDF, Ferroelectrics, 60, pp. 3–13 (1984).

[30] J. Kim, K. J. Loh, J.P. Lynch, Piezoelectric polymeric thin films tuned by carbon nanotube fillers, SPIE Smart Structures and Materials, San Diego, CA, San Diego, CA, 2008, pp. 1- 10.

[31] A. Ramaratnam, N. Jalili, Reinforcement of piezoelectric polymers with carbon nanotubes: Pathway to next-generation sensors, Journal of intelligent material systems and structures, 17, pp. 199- 208 (2006).

[32] E.T. Thostenson, T.-W. Chou, Aligned multi-walled carbon nanotube-reinforced composites: processing and mechanical characterization, J. Phys. D: Appl. Phys., 35, pp. L77- L80 (2002).

[33] R.L. Moreira, R. Almairac, M. Latour, Anchoring, memory and relaxation phenomena in the phase transition of poly(viny1idene fluoride-trifluoroethylene) copolymers, J. Phys.: Condens. Matter, 1, pp. 4273-4282 (1989).

[34] M.A. Barique, H. Ohigashi, Annealing effects on the Curie transition temperature and melting temperature of poly(vinylidene fluoride/trifluoroethylene) single crystalline films, Polymer, 42, pp. 4981-4987 (2001).

[35] R. Gregorio, M.M. Botta, Effect of crystallization temperature on the phase transitions of P(VDF/TrFE) copolymers, J Polym Sci Pol Phys, 36, pp. 403-414 (1998).

[36] R.L. Moreira, P. Saint-Gregoire, M. Lopez, M. Latour, Thermal and dielectric behaviors of Poly(vinylidene fluoride- trifluoroethylene) copolymers at the Curie transition, Journal of Polymer Science: Part B: Polymer Physics,, 27, pp. 709-722 (1989).

[37] R.L. Moreira, P. Saint-Gregoire, M. Latour, Thermal and dielectric investigations of the curie transition in Poly(vinylidene fluoride—

trifluoroethylene) copolymers, Phase Transitions: A Multinational Journal of Applied Physics, 14, pp. 243-249 (1989).

[38] T. Furukawa, Y. Tajitsu, X. Zhang, G.E. Johnson, Dielectric Relaxations in Copolymers of Vinylidene Fluoride, Ferroelectrics, 135, pp. 401-417 (1992).

[39] J. Kim, M.K. Chaudhury, M.J. Owen, Hydrophobicity loss and recovery of silicone HV insulation, Ieee T Dielect El In, 6, pp. 695-702 (1999).

[40] P. Du, X. Lin, X. Zhang, Dielectric constants of PDMS nanocomposites using conducting polymer nanowires, In The 16th International Conference on Solid-State Sensors, Actuators and Microsystems (Transducers), IEEE, Beijing, China, 2011.

[41] P. Klonos, A. Panagopoulou, A. Kyritsis, L. Bokobza, P. Pissis, Dielectric studies of segmental dynamics in poly(dimethylsiloxane)/titania nanocomposites, J Non-Cryst Solids, 357, pp. 610-614 (2011).

[42] T.B. Bateman, Elastic Moduli of Single-Crystal Zinc Oxide, J. Appl. Phys., 33, pp. 3309-3312 (1962).

[43] K. Omar, Investigation of dielectric constant of Zinc Oxide, Modern Applied Science, 3, pp. 110- 115 (2009).

[44] Y. Yang, W. Guo, X.Q. Wang, Z.Z. Wang, J. Qi, Y. Zhang, Size Dependence of Dielectric Constant in a Single Pencil-Like ZnO Nanowire, Nano Lett, 12, pp. 1919-1922 (2012).

[45] S.C. Tjong, G.D. Liang, Electrical properties of low-density polyethylene/ZnO nanocomposites, Mater Chem Phys, 100, pp. 1-5 (2006).

[46] B.K. Sharma, N. Khare, S.K. Dhawan, H.C. Guptaa, Dielectric properties of nano ZnO-polyaniline composite in the microwave frequency range, J Alloy Compd, 477, pp. 370-373 (2009).

[47] N. Gull, S.M. Khan, M.A. Munawar, M. Shafiq, F. Anjum, M.T.Z. Butt, T. Jamil, Synthesis and characterization of zinc oxide (ZnO) filled glass fiber reinforced polyester composites, Mater Design, 67, pp. 313-317 (2015).

[48] B. Zhao, F. Wang, H.Y. Chen, Y.P. Wang, M.M. Jiang, X.S. Fang, D.X. Zhao, Solar-Blind Avalanche Photodetector Based On Single ZnO-Ga2O3 Core-Shell Microwire, Nano Lett, 15, pp. 3988-3993 (2015).

[49] Y.M. Gu, Y.Z. Dai, Y. Liu, X.P. Chen, Electronic Artificial Skin for Application in Pressure Sensor, Adv Intell Syst, 345, pp. 433-439 (2015).

[50] G. Li, M. Parmar, D.W. Lee, An oxidized liquid metal-based microfluidic platform for tunable electronic device applications, Lab Chip, 15, pp. 766-775 (2015).

[51] S. Mohanty, S.K. Nayak, B.S. Kaith, S. Kalia, POLYMER NANOCOMPOSITES BASED ON INORGANIC AND ORGANIC NANOMATERIALS, Scrivener Publishing, Wiley, Beverly, MA, 600 2015.

[52] W.D.J. Callister, Materials Science and Engineering: An Introduction, 7th Edition, John Wiley & Sons, Inc., United States of America, 975 2006.

[53] A.K. Bakhshi, G. Bhalla, Electrically conducting polymers: Materials of the twentyfirst century, J Sci Ind Res India, 63, pp. 715-728 (2004).

[54] F. Kremer, A. Schönhals, Broadband Dielectric Spectroscopy, Springer, Berlin Heidelberg, 729 2003.

[55] R.E. Newnham, L.J. Bowen, K.A. Klicker, L.E. Cross, Composite piezoelectric transducers, Materials in engineering, 2, pp. 93 - 106 (1980).

[56] D.W. van Krevelen, K. te Nijenhuis, Properties of Polymers: Their Correlation with Chemical Structure; their Numerical Estimation and Prediction from Additive Group Contributions, Edition 4, Elsevier1030 2009.

[57] W. Schlesinger, H.M. Leeper, Single crystals of alpha-gutta, Journal of Polymer Science Part A-Polymer Chemistry, 11, pp. 203-2013 (1953).

[58] R. Hosemann, Der ideale Parakristall und die von ihm gestreute kohärente Röntgenstrahlung, Zeitschrift für Physik, 128, pp. 465-492 (1950).

[59] P. Frubing, A. Kremmer, R. Gerhard-Multhaupt, A. Spanoudaki, P. Pissis, Relaxation processes at the glass transition in polyamide 11: From rigidity to viscoelasticity, J Chem Phys, 125, pp. (2006).

[60] C. Schick, Study Rigid Amorphous Fraction in Polymer Nano-Composites by StepScan and HyperDSC, Application note. PerkinElmer, Inc., 008648_01, pp. 1-4 (2009).

[61] A. Sanz, A. Nogales, T.A. Ezquerra, M. Soccio, A. Munari, N. Lotti, Cold Crystallization of Poly(trimethylene terephthalate) As Revealed by Simultaneous WAXS, SAXS, and Dielectric Spectroscopy, Macromolecules, 43, pp. 671-679 (2010).

[62] A. Ridhore, J.P. Jog, A Dynamic Mechanical and Dielectric Relaxation Study of PP-g-MAH/Clay Nanocomposites, The Open Macromolecules Journal, 6, pp. 53-58 (2012).

[63] V. Sencadas, S. Lanceros-Mendez, R.S.I. Serra, A.A. Balado, J.L.G. Ribelles, Relaxation dynamics of poly(vinylidene fluoride) studied by dynamical mechanical measurements and dielectric spectroscopy, Eur Phys J E, 35, pp. (2012).

[64] R.H. Boyd, Relaxation processes in crystalline polymers: experimental behaviour — a review, Polymer, 26, pp. 323-347 (1985).

[65] J.F. Legrand, J. Lajzerowicz, B. Berge, P. Delzenne, F. Macchi, C. Bourgaux-Leonard, A. Wicker, J.K. Kruger, Ferroelectricity in VF2 based copolymers, Ferroelectrics, 78, pp. 151-158 (1988).

[66] C.L. Rohn, Analytical Polymer Rheology: Structure-processing-property Relationships, Hanser314 1995.

[67] Z. Ahmad, Polymeric Dielectric Materials, InTech, 2012, pp. 24.

[68] R.N. Capps, Elastomeric materials for acoustical applications, Naval Research Laboratory (U.S.), Washington, D.C., 1989.

[69] M. Sharma, G. Madras, S. Bose, Size dependent structural relaxations and dielectric properties induced by surface functionalized MWNTs in poly(vinylidene fluoride)/poly(methyl methacrylate) blends, Phys Chem Chem Phys, 16, pp. 2693-2704 (2014).

[70] G.M. Sessler, Electrets. Topics in Applied Physics, Springer-Verlag, Berlin-Heidelberg-New York, 1980.

[71] M.E. Lines, A.M. Glass, Principles and Applications of Ferroelectrics and Related Materials, Oxford University Press, Oxford, 680 1977.

[72] B.A. Strukov, A.P. Levanyuk, Ferroelectric Phenomena in Crystals, 1 ed., Springer-Verlag, Berlin Heidelberg, 308 1998.

[73] R.G. Kepler, Piezoelectricity, pyroelectricity, and ferroelecricity in organic materials, Ann. Rev. Phys. Chem., 29, pp. 497-518 (1978).

[74] K.S. Cole, R.H. Cole, Dispersion and Absorption in Dielectrics I. Alternating Current Characteristics, J. Chem. Phys. , 9, pp. 341–351 (1941).

[75] S. Havriliak, S. Negami, A complex plane representation of dielectric and mechanical relaxation processes in some polymers, Polymer, 8, pp. 161-210 (1967).

[76] R. Zorn, Logarithmic moments of relaxation time distributions, J Chem Phys, 116, pp. 3204-3209 (2002).

[77] K. Trachenko, The Vogel-Fulcher-Tammann law in the elastic theory of glass transition, J Non-Cryst Solids, 354, pp. 3903-3906 (2008).

[78] H. Vogel, The law of the relation between the viscosity of liquids and the temperature, Physikalische Zeitschrift, 22, pp. 645-646 (1921).

[79] R. Pirc, R. Blinc, Vogel-Fulcher freezing in relaxor ferroelectrics, Phys Rev B, 76, pp. (2007).

[80] A. Vary, H.E. Kautz, Analytical Ultrasonics in Materials Research and Testing, Analytical ultrasonics of materials. NASA Conference Publication 2383Cleveland, Ohio, 1984, pp. 257-298.

[81] L.D. Landau, I.M. Khalatnikov, On the anomalous absorption of a sound near to points of phase transition of the second kind, Dokl. Akad. Nauk SSSR, 96, pp. 469-472 (1954).

[82] W.A. Finzel, H.L. Vincent, Silicones in Coatings, Federation Series on Coatings Technology, Federation of Societies for Coatings Technology. Blue Bell, Philadelphia, 1996, pp. 34.

[83] L. Bistricic, V. Borjanovic, L. Mikac, V. Dananic, Vibrational spectroscopic study of poly(dimethylsiloxane)-ZnO nanocomposites, Vib Spectrosc, 68, pp. 1-10 (2013).

[84] A. Schonhals, H. Goering, C. Schick, B. Frick, R. Zorn, Polymers in nanoconfinement: What can be learned from relaxation and scattering experiments?, J Non-Cryst Solids, 351, pp. 2668-2677 (2005).

[85] M.E. Brown, P.K. Gallagher, Handbook of Thermal Analysis and Calorimetry, Elsiever B. V, Ohio, 780 2008.

[86] J.C.S. Moraes, M.M.D.S. Sostena, C.R. Grandini, The glass transition temperature in dental composites, in: J. Cuppoletti (Ed.) Metal, Ceramic and Polymeric Composites for Various Uses, InTech, Rijeka, 2011, pp. 659-684.

[87] J.C. Lotters, W. Olthuis, P.H. Veltink, P. Bergveld, The mechanical properties of the rubber elastic polymer polydimethylsiloxane for sensor applications, J Micromech Microeng, 7, pp. 145-147 (1997).

[88] T. Furukawa, Ferroelectric properties of vinylidene fluoride copolymers, Phase Transitions, 18, pp. 143-211 (1989).

[89] M.Y. Li, H.J. Wondergem, M.J. Spijkman, K. Asadi, I. Katsouras, P.W.M. Blom, D.M. de Leeuw, Revisiting the delta-phase of poly(vinylidene fluoride) for solution-processed ferroelectric thin films, Nat Mater, 12, pp. 433-438 (2013).

[90] R.A. Pethrick, The applications of ferroelectric polymers, Blackie, Glasgow, 387 1988.

[91] K. Tashiro, Crystal structure and phase transition of PVDF and related copolymers, in: H.S. Nalwa (Ed.) Ferroelectric Polymers: Chemistry, Physics and Applications, Marcel Dekker, New York, 1995, pp. 63-180.

[92] J.F. Legrand, J. Lajzerowicz, B. Berge, P. Delzenne, F. Macchi, C. Bourgaux-Leonard, A. Wicker, J.K. Kruger, Ferroelectricity in VF_2 based copolymers, Ferroelectrics, 78, pp. 151-158 (1988).

[93] T.R. Dargaville, M.C. Celina, J.M. Elliott, P.M. Chaplya, G.D. Jones, D.M. Mowery, R.A. Assink, R.L. Clough, J.W. Martin, Characterization, performance and optimization of PVDF as a piezoelectric film for advanced space mirror concepts, Sandia Report, Sandia National Laboratories, 2005, pp. 1-49.

[94] P. Martins, A.C. Lopes, S. Lanceros-Mendez, Electroactive phases of poly(vinylidene fluoride): Determination, processing and applications, Prog Polym Sci, 39, pp. 683-706 (2014).

[95] J. Kaszynska, B. Hilczer, P. Biskupski, Segmental dynamics in poly(vinylidene fluoride) studied by dielectric, mechanical and nuclear magnetic resonance spectroscopies, Polym Bull, 68, pp. 1121-1134 (2012).

[96] S.N. Fedosov, A.E. Sergeeva, Model of Polarization Buildup during Corona Charging of Ferroelectric Polymers, J Electrostat, 30, pp. 39-45 (1993).

[97] J.M.G. Neto, R.M. Faria, Spontaneous Electrical Current in P(Vdf/Trfe) Copolymer, Ise 8 - 8th International Symposium on Electrets, Proceedings, pp. 685-689 (1994).

[98] Z.F. Xia, S. Fedosov, A. Sergeeva, H.Y. Zhang, Thermally stimulated depolarization current in PVDF, P(VDF-TFE) and P(VDF-TrFE), Ise 9 - 9th International Symposium on Electrets, Proceedings, pp. 902-907 (1996).

[99] W. Eisenmenger, H. Schmidt, B. Dehlen, Space charge and dipoles in polyvinylidenefluoride, Braz J Phys, 29, pp. 295-305 (1999).

[100] A.F. Butenko, S.N. Fedosov, A.E. Sergeeva, Trapping of Compensating Charges in Corona Poled PVDF Films arXiv:0704.3449, pp. 1-6 (2007).

[101] S. Fedosov, A. Sergeeva, A.F. Butenko, Depolarization Currents in Fresh and Aged Corona Poled P(VDF-TFE) Films arXiv:0704.3993, pp. 1-5 (2007).

[102] S.N. Fedosov, A.F. Butenko, A.E. Sergeeva, Two components of depolarization currents in PVDF caused by relaxation of homo- and heterocharge, arXiv:0705.0149, pp. 1-6 (2007).

[103] N. Meng, X.J. Zhu, R. Mao, M.J. Reece, E. Bilotti, Nanoscale interfacial electroactivity in PVDF/PVDF-TrFE blended films with enhanced dielectric and ferroelectric properties, J Mater Chem C, 5, pp. 3296-3305 (2017).

[104] V.V. Kochervinskii, Piezoelectricity in crystallizing ferroelectric polymers: Poly(vinylidene fluoride) and its copolymers (A review), Crystallogr Rep+, 48, pp. 649-675 (2003).

[105] R.I. Mahdi, W.C. Gan , W.H.A. Majid, Hot plate annealing at a low temperature of a thin ferroelectric P(VDF-TRFE) film with an improved crystalline structure for sensors and actuators, Sensors, 14, pp. 19115- 19127 (2014).

[106] Z.Y. Fan, J.G. Lu, Zinc oxide nanostructures: Synthesis and properties, J Nanosci Nanotechno, 5, pp. 1561-1573 (2005).

[107] M. Vaseem, A. Umar, Y.-B. Hahn, ZnO Nanoparticles: Growth, Properties, and Applications, in: A. Umar, Y.-B. Hahn (Eds.) Metal Oxide Nanostructures and Their Applications, American Scientific Publishers 2010.

[108] K. Uchino, Advanced piezoelectric materials. Science and technology, Woodhead Publishing Limited, Oxford, Cambridge, Philadelphia, New Delhi, 678 2010.

[109] C. Journet, P. Bernier, Production of carbon nanotubes, Appl Phys a-Mater, 67, pp. 1-9 (1998).

[110] J. Banys, S. Lapinskas, S. Rudys, S. Greicius, R. Grigalaitis, High Frequency Measurements of Ferroelecrics and Related Materials in Coaxial Line, Ferroelectrics, 414, pp. 64-69 (2011).

[111] V. Samulionis, J. Banys, A. Sanchez-Ferrer, R. Mezzenga, Ultrasonic characterization of dynamic elastic properties of polymer composites with inorganic nanotubes, Sens. Transducers J. , 12, pp. 66-70 (2011).

[112] N. Mohmeyer, B. Muller, N. Behrendt, J. Hillenbrand, M. Klaiber, X.Q. Zhang, P. Smith, V. Altstadt, G.M. Sessler, H.W. Schmidt, Nucleation of isotactic polypropylene by triphenylarnine-based trisamide derivatives and their influence on charge-storage properties, Polymer, 45, pp. 6655-6663 (2004).

[113] J.A. Giacometti, S. Fedosov, M.M. Costa, Corona charging of polymers: Recent advances on constant current charging, Braz J Phys, 29, pp. 269-279 (1999).

[114] P.K. Khare, J.M. Keller, M.S. Gaur, R. Singh, S.C. Datt, Open- and short-circuit thermally stimulated currents in ethyl cellulose, Polym Int, 39, pp. 303-307 (1996).

[115] G.M. Yang, Thermally Stimulated Discharge of Electron-Beam-Charged and Corona-Charged Polypropylene Films, J Phys D Appl Phys, 26, pp. 690-693 (1993).

[116] M.H. Youssef, Influence of sulfur content and curing time on the glass transition parameters in SBR vulcanizates: an ultrasonic study, Polymer Testing, 22, pp. 235-242 (2003).

[117] D. Fragiadakis, P. Pissis, L. Bokobza, Glass transition and molecular dynamics in poly (dimethylsiloxane)/silica nanocomposites, Polymer, 46, pp. 6001-6008 (2005).

[118] H. Adachi, K. Adachi, Y. Ishida, T. Kotaka, Dielectric relaxation of polydimethylsiloxane, Journal of polymer science part B: Polymer physics, 17, pp. 851-857 (1979).

[119] J.Y. Ouyang, Y. Pan, S.Q. Zhou, S.H. Goh, Supramolecular assembled C-60-containing carboxylated poly(dimethylsiloxane) composites, Polymer, 47, pp. 6140-6148 (2006).

[120] C.M. Roland, R. Casalini, Temperature dependence of local segmental motion in polystyrene and its variation with molecular weight, J Chem Phys, 119, pp. 1838-1842 (2003).

[121] V. Samulionis, J. Macutkevic, J. Banys, J. Belovickis, O. Shenderova, Ultrasonic studies of onion-like carbons/polydimethysiloxane composites, 2014 Ieee International Ultrasonics Symposium (Ius), pp. 1986-1987 (2014).

[122] C.M. Sehgal, J.F. Greenleaf, Scattering Of Ultrasound by Tissues, Ultrasonic Imaging, 6, pp. 60-80 (1984).

[123] K.I. Lee, Dependencies of the Attenuation Coefficient on the Frequency and the Trabecular Thickness in Trabecular-bone-mimicking Phantoms: Application of a Scattering Model, J Korean Phys Soc, 58, pp. 1124-1128 (2011).

[124] L. Piche, Phenomena Related to the Propagation of Ultrasound in Polymers (a Paradigm for Disordered Materials), Ieee 1989 Ultrasonics Symposium : Proceedings, Vols 1 and 2, pp. 599-608 (1989).

[125] F. Lionetto, F. Montagna, A. Maffezzoli, Ultrasonic dynamic mechanical analysis of polymers, Appl Rheol, 15, pp. 326-335 (2005).

[126] F. Faghihi, N. Mohammadi, M. Haghgoo, The Effects of Rigid Polystyrene Particles on the Glass Transition Characteristics and Mechanical Wave Attenuation of Styrene-Butadiene Rubber: Particle Size and Acoustic Mismatch, J Polym Sci Pol Phys, 48, pp. 82-88 (2010).

[127] A.I. Beltzer, N. Brauner, The Dynamic Response Of Random Composites by a Causal Differential Method, Mechanics of Materials 6, pp. 337- 445 (1987).

[128] J. Belovickis, J. Macutkevic, S. Svirskas, V. Samulionis, J. Banys, O. Shenderova, V. Borjanovic, Dielectric Spectroscopy of Polymer Based PDMS Nanocomposites with ZnO Nanoparticles, Ferroelectrics, 479, pp. 82-89 (2015).

[129] T. Dollase, M. Wilhelm, H.W. Spiess, Y. Yagen, R. Yerushalmi-Rozen, M. Gottlieb, Effect of interfaces on the crystallization behavior of PDMS, Interface Sci, 11, pp. 199-209 (2003).

[130] L. del Valle-Carrandi, A. Alegria, J. Colmenero, PDMS behaviour under confinement in strongly segregated mesophases of PS-PDMS diblock copolymers, Eur Phys J-Spec Top, 189, pp. 257-261 (2010).

[131] Y. Bai, L. Jin, Characterization of frequency-dependent glass transition temperature by Vogel-Fulcher relationship, J Phys D Appl Phys, 41, pp. (2008).

[132] R. Sushko, M. Filimon, R. Dannert, P. Elens, R. Sanctuary, J. Baller, Anomalous glass transition behaviorof SBR-Al2O3 nanocomposites at small filler concentrations, Nanotechnology, 25, pp. (2014).

[133] S. Ansorge, F. Schmuck, K.O. Papailiou, Impact of different Fillers and Filler Treatments on the Erosion Suppression Mechanism of Silicone Rubber for Use as Outdoor Insulation Material, Ieee T Dielect El In, 22, pp. 979-989 (2015).

[134] A. Leschhorn, H. Kliem, Influence of the piezoeffect on static and dynamic ferroelectric properties, J Appl Phys, 114, pp. (2013).

[135] H. Kliem, M. Kuehn, Modeling the switching kinetics in ferroelectrics, J Appl Phys, 110, pp. (2011).

[136] U. Robels, J.H. Calderwood, G. Arlt, Shift and Deformation of the Hysteresis Curve of Ferroelectrics by Defects - Electrostatic Model, J Appl Phys, 77, pp. 4002-4008 (1995).

[137] A.N. Morozovska, I.S. Golovina, S.V. Lemishko, A.A. Andriiko, S.A. Khainakov, E.A. Eliseev, Effect of Vegard strains on the extrinsic size effects in ferroelectric nanoparticles, Phys Rev B, 90, pp. (2014).

[138] T. Ikeda, Studies on (Ba-Pb)(Ti-Zr)O3 system, J. Phys. Soc. Jpn., 14, pp. 168-174 (1959).

[139] A.V. Solnyshkin, I.L. Kislova, M.V. Silibin, D.A. Kiselev, Polarization Effect on Dielectric Response of Ferroelectric Copolymer P(VDF-TrFE), Ferroelectrics, 469, pp. 144-149 (2014).

[140] V. Pascariu, L. Padurariu, O. Avadanei, L. Mitoseriu, Dielectric properties of PZT-epoxy composite thick films, J Alloy Compd, 574, pp. 591-599 (2013).

[141] Y. Wang, S.G. Lu, M. Lanagan, Q.M. Zhang, Dielectric Relaxation of Relaxor Ferroelectric P(VDF-TrFE-CFE) Terpolymer over Broad Frequency Range, Ieee T Ultrason Ferr, 56, pp. 444-449 (2009).

[142] X.X. Wang, K.H. Lam, X.G. Tang, H.L.W. Chan, Dielectric characteristics and polarization response of lead-free ferroelectric (Bi0.5Na0.5)(0.94)Ba0.06TiO3-P(VDF-TrFE) 0-3 composites, Solid State Commun, 130, pp. 695-699 (2004).

[143] B. Sareni, L. Krahenbuhl, A. Beroual, C. Brosseau, Effective dielectric constant of random composite materials, J Appl Phys, 81, pp. 2375-2383 (1997).

[144] M.J. MIKSIS, EFFECTIVE DIELECTRIC CONSTANT OF A NONLINEAR COMPOSITE MATERIAL, SIAM J. APP, 43, pp. 1140-1155 (1983).

[145] Y.G. Wu, X.H. Zhao, F. Li, Z.G. Fan, Evaluation of mixing rules for dielectric constants of composite dielectrics by MC-FEM calculation on 3D cubic lattice, J Electroceram, 11, pp. 227-239 (2003).

[146] K. Lichtenecker, Die dielektrizitatskonstante naturlicher und kunstlicher mischkorper, Phys. Z., 27, pp. 115-158 (1926).

[147] W.P. Li, L.J. Yu, Y.J. Zhu, D.Y. Hua, J. Wang, L.H. Luo, J. Zhang, Annealing Effect on Poly(vinylidene fluoride/trifluoroethylene) (70/30) Copolymer Thin Films Above the Melting Point, J Appl Polym Sci, 116, pp. 663-667 (2010).

[148] K. Lau, Y. Liu, H. Chen, R.L. Withers, Effect of Annealing Temperature on the Morphology and Piezoresponse Characterisation of Poly(vinylidene fluoride-trifluoroethylene) Films via Scanning Probe Microscopy, Adv Cond Matter Phys, pp. (2013).

[149] R. Luiz Moreira, P. Saint-Gregoire, M. Latour, Thermal and dielectric investigations of the Curie transition in Poly(vinylidene Fluoride-Trifluoroethylene) copolymers, Phase Transitions, 14, pp. 243-249 (1989).

[150] J.D. Hoffman, Anelastic and Dielectric Effects in Polymeric Solids, Wiley, New York, 617 1967.

[151] A. Lonjon, Nanocomposite conducteur polymère/nanofils métalliques : élaboration et analyse des propriétés physiques. Directeur de these, 2010.

[152] J. Belovickis, J. Macutkevic, S. Svirskas, V. Samulionis, J. Banys, O. Shenderova, V. Borjanovic, Ultrasonic and dielectric relaxations in PDMS/ZnO nanocomposite, Phys Status Solidi B, 252, pp. 2778-2783 (2015).

[153] L.M. Ganesan, P. Frubing, A. Mellinger, R. Gerhard, Dielectric relaxation behaviour of nematic liquid crystals dispersed in poly(vinylidene fluoride-trifluoroethylene), J Phys D Appl Phys, 42, pp. (2009).

[154] Y. Zhen, J. Arredondo, G.-L. Zhao, Unusual dielectric loss properties of carbon nanotube—polyvinylidene fluoride composites in low frequency region (100 Hz < f < 1 MHz), Open Journal of Organic Polymer Materials, 3, pp. 99-103 (2013).

[155] J. Macutkevic, I. Kranauskaite, J. Banys, S. Moseenkov, V. Kuznetsov, O. Shenderova, Metal-insulator transition and size dependent electrical

percolation in onion-like carbon/polydimethylsiloxane composites, J Appl Phys, 115, pp. (2014).

[156] A. Dziaugys, J. Macutkevic, S. Svirskas, R. Juskenas, M. Wencka, J. Banys, S.F. Motria, Y. Vysochanskii, Maxwell-Wagner relaxation and anomalies of physical properties in Cu0.15Fe1.7PS3 mixed material, J Alloy Compd, 650, pp. 386-392 (2015).

[157] P. Khodaparast, Z. Ounaies, Influence of dispersion states on the performance of polymer-based nanocomposites, Smart Mater Struct, 23, pp. (2014).

[158] M. Ahmed, Polypropylene FiberScience and Technology, Elsevier, New York, 1982.

[159] G. Teyssedre, C. Lacabanne, Compositional Variation of the Glass-Transition and the Associated Dielectric-Relaxation in Copolymers of Vinylidene Fluoride and Trifluoroethylene, Polymer, 36, pp. 3641-3648 (1995).